(12) **INTERNATIONAL APPLICATION PUBLISHED UNDER THE PATENT COOPERATION TREATY (PCT)**

(19) **World Intellectual Property Organization**
International Bureau

(43) **International Publication Date**
15 March 2018 (15.03.2018)

WIPO I PCT

(10) **International Publication Number**
WO 2018/049109 A1

(72) **Inventors: ZHENG, Yuebing**; 2205 Rivina Dr., Austin, Texas 78733 (US). **LIN, Linhan**; 1000 Floradale Dr., Austin, Texas 78753 (US). **PENG, Xiaolei**; 2501 Lake Austin Blvd., Austin, Texas 78703 (US).

(54) **Title:** METHODS AND SYSTEMS FOR OPTICAL CONTROL OF METAL PARTICLES WITH THERMOPHORESIS
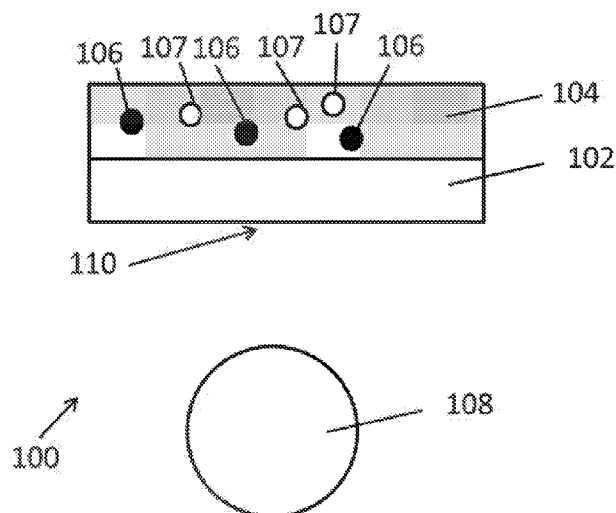
FIG. 1

(57) **Abstract:** Disclosed herein are methods comprising illuminating a first location of a plasmonic substrate with electromagnetic radiation, wherein the electromagnetic radiation comprises a wavelength that overlaps with at least a portion of the plasmon resonance energy of the plasmonic substrate. The plasmonic substrate can be in thermal contact with a liquid sample comprising a plurality of metal particles and a surfactant, the liquid sample having a first temperature. The methods can further comprise generating a confinement region at a location in the liquid sample proximate to the first location of the plasmonic substrate, wherein at least a portion of the confinement region has a second temperature that is greater than the first temperature such that the confinement region is bound by a temperature gradient. The methods can further comprise trapping at least a portion of the plurality of metal particles within the confinement region.

UG, ZM, ZW), Eurasian (AM, AZ, BY, KG, KZ, RU, TJ, TM), European (AL, AT, BE, BG, CH, CY, CZ, DE, DK, EE, ES, FI, FR, GB, GR, HR, HU, IE, IS, IT, LT, LU, LV, MC, MK, MT, NL, NO, PL, PT, RO, RS, SE, SI, SK, SM, TR), OAPI (BF, BJ, CF, CG, CI, CM, GA, GN, GQ, GW, KM, ML, MR, NE, SN, TD, TG).

Published:
— *with international search report (Art. 21(3))*

METHODS AND SYSTEMS FOR OPTICAL CONTROL OF METAL PARTICLES WITH THERMOPHORESIS

CROSS-REFERENCE TO RELATED APPLICATIONS

This application claims the benefit of U.S. Provisional Application No. 62/385,454, filed September 9, 2016, which is hereby incorporated herein by reference in its entirety.

BACKGROUND

Associated with the excitation of surface plasmons, metallic nanoparticles can manipulate light at the subwavelength scale where the intensive localized electromagnetic field strongly couples with nanoscale matters for new physical phenomena and applications. Optical and electrical properties of the plasmonic nanoparticles depend on the particle compositions, sizes, shapes, and the inter-particle interactions. Plasmonic nanoparticle assemblies that feature high particle density and small inter-particle distance are of importance for many applications that utilize the multiple and intensive electromagnetic "hot spots" in the assemblies. The capability of reversibly controlling the particle assemblies with external stimuli enables the dynamically tunable plasmonic coupling for advanced applications. Reversible assembly of functionalized metallic nanoparticles driven by pH of the solution (Taladriz-Blanco P et al. *J. Mater. Chem.* **2011**, 21, 16880-16887; Li W et al. *Nanoscale* **2015**, 7, 956-964), environmental temperature (Li Z et al. *J. Am. Chem. Soc.* **2012**, 134, 3322-3325; Liu Y et al. *Angew. Chem. Int. Ed.* **2012**, 51, 6373-6377), metal-ion coordination (Si S et al. *ChemPhysChem* **2008**, 9, 1578-1584), voltage (Su B et al. *J. Am. Chem. Soc.* **2004**, 126, 915-919), and light (Klajn R et al. *Proc. Natl. Acad. Sci.* **2007**, 104, 10305-10309; Kundu PK et al. *Nat. Chem* **2015**, 7, 646-652) has been demonstrated.

Optical manipulation of plasmonic nanoparticles has advantages for applications such as nanofabrication, drug delivery and bio-sensing. Optical tweezers, which provide remote, real-time and versatile manipulation of colloidal particles in solutions, have proven effective in the reversible assembly of plasmonic nanoparticles (Tong L et al. *Lab Chip* **2009**, 9, 193-195; Messina E et al. *J. Phys. Chem. C* **2011**, 115, 5115-5122; Stetciura IY et al. *Analyst* **2015**, 140, 4981-4986; Svedberg F et al. *Nano Lett.* **2006**, 6, 2639-2641; Yoshikawa H et al. *Phys. Rev. E* **2004**, 70, 061406). In optical tweezers, the optical forces assemble the nanoparticles into aggregates. When the working light is turned off, the assemblies can re-disperse into solution due to repulsive electrostatic interaction among the nanoparticles that have charges of the same sign. However, due to the strong light scattering from plasmonic nanoparticles, optical tweezers

demand tightly focused laser beam of high power intensity (10-100 mW/μm^2) in order to generate a strong optical gradient force for the assembly of the nanoparticles. The requirements of high optical power and sophisticated optics for beam control of optical tweezers have limited the applications of these nanoparticle assemblies. For example, un-expected photochemical or

5   thermal reactions (or damages) can occur to molecular analytes at the assemblies under the high-power laser illumination. Due to their enhanced local electromagnetic field and optical force, surface plasmon polaritons (SPPs) on a metallic thin film have been harnessed to reduce the power requirement for optical assembly of nanoparticles over the film (Patra PP et al. *Nat. Commun.* **2014**, 5, 4357). However, there are a couple of limitations in exploiting the plasmon-

10   enhanced optical force for the assembly of plasmonic nanoparticles. One is that the high sensitivity of optical force to plasmon resonances requires strict matching between the plasmon resonant wavelength of nanoparticles and the working wavelength of laser beam, meaning that a certain laser beam can only work well for limited types of nanoparticles with specific plasmon resonances. Another limitation is that, despite the rapid and even ultrafast optical responses, it

15   takes a relatively long time (~10 min) to achieve the assembly of nanoparticles in solutions because the near-field optical trapping on a plasmonic substrate relies on diffusion to bring nanoparticles into the working regime. Methods for the non-invasive and versatile manipulation of general particles with low optical power are still needed. The methods and systems discussed herein addresses these and other needs.

20   **SUMMARY**

In accordance with the purposes of the disclosed systems and methods, as embodied and broadly described herein, the disclosed subject matter relates to systems and methods for optical control of metal particles with thermophoresis.

Disclosed herein are methods comprising illuminating a first location of a plasmonic

25   substrate with electromagnetic radiation, wherein the electromagnetic radiation comprises a wavelength that overlaps with at least a portion of the plasmon resonance energy of the plasmonic substrate. In some examples, the power density of the electromagnetic radiation can be 0.1 mW/μm^2 or less (e.g., 0.05 mW/μm^2 or less). The electromagnetic radiation can, for example, be provided by a light source. Examples of suitable light sources include artificial light

30   sources, such as a laser.

In some examples, the light source is configured to illuminate a mirror, the mirror being configured to reflect the electromagnetic radiation from the light source to illuminate the first

location of the plasmonic substrate. In some examples, the mirror can comprise a plurality of mirrors, such as an array of micromirrors (e.g., a digital micromirror device).

The plasmonic substrate can, in some examples, comprise a plurality of plasmonic particles. In some examples, the plurality of plasmonic particles can comprise a plurality of metal particles. The plurality of metal particles can, for example, comprise a metal selected from the group consisting of Au, Ag, Al, and combinations thereof. The plurality of plasmonic particles can have an average particle size of from 10 nm to 500 nm. In some examples, the plurality of plasmonic particles are substantially spherical. In some examples, each plasmonic particle within the plurality of plasmonic particles on the substrate is separated from its neighboring plasmonic particles by an average distance of from 3 nm to 1500 nm. The density of the plurality of plasmonic particles on the plasmonic substrate can, for example, be 10^{11} particles/cm^2 or less.

The methods can further comprise, for example, making the plasmonic substrate by depositing the plurality of plasmonic particles on a substrate. Depositing the plurality of plasmonic particles can comprise, for example, printing, lithographic deposition, electron beam deposition, thermal deposition, spin coating, drop-casting, zone casting, dip coating, blade coating, spraying, vacuum filtration, or combinations thereof.

The methods can further comprise, for example, making the plasmonic substrate by thermally annealing a film of a plasmonic metal deposited on a substrate, thereby forming the plurality of plasmonic particles on the substrate. In some examples, the methods can further comprise depositing the film of the plasmonic metal on the substrate. In some examples, the film of the plasmonic metal can have a thickness of from 2 nm to 10 nm. Thermally annealing the film can, for example, comprise heating the film at a temperature of from 400°C to 600°C (e.g., at a temperature of 550°C). In some examples, the film can be thermally annealed for from 1 hour to 12 hours (e.g., for 2 hours).

The plasmonic substrate can be, for example, in thermal contact with a liquid sample comprising a plurality of metal particles and a surfactant, the liquid sample having a first temperature. The liquid sample can further comprise, for example, an aqueous solvent. The first temperature can be, for example, from 273 K to 343.

The surfactant can, for example, comprise a cationic surfactant or an anionic surfactant. In some examples, the surfactant can comprise cetrimonium bromide (CTAB), cetrimonium chloride (CTAC), sodium dodecyl sulfate (SDS), or a combination thereof. The concentration of the surfactant in the liquid sample can be from 1 mM to 75 mM. In some examples, the

concentration of the surfactant in the liquid sample is above the critical micelle concentration of the surfactant, such that the surfactant forms a plurality of surfactant micelles in the liquid sample.

The concentration of the plurality of metal particles in the liquid sample can be, for example, from 10^{10} particle/mm^3 to 10^{12} particles/mm^3. The plurality of metal particles in the liquid sample can have, for example, an average particle size of from 60 nm to 1 μm. In some examples, the plurality of metal particles in the liquid sample can comprise a metal selected from the group consisting of Al, Ag, Au, and combinations thereof. In some examples, the plurality of metal particles can comprise a plurality of plasmonic particles.

The plurality of metal particles can, for example, further comprise a capping layer comprising a capping material such that the plurality of metal particles comprise a plurality of capped metal particles. In some examples, the capping material is selected from the group consisting of cetrimonium bromide (CTAB), cetrimonium chloride (CTAC), sodium dodecyl sulfate (SDS), and combinations thereof. In some examples, the capping material and the surfactant are the same material.

The methods can further comprise, for example, generating a confinement region at a location in the liquid sample proximate to the first location of the plasmonic substrate, wherein at least a portion of the confinement region has a second temperature that is greater than the first temperature such that the confinement region is bound by a temperature gradient. In some examples, the method further comprises repulsing at least a portion of the surfactant from the confinement region such that the concentration of the surfactant within the confinement region is lower than the concentration of the surfactant outside the confinement region.

The second temperature can be, for example, from 273 K to 363 K. In some examples, the second temperature can be greater than the first temperature by from 3 K to 10 K.

In some examples, the confinement region is generated by plasmon-enhanced photothermal effects. The confinement region can, for example, have a diameter of from 500 nm to 10 μm.

The methods can further comprise, for example, trapping at least a portion of the plurality of metal particles within the confinement region. The portion of the plurality of metal particles trapped within the confinement region can be trapped, for example, by an electrostatic force, a thermophoretic force, van der Waals force, or combinations thereof. In some examples, the portion of the plurality of metal particles are not damaged during the trapping. In some

examples, the portion of the plurality of metal particles trapped is one metal particle. In other words, also disclosed herein are methods for single-particle trapping.

The methods can further comprise, for example, illuminating a second location of the plasmonic substrate thereby: generating a second confinement region at a location in the liquid sample proximate to the second location of the plasmonic substrate, wherein at least a portion of the second confinement region has a third temperature that is greater than the first temperature such that the second confinement region is bound by a temperature gradient; and translocating the trapped portion of the plurality of metal particles from the first confinement region to the second confinement region, trapping at least a second portion of the plurality of metal particles within the second confinement region, or a combination thereof. In some examples, the plasmonic substrate, the light source, the mirror, or a combination thereof can be translocated to illuminate the second location.

In some examples, the plasmonic substrate comprises a portion of a substrate, the substrate further comprising a non-plasmonic portion and wherein the substrate is in thermal contact with the liquid sample. In some examples, the non-plasmonic portion of the substrate can comprise glass, quartz, silicon dioxide, a polymer, and combinations thereof.

In certain examples, wherein the plasmonic substrate comprises a portion of a substrate, the substrate further comprising a non-plasmonic portion and wherein the substrate is in thermal contact with the liquid sample, the methods can further comprise illuminating a location of the non-plasmonic portion of the substrate, thereby: generating a second confinement region at a location in the liquid sample proximate to the location of the non-plasmonic portion of the substrate, wherein at least a portion of the second confinement region has a third temperature that is greater than the first temperature such that the second confinement region is bound by a temperature gradient; and translocating the trapped portion of the plurality of metal particles from the first confinement region to the second confinement region. In some examples, the substrate can be translocated to illuminate the location of the non-plasmonic portion of the substrate. In some examples, wherein the electromagnetic radiation is provided by a light source, the light source can be translocated to illuminate the location of the non-plasmonic portion of the substrate. In some examples, wherein the electromagnetic radiation is provided by a light source, the light source being configured to illuminate a mirror and the mirror is configured to reflect the electromagnetic radiation from the artificial light source to illuminate the substrate, the mirror can be translocated to illuminate the location of the non-plasmonic portion of the substrate.

Also disclosed herein are patterned sample made using the methods described herein. Also disclosed herein are methods of use of patterned sample made using the methods described herein, for example using the patterned samples for single-particle sensing, functional optical devices, or combinations thereof. In some examples, the patterned sample can be used for surface-enhanced Raman spectroscopy (SERS).

Also disclosed herein are systems for performing the methods described herein. The systems can comprise a plasmonic substrate in thermal contact with a liquid sample comprising a plurality of metal particles and a surfactant; and a light source configured to illuminate the plasmonic substrate at a first location. In some examples, the system can include a single light source. In some examples, the systems can further comprise a means for translocating the plasmonic substrate and/or the light source.

The system can, in some examples, further comprise a mirror, wherein the system can be aligned such that the light source is configured to illuminate the mirror and the mirror is configured to reflect the electromagnetic radiation from the light source to illuminate the first location of the plasmonic substrate. In some examples, the systems can further comprise a means for translocating the mirror.

The system can, in some examples, further comprise an instrument configured to capture an electromagnetic signal from the plasmonic substrate. The instrument can comprise, for example, Raman spectrometers, UV-vis absorption spectrometers, IR absorption spectrometers, fluorescence spectrometers, and combinations thereof. In some examples, the systems can further comprise a computing device configured to receive and process electromagnetic signals from the instrument.

In some examples, the system can further comprise a first lens. In some examples, the system can be configured such that the light source is below the first lens and the plasmonic substrate is above the first lens. In some examples, the system can further comprise a second lens. In some examples, the system is aligned such that the light source is below the first lens, the plasmonic substrate is above the first lens, the second lens is above the plasmonic substrate, and the instrument is above the second lens.

Additional advantages of the disclosed systems and methods will be set forth in part in the description which follows, and in part will be obvious from the description. The advantages of the disclosed systems and methods will be realized and attained by means of the elements and combinations particularly pointed out in the appended claims. It is to be understood that both the

foregoing general description and the following detailed description are exemplary and explanatory only and are not restrictive of the disclosed systems and methods, as claimed.

The details of one or more embodiments of the invention are set forth in the accompanying drawings and the description below. Other features, objects, and advantages of 5   the invention will be apparent from the description and drawings, and from the claims.

BRIEF DESCRIPTION OF THE FIGURES

The accompanying figures, which are incorporated in and constitute a part of this specification, illustrate several aspects of the disclosure, and together with the description, serve to explain the principles of the disclosure.

10   Figure 1 is a schematic of an exemplary system as disclosed herein.

Figure 2 is a schematic of an exemplary system as disclosed herein.

Figure 3 is a schematic of an exemplary system as disclosed herein.

Figure 4 is a schematic of an exemplary system as disclosed herein.

Figure 5 is a schematic of an exemplary system as disclosed herein.

15   Figure 6 is a schematic of an exemplary system as disclosed herein.

Figure 7 is a schematic of an exemplary computing device.

Figure 8 is a schematic of the light-directed reversible assembly of Au nanotriangles that are surface-functionalized with CTAC based on the plasmon-enhanced thermophoresis light-directed reversible assembly of. The CTA^+ groups form double layers on the nanoparticle 20   surfaces, which become positively charged and hydrophilic (inset).

Figure 9 is a scanning electron micrograph (SEM) of a single Au nanotriangle.

Figure 10 shows the normalized optical transmission spectra of Au nanotriangles (AuNTs), Ag nanospheres (AgNSs), and Au nanospheres (AuNSs) in suspensions.

Figure 11 is a scanning electron micrograph of the Au nanoislands as a plasmonic 25   substrate.

Figure 12 is an optical transmission spectrum of the Au nanoislands as a plasmonic substrate.

Figure 13 shows successive optical images for the light-directed assembly of Au nanotriangles. The red and blue dot circles indicate that the laser is off and on, respectively. The 30   scale bar is 10 μm.

Figure 14 shows successive optical images for the disassembly of an Au nanotriangle aggregate when the laser is off. The red and blue dot circles indicate that the laser is off and on, respectively. The scale bar is 10 μm.

Figure 15 is a schematic illustration of the migration of a CTA$^+$-modified Au nanotriangle from cold to hot regime in the light-induced temperature-gradient field, which is known as thermophoresis.

Figure 16 is a schematic illustration of the release or re-dispersion of an Au nanotriangle assembly due to electrostatic repulsive interaction when the laser is off and the temperature-gradient field disappears.

Figure 17 shows the simulated temperature distribution at the interface between plasmonic substrate and particle solution in a cross-sectional view before the formation of Au nanotriangle assembly.

Figure 18 shows the simulated temperature distribution at the interface between plasmonic substrate and particle solution in a cross-sectional view after the formation of Au nanotriangle assembly.

Figure 19 shows the simulated temperature distribution at the interface between glass substrate and nanoparticle solution in a cross-sectional view.

Figure 20 shows time-evolved optical images of Au nanotriangle assembly (and disassembly) at the variable optical power. t_1: A stable Au nanotriangle assembly formed at optical power of 0.2 mW. t_2-t_4: An increased thermal convection disassembled the Au nanotriangle assembly when the optical power was increased to 0.5 mW. The scale bar is 10 μm.

Figure 21 shows time-evolved optical images illustrate that the Au nanotriangle assembly can be transported from the plasmonic substrate to the glass substrate by translating the sample stage. The scale bar is 10 μm.

Figure 22 shows the schematics of the optical setup for parallel and dynamic manipulation of multiple nanoparticle assemblies and "multiplex" *in-situ* SERS.

Figure 23 is an optical image of 25 Au nanotriangle assemblies in a 5×5 square array. The total power of 532 nm working laser beam is 7.9 mW for the parallel manipulation. The diameter of individual laser beams for single assemblies is 2 μm. The scale bar is 10 μm.

Figure 24 is a dark-field optical image of 17 Au nanotriangle assemblies in an "Au" pattern. The total power of 532 nm working laser beam is 3.6 mW for the parallel manipulation. The diameter of individual laser beams for single assemblies is 2 μm. The scale bar is 10 μm.

Figure 25 shows the time-evolved optical images of dynamic manipulation of selected Au nanotriangle assemblies to transform the pattern. The total power of 532 nm working laser beam is 3.6 mW for the parallel manipulation. The diameter of individual laser beams for single assemblies is 2 μm. The scale bar is 10 μm.

Figure 26 shows the Raman spectrum of rhodamine 6G measured from a single Ag nanosphere assembly. The assembly size is 5.0 ± 0.2 µm. The concentrations of CTAC and rhodamine 6G are 10 mM and 1 mM, respectively.

Figure 27 shows the parametric study of SERS of rhodamine 6G based on plasmonic nanoparticle assemblies. Raman intensities of 614 cm⁻¹ and 1510 cm⁻¹ modes as a function of the CTAC concentration in Au nanosphere solution. The size of Au nanosphere assemblies over the plasmonic substrate was maintained at 4.0±0.2 µm. A 660 nm laser beam with a power of 0.27 mW and a diameter of 2 µm is used for both nanoparticle assembly and Raman measurement. The rhodamine 6G concentration is 1 mM. The acquisition time is 10 s.

Figure 28 shows the parametric study of SERS of rhodamine 6G based on plasmonic nanoparticle assemblies. Assembly-size-dependent Raman intensities of 614 cm⁻¹ and 1510 cm⁻¹ modes based on Au nanotriangle assemblies over the plasmonic substrate. A 660 nm laser beam with a power of 0.27 mW and a diameter of 2 µm is used for both nanoparticle assembly and Raman measurement. The rhodamine 6G concentration is 1 mM. The acquisition time is 1 s.

Figure 29 shows the parametric study of SERS of rhodamine 6G based on plasmonic nanoparticle assemblies. Assembly-size-dependent Raman intensities of 614 cm⁻¹ and 1510 cm⁻¹ modes based on Au nanotriangle assemblies over the glass substrate. A 660 nm laser beam with a power of 0.27 mW and a diameter of 2 µm is used for both nanoparticle assembly and Raman measurement. The rhodamine 6G concentration is 1 mM. The acquisition time is 1 s.

Figure 30 shows the parametric study of SERS of rhodamine 6G based on plasmonic nanoparticle assemblies. Assembly-size-dependent Raman intensities of 614 cm⁻¹ and 1510 cm⁻¹ modes based on Ag nanosphere assemblies over the plasmonic substrate. A 660 nm laser beam with a power of 0.27 mW and a diameter of 2 µm is used for both nanoparticle assembly and Raman measurement. The rhodamine 6G concentration is 1 mM. The acquisition time is 1 s.

Figure 31 shows the Raman spectra recorded from single Ag nanosphere assemblies over the plasmonic substrate for rhodamine 6G of different concentrations. The assembly size is 5.0 ± 0.2 µm. A 660 nm laser beam with a diameter of 2 µm and a power of 0.27 mW is used for both nanoparticle assembly and Raman measurement. Raman acquisition time is 10 s.

Figure 32 shows the time-resolved Raman spectra of rhodamine 6G (10 µM) based on a single Ag nanosphere assembly during the solvent evaporation. At t_1, the assembly is immersed in the solvent. At t_{10}, the assembly is 100% dry. The assembly size increases from 4 µm to 6 µm after the complete evaporation of solvent. A 660 nm laser beam with a diameter of 2 µm and a

power of 0.32 mW is used for both nanoparticle assembly and Raman measurement. Raman acquisition time is 15 s.

Figure 33 shows the Raman spectra of rhodamine 6G measured from one Ag nanosphere assembly, two Ag nanosphere assemblies and three Ag nanosphere assemblies generated by single beam, two beams and three beams through spatial light modulator.

Figure 34 shows the Raman spectra of methyl orange of variable concentrations based on Au nanotriangle assembly over the plasmonic substrate (assembly size: 5.3±0.2 μm). A 660 nm laser beam with a diameter of 2 μm and a power of 0.32 mW is used for both the nanoparticle assembly and SERS measurement. Raman acquisition time is 10 s.

Figure 35 shows the Raman spectra of methyl orange of variable concentrations based on Ag nanosphere assembly over the plasmonic substrate (assembly size: 3.8±0.2 μm). A 660 nm laser beam with a diameter of 2 μm and a power of 0.32 mW is used for both the nanoparticle assembly and SERS measurement. Raman acquisition time is 10 s.

Figure 36 is a scanning electron microscopy (SEM) image of the 4.5 nm porous Au film after thermal annealing. Scale bar: 200 nm.

Figure 37 is a scanning electron microscopy (SEM) image of the 6.5 nm porous Au films after thermal annealing. Scale bar: 200 nm.

Figure 38 is the transmission spectra of the 4.5 nm and 6.5 nm porous Au films after thermal annealing.

Figure 39 is a schematic view of the surface charge modification of a metal nanoparticle by CTAC adsorption.

Figure 40 is a schematic view of the formation of CTAC micelles, which can act as macro-positive ions.

Figure 41 is a schematic view of a Cl⁻ ion.

Figure 42 is a schematic view of the dispersion of a single metal particle and multiple ions (micellar ions and Cl⁻ ions) in the solution without optical heating.

Figure 43 is a schematic view of the thermophoretic migration of the ions under optical heating. The incident laser beam has a diameter of 2 μm and an optical power of 0.216 mW.

Figure 44 is a schematic view of the steady ionic distribution under optical heating generates a thermoelectric field E_T for trapping the metal nanoparticle. The repulsive electric field E_r arises from the positive charge of the thermoplasmonic substrate and balances E_T. The incident laser beam has a diameter of 2 μm and an optical power of 0.216 mW.

Figure 45 is the simulated in-plane temperature gradient and direction of the corresponding trapping force. The incident laser beam has a diameter of 2 µm and an optical power of 0.216 mW. The arrows show the direction of the trapping force.

Figure 46 is the simulated out-of-plane temperature gradient and direction of the corresponding trapping force. The incident laser beam has a diameter of 2 µm and an optical power of 0.216 mW. The arrows show the direction of the trapping force.

Figure 47 is a schematic illustration and successive optical images showing trapping of a single 100 nm Ag nanosphere (AgNS). The grey disks in the optical images indicate that the laser is on. The optical power was 0.4 mW. Scale bar: 10 µm.

Figure 48 is a schematic illustration and successive optical images showing dynamic manipulation of a single 100 nm Ag nanosphere (AgNS). The grey lines in the optical images show the manipulation trajectory of the trapped Ag nanosphere. The optical power was 0.4 mW. Scale bar: 20 µm.

Figure 49 is a schematic illustration and successive optical images showing release of a single 100 nm Ag nanosphere (AgNS). The central disks in the optical images mean that the laser is turned off. The optical power was 0.4 mW. Scale bar: 10 µm.

Figure 50 is the measured escape velocities of 200 nm Au nanosphere (AuNS), 100 nm Au nanosphere, and 100 nm Ag nanosphere (ag NS), as a function of optical power. The maximum in-plane temperature gradients at the planes that are 50 nm and 100 nm above the thermoplasmonic substrate (i.e. around the center of the trapped 100 nm and 200 nm nanospheres) were simulated as a function of the optical power (h=50 nm and h = 100 nm curves, respectively). CTAC concentration was 1 mM.

Figure 51 is the escape velocity of a single 200 nm Au nanosphere (AuNS) as a function of SDS concentration. The Au nanosphere was trapped with a 532 nm laser beam through a 100× air objective (NA 0.9). The laser beam has a diameter of 1 µm at an optical power of 0.05 mW. A maximum escape velocity was observed at a SDS concentration of 20 mM, which is about 3 times higher than the critical micelle concentration (cmc) of SDS.

Figure 52 is the simulated out-of-plane temperature gradients at the planes that are 50 nm and 100 nm above the substrate, corresponding to around spherical centers of the trapped 100 nm Au nanosphere and 200 nm Au nanosphere, as a function of the incident optical power.

Figure 53 is the Measured escape velocities of 200 nm Au nanosphere (AuNS, 100 nm Au nanosphere, and 100 nm Ag nanosphere (AgNS) as a function of CTAC concentration.

Figure 54 is a schematic diagram of the optical setup of the OTENT with *in-situ* dark-field optical imaging and spectroscopy. The listed optical components: L-Laser; BE-Beam expander; DMD-Digital micromirror device; WL-White light; CO-Condenser; O-Objective; BS-Beam splitter; NF-Notch filter; MO-Monitor; CA-Camera; MI-Mirror; S-Spectrometer. For trapping and spectroscopy of Au nanospheres and Ag nanospheres, a 660 nm laser with a 650 nm shortpass filter was used. For trapping and spectroscopy of Au nanotriangles (AuNTs) and Au nanorods (AuNRs), a 532 nm laser with a 533 nm notch filter was used.

Figure 55 is the dark-field optical images (insets in right panels), experimental and simulated scattering spectra (right panels), and electric field profiles (left) of single Ag nanospheres with diameters of 80 nm (top), 90 nm (middle) and 100 nm (bottom). The solid and dashed curves represent experimental and simulated scattering spectra, respectively.

Figure 56 is the dark-field optical images (insets in right panels), experimental and simulated scattering spectra (right panels), and electric field profiles (left) of single Au nanospheres with diameters of 80 nm (top), 90 nm (middle) and 100 nm (bottom). The solid and dashed curves represent experimental and simulated scattering spectra, respectively.

Figure 57 is the *in-situ* scattering spectra of a 100 nm Ag nanosphere rapped with a 532 nm laser beam. The solid and dashed curves are the experimental and simulated spectra. Since a 533 nm notch filter was used to record the spectra, the data around 533 nm was removed.

Figure 58 is the *in-situ* scattering spectra of a 100 nm Au nanosphere trapped with a 532 nm laser beam. The solid and dashed curves are the experimental and simulated spectra. Since a 533 nm notch filter was used to record the spectra, the data around 533 nm was removed.

Figure 59 is the dark-field optical images (insets in right panels), experimental and simulated scattering spectra (right panels), and electric field profiles (left) of single Au nanotriangles with side lengths of 60 nm (top) and 140 nm (bottom). The solid and dashed curves represent experimental and simulated scattering spectra, respectively.

Figure 60 is the background spectrum of the thermoplasmonic substrate recorded by turning on the 532 nm laser beam without trapping of any particle.

Figure 61 is the dark-field optical images (insets in right panels), experimental and simulated scattering spectra (right panels), and electric field profiles (left) of single Au nanorods with dimensions of 63 nm × 23 nm (top), 65 nm × 25 nm (middle), and 67 nm × 25 nm (bottom) (length×diameter). The solid and dashed curves represent experimental and simulated scattering spectra, respectively.

Figure 62 is the dark-field optical image recorded before a single Au nanorod (AuNR) was trapped by a single 532 nm laser beam.

Figure 63 is the dark-field optical image recorded after a single Au nanorod (AuNR) was trapped by a single 532 nm laser beam. The scattering intensity of the Au nanorod was much weaker than the transmitted laser beam and the fluorescence light from the thermoplasmonic substrate, preventing the observation of the red color from the single Au nanorod.

Figure 64 is a SEM image of a single 100 nm Au nanosphere printed on the thermoplasmonic substrate after being trapped by the opto-thermoelectric nanotweezers (OTENTs). The micrograph further verified the single nanoparticles trapped by our OTENTs. The printed particle is indicated by the arrow. Scale bar: 1 μm.

Figure 65 is a SEM image of a single 150 nm Au nanotriangle printed on the thermoplasmonic substrate after being trapped by the opto-thermoelectric nanotweezers (OTENTs). The micrograph further verified the single nanoparticles trapped by our OTENTs. The printed particle is indicated by the arrow. Scale bar: 500 nm.

Figure 66 is a SEM image of a single Au nanorod printed on the thermoplasmonic substrate after being trapped by the opto-thermoelectric nanotweezers (OTENTs). The micrograph further verified the single nanoparticles trapped by our OTENTs. The printed particle is indicated by the arrow. Scale bar: 500 nm.

Figure 67 is a schematic illustration and successive optical images showing parallel trapping of six 100 nm Ag nanospheres into a circular pattern, with six laser beams where each beam traps one Ag nanosphere.

Figure 68 is a schematic illustration and successive optical images showing parallel trapping of six 150 nm Au nanotriangles into a triangular pattern with six laser beams, where each beam traps one Au nanotriangle.

Figure 69 is the scattering intensity as a function of time, showing the trapping dynamics of a single 100 nm Au nanosphere. The scattering intensity was recorded at a wavelength of 580 nm.

Figure 70 is the scattering intensity as a function of time showing the trapping dynamics of multiple 100 nm Au nanospheres at a single laser beam. The scattering intensity was recorded at a wavelength of 580 nm.

Figure 71 is a schematic illustration and successive optical images showing the trapping process of a single Ag nanowire (AgNW) with a 1D optical image. Scale bar: 10 μm.

13

Figure 72 is a schematic illustration and successive optical images showing the rotation of a single Ag nanowire with a 1D optical image. The grey line represents the 1D optical image. Scale bar: 10 μm.

Figure 73 is the dark-field optical image (left) and simulated electric field intensity (right) when longitudinal surface plasmons are excited along the nanowire (λ=703 nm). The Ag nanowire has a length of 11.7 μm. The arrows in the optical image show the polarization of the incident white light. Scale bar: 10 μm.

Figure 74 is the dark-field optical image (left) and simulated electric field intensity (right) when transverse surface plasmons are excited along the nanowire (λ=420 nm). The Ag nanowire has a length of 11.7 μm. The arrows in the optical image show the polarization of the incident white light. Scale bar: 10 μm.

DETAILED DESCRIPTION

The systems and methods described herein may be understood more readily by reference to the following detailed description of specific aspects of the disclosed subject matter and the Examples included therein.

Before the present systems and methods are disclosed and described, it is to be understood that the aspects described below are not limited to specific synthetic methods or specific reagents, as such may, of course, vary. It is also to be understood that the terminology used herein is for the purpose of describing particular aspects only and is not intended to be limiting.

Also, throughout this specification, various publications are referenced. The disclosures of these publications in their entireties are hereby incorporated by reference into this application in order to more fully describe the state of the art to which the disclosed matter pertains. The references disclosed are also individually and specifically incorporated by reference herein for the material contained in them that is discussed in the sentence in which the reference is relied upon.

In this specification and in the claims that follow, reference will be made to a number of terms, which shall be defined to have the following meanings.

Throughout the description and claims of this specification the word "comprise" and other forms of the word, such as "comprising" and "comprises," means including but not limited to, and is not intended to exclude, for example, other additives, components, integers, or steps.

As used in the description and the appended claims, the singular forms "a," "an," and "the" include plural referents unless the context clearly dictates otherwise. Thus, for example,

14

reference to "a composition" includes mixtures of two or more such compositions, reference to "an agent" includes mixtures of two or more such agents, reference to "the component" includes mixtures of two or more such components, and the like.

"Optional" or "optionally" means that the subsequently described event or circumstance
5   can or cannot occur, and that the description includes instances where the event or circumstance occurs and instances where it does not.

Ranges can be expressed herein as from "about" one particular value, and/or to "about" another particular value. By "about" is meant within 5% of the value, e.g., within 4, 3, 2, or 1% of the value. When such a range is expressed, another aspect includes from the one particular
10   value and/or to the other particular value. Similarly, when values are expressed as approximations, by use of the antecedent "about," it will be understood that the particular value forms another aspect. It will be further understood that the endpoints of each of the ranges are significant both in relation to the other endpoint, and independently of the other endpoint.

It is understood that throughout this specification the identifiers "first" and "second" are
15   used solely to aid in distinguishing the various components and steps of the disclosed subject matter. The identifiers "first" and "second" are not intended to imply any particular order, amount, preference, or importance to the components or steps modified by these terms.

Disclosed herein are systems and methods, for example, for dynamically controlling colloidal particles and/or biological cells using thermally controlled confinement regions. In
20   some examples, the methods and systems can comprise locally exposing a substrate to an optical signal according to a desired pattern to thereby confine the colloidal particles and/or biological cells within said pattern.

Disclosed herein are methods comprising illuminating a first location of a plasmonic substrate with electromagnetic radiation, wherein the electromagnetic radiation comprises a
25   wavelength that overlaps with at least a portion of the plasmon resonance energy of the plasmonic substrate. As used herein, "a first location" and "the first location" are meant to include any number of locations in any arrangement on the plasmonic substrate. Thus, for example "a first location" includes one or more first locations. In some embodiments, the first location can comprise a plurality of locations. In some embodiments, the first locations can
30   comprise a plurality of locations arranged in an ordered array.

In some examples, the power density of the electromagnetic radiation can be 0.1 mW/μm^2 or less (e.g., 0.09 mW/μm^2 or less, 0.08 mW/μm^2 or less, 0.07 mW/μm^2 or less, 0.06 mW/μm^2 or less, 0.05 mW/μm^2 or less, 0.04 mW/μm^2 or less, 0.03 mW/μm^2 or less, 0.02

mW/μm^2 or less, 0.01 mW/μm^2 or less, 0.009 mW/μm^2 or less, 0.008 mW/μm^2 or less, 0.007

mW/μm^2 or less, or 0.006 mW/μm^2 or less). In some examples, the power density of the

electromagnetic radiation can be 0.005 mW/μm^2 or more (e.g., 0.006 mW/μm^2 or more, 0.007

mW/μm^2 or more, 0.008 mW/μm^2 or more, 0.009 mW/μm^2 or more, 0.01 mW/μm^2 or more, 0.02

5   mW/μm^2 or more, 0.03 mW/μm^2 or more, 0.04 mW/μm^2 or more, 0.05 mW/μm^2 or more, 0.06

mW/μm^2 or more, 0.07 mW/μm^2 or more, 0.08 mW/μm^2 or more, or 0.09 mW/μm^2 or more).

The power density of the electromagnetic radiation can range from any of the minimum values

described above to any of the maximum values described above. For example, the power density

of the electromagnetic radiation can range from 0.005 mW/μm^2 to 0.1 mW/μm^2 (e.g., from 0.005

10   mW/μm^2 to 0.05 mW/μm^2, from 0.05 mW/μm^2 to 0.1 mW/μm^2, from 0.005 mW/μm^2 to 0.01

mW/μm^2, from 0.01 mW/μm^2 to 0.05 mW/μm^2, from 0.05 mW/μm^2 to 0.1 mW/μm^2, or from

0.01 mW/μm^2 to 0.09 mW/μm^2).

The electromagnetic radiation can, for example, be provided by a light source. The light

source can be any type of light source. Examples of suitable light sources include natural light

15   sources (*e.g.*, sunlight) and artificial light sources (*e.g.*, incandescent light bulbs, light emitting

diodes, gas discharge lamps, arc lamps, lasers, etc.). In some examples, the light source is a

laser.

In some examples, the light source is configured to illuminate a mirror, the mirror being

configured to reflect the electromagnetic radiation from the light source to illuminate the first

20   location of the plasmonic substrate. In some examples, the mirror can comprise a plurality of

mirrors, such as an array of micromirrors (e.g., a digital micromirror device).

The plasmonic substrate can, in some examples, comprise a plurality of plasmonic

particles. In some examples, the plurality of plasmonic particles can comprise a plurality of

metal particles. The plurality of metal particles can, for example, comprise a metal selected from

25   the group consisting of Au, Ag, Al, and combinations thereof. In some examples, the plurality of

plasmonic particles can comprise a plurality of gold particles, a plurality of silver particles, or a

combination thereof.

The plurality of plasmonic particles can have an average particle size. "Average particle

size" and "mean particle size" are used interchangeably herein, and generally refer to the

30   statistical mean particle size of the particles in a population of particles. For example, the

average particle size for a plurality of particles with a substantially spherical shape can comprise

the average diameter of the plurality of particles. For a particle with a substantially spherical

shape, the diameter of a particle can refer, for example, to the hydrodynamic diameter. As used

herein, the hydrodynamic diameter of a particle can refer to the largest linear distance between two points on the surface of the particle. For an anisotropic particle, the average particle size can refer to, for example, the average maximum dimension of the particle (e.g., the length of a rod shaped particle, the diagonal of a cube shape particle, the bisector of a triangular shaped particle, etc.) For an anisotropic particle, the average particle size can refer to, for example, the hydrodynamic size of the particle. Mean particle size can be measured using methods known in the art, such as evaluation by scanning electron microscopy, transmission electron microscopy, and/or dynamic light scattering.

The plurality of plasmonic particles have, for example, an average particle size of 10 nm or more (e.g., 15 nm or more, 20 nm or more, 25 nm or more, 30 nm or more, 35 nm or more, 40 nm or more, 45 nm or more, 50 nm or more, 55 nm or more, 60 nm or more, 65 nm or more, 70 nm or more, 75 nm or more, 80 nm or more, 85 nm or more, 90 nm or more, 95 nm or more, 100 nm or more, 110 nm or more, 120 nm or more, 130 nm or more, 140 nm or more, 150 nm or more, 160 nm or more, 170 nm or more, 180 nm or more, 190 nm or more, 200 nm or more, 210 nm or more, 220 nm or more, 230 nm or more, 240 nm or more, 250 nm or more, 275 nm or more, 300 nm or more, 325 nm or more, 350 nm or more, 375 nm or more, 400 nm or more, 425 nm or more, 450 nm or more, or 475 nm or more).

In some examples, the plurality of plasmonic particles can have an average particle size of 500 nm or less (e.g., 475 nm or less, 450 nm or less, 425 nm or less, 400 nm or less, 375 nm or less, 350 nm or less, 325 nm or less, 300 nm or less, 290 nm or less, 280 nm or less, 270 nm or less, 260 nm or less, 250 nm or less, 240 nm or less, 230 nm or less, 220 nm or less, 210 nm or less, 200 nm or less, 190 nm or less, 180 nm or less, 170 nm or less, 160 nm or less, 150 nm or less, 140 nm or less, 130 nm or less, 120 nm or less, 110 nm or less, 100 nm or less, 95 nm or less, 90 nm or less, 85 nm or less, 80 nm or less, 75 nm or less, 70 nm or less, 65 nm or less, 60 nm or less, 55 nm or less, 50 nm or less, 45 nm or less, 40 nm or less, 35 nm or less, 30 nm or less, 25 nm or less, 20 nm or less, or 15 nm or less).

The average particle size of the plurality of plasmonic particles can range from any of the minimum values described above to any of the maximum values described above. For example, the plurality of plasmonic particles can have an average particle size of from 10 nm to 500 nm (e.g., from 10 nm to 250 nm, from 250 nm to 500 nm, from 10 nm to 100 nm, from 100 nm to 200 nm, from 200 nm to 300 nm, from 300 nm to 400 nm, from 400 nm to 500 nm, or from 10 nm to 300 nm).

In some examples, the plurality of plasmonic particles can be substantially monodisperse. "Monodisperse" and "homogeneous size distribution," as used herein, and generally describe a population of particles where all of the particles are the same or nearly the same size. As used herein, a monodisperse distribution refers to particle distributions in which 80% of the

5   distribution (e.g., 85% of the distribution, 90% of the distribution, or 95% of the distribution) lies within 25% of the median particle size (e.g., within 20% of the median particle size, within 15% of the median particle size, within 10% of the median particle size, or within 5% of the median particle size).

The plurality of plasmonic particles can comprise particles of any shape (e.g., a sphere, a

10   rod, a quadrilateral, an ellipse, a triangle, a polygon, etc.). In some examples, the plurality of plasmonic particles can have an isotropic shape. In some examples, the plurality of plasmonic particles can have an anisotropic shape. In some examples, the plurality of plasmonic particles are substantially spherical.

In some examples, each plasmonic particle within the plurality of plasmonic particles on

15   the substrate is separated from its neighboring plasmonic particles by an average distance of 3 nm or more (e.g., 4 nm or more, 5 nm or more, 6 nm or more, 7 nm or more, 8 nm or more, 9 nm or more, 10 nm or more, 11 nm or more, 12 nm or more, 13 nm or more, 14 nm or more, 15 nm or more, 16 nm or more, 17 nm or more, 18 nm or more, 19 nm or more, 20 nm or more, 25 nm or more, 30 nm or more, 35 nm or more, 40 nm or more, 45 nm or more, 50 nm or more, 55 nm

20   or more, 60 nm or more, 65 nm or more, 70 nm or more, 75 nm or more, 80 nm or more, 85 nm or more, 90 nm or more, 95 nm or more, 100 nm or more, 125 nm or more, 150 nm or more, 175 nm or more, 200 nm or more, 225 nm or more, 250 nm or more, 275 nm or more, 300 nm or more, 325 nm or more, 350 nm or more, 375 nm or more, 400 nm or more, 425 nm or more, 450 nm or more, 475 nm or more, 500 nm or more, 550 nm or more, 600 nm or more, 650 nm or

25   more, 700 nm or more, 750 nm or more, 800 nm or more, 850 nm or more, 900 nm or more, 950 nm or more, 1000 nm or more, 1100 nm or more, 1200 nm or more, 1300 nm or more, or 1400 nm or more).

In some examples, each plasmonic particle within the plurality of plasmonic particles on the substrate is separated from its neighboring plasmonic particles by an average distance of

30   1500 nm or less (e.g., 1400 nm or less, 1300 nm or less, 1200 nm or less, 1100 nm or less, 1000 nm or less, 950 nm or less, 900 nm or less, 850 nm or less, 800 nm or less, 750 nm or less, 700 nm or less, 650 nm or less, 600 nm or less, 550 nm or less, 500 nm or less, 475 nm or less, 450 nm or less, 425 nm or less, 400 nm or less, 375 nm or less, 350 nm or less, 325 nm or less, 300

nm or less, 275 nm or less, 250 nm or less, 225 nm or less, 200 nm or less, 175 nm or less, 150 nm or less, 125 nm or less, 100 nm or less, 95 nm or less, 90 nm or less, 85 nm or less, 80 nm or less, 75 nm or less, 70 nm or less, 65 nm or less, 60 nm or less, 55 nm or less, 50 nm or less, 45 nm or less, 40 nm or less, 35 nm or less, 30 nm or less, 25 nm or less, 20 nm or less, 19 nm or less, 18 nm or less, 17 nm or less, 16 nm or less, 15 nm or less, 14 nm or less, 13 nm or less, 12 nm or less, 11 nm or less, 10 nm or less, 9 nm or less, 8 nm or less, 7 nm or less, 6 nm or less, 5 nm or less, or 4 nm or less).

The average distance that each plasmonic particle within the plurality of plasmonic particles on the substrate is separated from its neighboring plasmonic particles can range from any of the minimum values described above to any of the maximum values described above. For example, each plasmonic particle within the plurality of plasmonic particles on the substrate is separated from its neighboring plasmonic particles by an average distance of from 3 nm to 1500 nm (e.g., from 3 nm to 750 nm, from 750 nm to 1500 nm, from 3 nm to 500 nm, from 500 nm to 1000 nm, from 1000 nm to 1500 nm, or from 5 nm to 1000 nm).

The density of the plurality of plasmonic particles on the plasmonic substrate can, for example, be 10^7 particles/cm^2 or more (e.g., 2.5×10^7 particles/cm^2 or more, 5×10^7 particles/cm^2 or more, 7.5×10^7 particles/cm^2 or more, 1×10^8 particles/cm^2 or more, 2.5×10^8 particles/cm^2 or more, 5×10^8 particles/cm^2 or more, 7.5×10^8 particles/cm^2 or more, 1×10^9 particles/cm^2 or more, 2.5×10^9 particles/cm^2 or more, 5×10^9 particles/cm^2 or more, 7.5×10^9 particles/cm^2 or more, 1×10^{10} particles/cm^2 or more, 2.5×10^{10} particles/cm^2 or more, 5×10^{10} particles/cm^2 or more, or 7.5×10^{10} particles/cm^2 or more). In some examples, the density of the plurality of plasmonic particles on the plasmonic substrate can be 10^{11} particles/cm^2 or less (e.g., 7.5×10^{10} particles/cm^2 or less, 5×10^{10} particles/cm^2 or less, 2.5×10^{10} particles/cm^2 or less, 1×10^{10} particles/cm^2 or less, 7.5×10^9 particles/cm^2 or less, 5×10^9 particles/cm^2 or less, 2.5×10^9 particles/cm^2 or less, 1×10^9 particles/cm^2 or less, 7.5×10^8 particles/cm^2 or less, 5×10^8 particles/cm^2 or less, 2.5×10^8 particles/cm^2 or less, 1×10^8 particles/cm^2 or less, 7.5×10^7 particles/cm^2 or less, 5×10^7 particles/cm^2 or less, or 2.5×10^7 particles/cm^2 or less). The density of the plasmonic particles on the plasmonic substrate can range from any of the minimum values described above to any of the maximum values described above. For example, the density of the plurality of plasmonic particles on the plasmonic substrate can be from 10^7 particles/cm^2 to 10^{11} particles/cm^2 (e.g., from 1×10^7 particles/cm^2 to 1×10^9 particles/cm^2, from 1×10^9 particles/cm^2 to 1×10^{11} particles/cm^2, from 1×10^7 particles/cm^2 to 1×10^8 particles/cm^2, from 1×10^8 particles/cm^2 to 1×10^9 particles/cm^2, from 1×10^9 particles/cm^2 to 1×10^{10}

19

particles/cm^2, from 1×10^{10} particles/cm^2 to 1×10^{11} particles/cm^2, or from 2.5×10^7 particles/cm^2 to 7.5×10^{10} particles/cm^2).

The size, shape, and/or composition of the plurality of plasmonic particles; the separation between each particle within the plurality of plasmonic particles; the density of the plasmonic

5   particles on the substrate; or combinations thereof can be selected in view of a variety of factors. In some examples, the size, shape, and/or composition of the plurality of plasmonic particles can be selected to maximize the electromagnetic field enhancement. For example, the size, shape, and/or composition of the plurality of plasmonic particles; the separation between each particle within the plurality of plasmonic particles; the density of the plasmonic particles on the

10   substrate; or combinations thereof can be selected such that the intensity of an incident electromagnetic field is enhanced by a factor of 5 or more by the plurality of plasmonic particles (e.g., 10 or more, 20 or more, 30 or more, 40 or more, 50 or more, 60 or more 70 or more, 80 or more, 90 or more, or 100 or more). In some examples, the size, shape, and/or composition of the plurality of plasmonic particles; the separation between each particle within the plurality of

15   plasmonic particles; the density of the plasmonic particles on the substrate; or combinations thereof can be selected such that the plasmon resonance energy of the plasmonic substrate overlaps with at least a portion of the electromagnetic radiation used to illuminate the plasmonic substrate.

The methods can further comprise, for example, making the plasmonic substrate by

20   depositing the plurality of plasmonic particles on a substrate. Depositing the plurality of plasmonic particles can comprise, for example, printing, lithographic deposition, electron beam deposition, thermal deposition, spin coating, drop-casting, zone casting, dip coating, blade coating, spraying, vacuum filtration, or combinations thereof.

The methods can further comprise, for example, making the plasmonic substrate by

25   thermally annealing a film of a plasmonic metal deposited on a substrate, thereby forming the plurality of plasmonic particles on the substrate. In some examples, the methods can further comprise depositing the film of the plasmonic metal on the substrate. The film of plasmonic metal can be deposited on the substrate, for example, by thin film processing techniques, such as sputtering, pulsed layer deposition, molecular beam epitaxy, evaporation, atomic layer

30   deposition, or combinations thereof. In some examples, the film of the plasmonic metal can have a thickness of 2 nm or more (e.g., 2.5 nm or more, 3 nm or more, 3.5 nm or more, 4 nm or more, 4.5 nm or more, 5 nm or more, 5.5 nm or more, 6 nm or more, 6.5 nm or more, 7 nm or more, 7.5 nm or more, 8 nm or more, 8.5 nm or more, 9 nm or more, or 9.5 nm or more). In some

examples, the film of the plasmonic metal can have a thickness of 10 nm or less (e.g., 9.5 nm or less, 9 nm or less, 8.5 nm or less, 8 nm or less, 7.5 nm or less, 7 nm or less, 6.5 nm or less, 6 nm or less, 5.5 nm or less, 5 nm or less, 4.5 nm or less, 4 nm or less, 3.5 nm or less, 3 nm or less, or 2.5 nm or less). The thickness of the film of the plasmonic metal can range from any of the minimum values described above to any of the maximum values described above. For example, the film of the plasmonic metal can have a thickness of from 2 nm to 10 nm (e.g., from 2 nm to 5 nm, from 5 nm to 10 nm, from 2 nm to 4 nm, from 4 nm to 6 nm, from 6 nm to 8 nm, from 8 nm to 10 nm, or from 3 nm to 9 nm).

Thermally annealing the film can, for example, comprise heating the film at a temperature of 400°C or more (e.g., 410°C or more, 420°C or more, 430°C or more, 440°C or more, 450°C or more, 460°C or more, 470°C or more, 480°C or more, 490°C or more, 500°C or more, 510°C or more, 520°C or more, 530°C or more, 540°C or more, 550°C or more, 560°C or more, 570°C or more, 580°C or more, or 590°C or more). In some examples, thermally annealing the film can comprise heating the film at a temperature of 600°C or less (e.g., 590°C or less, 580°C or less, 570°C or less, 560°C or less, 550°C or less, 540°C or less, 530°C or less, 520°C or less, 510°C or less, 500°C or less, 490°C or less, 480°C or less, 470°C or less, 460°C or less, 450°C or less, 440°C or less, 430°C or less, 420°C or less, or 410°C or less). The temperature at which the film is heated during thermal annealing can range from any of the minimum values described above to any of the maximum values described above. For example, thermally annealing the film can comprise heating the film at a temperature of from 400°C to 600°C (e.g., from 400°C to 500°C, from 500°C to 600°C, from 400°C to 450°C, from 450°C to 500°C, from 500°C to 550°C, from 550°C to 600°C, from 450°C to 550°C, or from 520°C to 580°C). In some examples, thermally annealing the film can comprise heating the film at a temperature of 550°C.

In some examples, the film can be thermally annealed for 1 hour or more (e.g., 1.5 hours or more, 2 hours or more, 2.5 hours or more, 3 hours or more, 3.5 hours or more, 4 hours or more, 4.5 hours or more, 5 hours or more, 5.5 hours or more, 6 hours or more, 6.5 hours or more, 7 hours or more, 7.5 hours or more, 8 hours or more, 8.5 hours or more, 9 hours or more, 9.5 hours or more, 10 hours or more, 10.5 hours or more, 11 hours or more, or 11.5 hours or more). In some examples, the film can be thermally annealed for 12 hours or less (e.g., 11.5 hours or less, 11 hours or less, 10.5 hours or less, 10 hours or less, 9.5 hours or less, 9 hours or less, 8.5 hours or less, 8 hours or less, 7.5 hours or less, 7 hours or less, 6.5 hours or less, 6 hours or less, 5.5 hours or less, 5 hours or less, 4.5 hours or less, 4 hours or less, 3.5 hours or less, 3 hours or

less, 2.5 hours or less, 2 hours or less, or 1.5 hours or less). The time for which the film can be thermally annealed can range from any of the minimum values described above to any of the maximum values described above. For example, the film can be thermally annealed for from 1 hour to 12 hours (e.g., from 1 hour to 6 hours, from 6 hours to 12 hours, from 1 hour to 4 hours,

5   from 4 hours to 8 hours, from 8 hours to 12 hours, from 1 hour to 10 hours, or from 1 hour to 3 hours). In some examples, the film can be thermally annealed for 2 hours.

The plasmonic substrate can be, for example, in thermal contact with a liquid sample comprising a plurality of metal particles and a surfactant, the liquid sample having a first temperature. The liquid sample can further comprise, for example, an aqueous solvent. The first

10   temperature can be, for example, 273 K or more (e.g., 275 K or more, 280 K or more, 285 K or more, 290 K or more, 295 K or more, 300 K or more, 305 K or more, 310 K or more, 315 K or more, 320 K or more, 325 K or more, 330 K or more, 335 K or more, or 340 K or more). In some examples, the first temperature can be 343 K or less (e.g., 340 K or less, 335 K or less, 330 K or less, 325 K or less, 320 K or less, 315 K or less, 310 K or less, 305 K or less, 300 K or less,

15   295 K or less, 290 K or less, 285 K or less, 280 K or less, or 275 K or less). The first temperature can range from any of the minimum values described above to any of the maximum values described above. For example, the first temperature can be from 273 K to 343 K (e.g., from 273 K to 305 K, from 305 K to 343 K, from 273 K to 285 K, from 285 K to 300 K, from 300 K to 315 K, from 315 K to 330 K, from 330 K to 434 K, or from 275 K to 340 K).

20   The surfactant can, for example, be a non-photoresponsive surfactant. In some examples, the surfactant can comprise a cationic surfactant or an anionic surfactant. Examples of cationic surfactants include, but are not limited to, cetrimonium bromide (CTAB), cetrimonium chloride (CTAC), benzalkonium chloride, benzethonium chloride, bronidox, distearyldimethylammonium chloride, tetramethylammonium hydroxide, and combinations thereof. Examples of anionic

25   surfactants include, but are not limited to, ammonium lauryl sulfate, ammonium perfluorononanoate, docusate, perfluorobutanesulfonic acid, perfluorononanoic acid, perfluorooctanesulfonic acid, perfluorooctanoic acid, phospholipid, potassium lauryl sulfate, sodium dodecyl sulfate (SDS), sodium dodecylbenzenesulfonate, sodium laurate, sodium laureth sulfate, sodium lauroyl sarcosinate, sodium myreth sulfate, sodium pareth sulfate, sodium

30   stearate, and combinations thereof. In some examples, the surfactant can comprise cetrimonium bromide (CTAB), cetrimonium chloride (CTAC), sodium dodecyl sulfate (SDS), or a combination thereof.

The concentration of the surfactant in the liquid sample is 1 mM or more (e.g., 5 mM or more, 10 mM or more, 15 mM or more, 20 mM or more, 25 mM or more, 30 mM or more, 35 mM or more, 40 mM or more, 45 mM or more, 50 mM or more, 55 mM or more, 60 mM or more, 65 mM or more, or 70 mM or more). In some examples, the concentration of the

5   surfactant in the liquid sample is 75 mM or less (e.g., 70 mM or less, 65 mM or less, 60 mM or less, 55 mM or less, 50 mM or less, 45 mM or less, 40 mM or less, 35 mM or less, 30 mM or less, 25 mM or less, 20 mM or less, 15 mM or less, 10 mM or less, or 5 mM or less). The concentration of the surfactant in the liquid sample can range from any of the minimum values described above to any of the maximum values described above. For example, the concentration

10   of the surfactant in the liquid sample can be from 1 mM to 75 mM (e.g., from 1 mM to 35 mM, from 35 mM to 75 mM, from 1 mM to 25 mM, from 25 mM to 50 mM, from 50 mM to 75 mM, or from 5 mM to 70 mM). In some examples, the concentration of the surfactant in the liquid sample is above the critical micelle concentration of the surfactant, such that the surfactant forms a plurality of surfactant micelles in the liquid sample.

15   The concentration of the plurality of metal particles in the liquid sample can be, for example, 10^{10} particle/mm^3 or more (e.g., 2×10^{10} particles/mm^3 or more, 3×10^{10} particles/mm^3 or more, 4×10^{10} particles/mm^3 or more, 5×10^{10} particles/mm^3 or more, 6×10^{10} particles/mm^3 or more, 7×10^{10} particles/mm^3 or more, 8×10^{10} particles/mm^3 or more, 9×10^{10} particles/mm^3 or more, 1×10^{11} particles/mm^3 or more, 2×10^{11} particles/mm^3 or more, 3×10^{11} particles/mm^3

20   or more, 4×10^{11} particles/mm^3 or more, 5×10^{11} particles/mm^3 or more, 6×10^{11} particles/mm^3 or more, 7×10^{11} particles/mm^3 or more, 8×10^{11} particles/mm^3 or more, or 9×10^{11} particles/mm^3 or more). In some examples, the concentration of the plurality of metal particles can be 10^{12} particles/mm^3 or less (e.g., 9×10^{11} particles/mm^3 or less, 8×10^{11} particles/mm^3 or less, 7×10^{11} particles/mm^3 or less, 6×10^{11} particles/mm^3 or less, 5×10^{11} particles/mm^3 or less,

25   4×10^{11} particles/mm^3 or less, 3×10^{11} particles/mm^3 or less, 2×10^{11} particles/mm^3 or less, 1×10^{11} particles/mm^3 or less, 9×10^{10} particles/mm^3 or less, 8×10^{10} particles/mm^3 or less, 7×10^{10} particles/mm^3 or less, 6×10^{10} particles/mm^3 or less, 5×10^{10} particles/mm^3 or less, 4×10^{10} particles/mm^3 or less, 3×10^{10} particles/mm^3 or less, or 2×10^{10} particles/mm^3 or less).

The concentration of the plurality of metal particles in the liquid sample can range from

30   any of the minimum values described above to any of the maximum values described above. For example, the concentration of the plurality of metal particles in the liquid sample can be from 10^{10} particle/mm^3 to 10^{12} particles/mm^3 (e.g., from 10^{10} particle/mm^3 to 10^{11} particles/mm^3, from 10^{11} particles/mm^3 to 10^{12} particles/mm^3, from 1×10^{10} particle/mm^3 to 5×10^{10} particles/mm^3,

from 5×10^{10} particles/mm^3 to 1×10^{11} particles/mm^3, from 1×10^{11} particles/mm^3 to 5×10^{11} particles/mm^3, from 5×10^{11} particles/mm^3 to 1×10^{12} particles/mm^3, or from 2×10^{10} particles/mm^3 to 9×10^{11} particles/mm^3).

The plurality of metal particles in the liquid sample can have, for example, an average particle size of 60 nm or more (e.g., 70 nm or more, 80 nm or more, 90 nm or more, 100 nm or more, 125 nm or more, 150 nm or more, 175 nm or more, 200 nm or more, 225 nm or more, 250 nm or more, 275 nm or more, 300 nm or more, 325 nm or more, 350 nm or more, 375 nm or more, 400 nm or more, 425 nm or more, 450 nm or more, 475 nm or more, 500 nm or more, 550 nm or more, 600 nm or more, 650 nm or more, 700 nm or more, 750 nm or more, 800 nm or more, 850 nm or more, 900 nm or more, or 950 nm or more).

In some examples, the plurality of metal particles in the liquid sample can have an average particle diameter of 1 µm or less (e.g., 950 nm or less, 900 nm or less, 850 nm or less, 800 nm or less, 750 nm or less, 700 nm or less, 650 nm or less, 600 nm or less, 550 nm or less, 500 nm or less, 475 nm or less, 450 nm or less, 425 nm or less, 400 nm or less, 375 nm or less, 350 nm or less, 325 nm or less, 300 nm or less, 275 nm or less, 250 nm or less, 225 nm or less, 200 nm or less, 175 nm or less, 150 nm or less, 125 nm or less, 100 nm or less, 90 nm or less, 80 nm or less, or 70 nm or less).

The average particle size of the plurality of metal particles in the liquid sample can range from any of the minimum values described above to any of the maximum values described above. For example the plurality of metal particles in the liquid sample can have an average particle size of from 60 nm to 1 µm (e.g., from 60 nm to 500 nm, from 500 nm to 1 µm, from 60 nm to 300 nm, from 300 nm to 550 nm, from 550 nm to 800 nm, from 800 nm to 1 µm, from 60 nm to 800 nm, from 60 nm to 600 nm, from 60 nm to 400 nm, from 60 nm to 200 nm, from 70 nm to 180 nm, from 80 nm to 170 nm, from 90 nm to 160 nm, or from 100 nm to 150 nm).

In some examples, the plurality of metal particles in the liquid sample can comprise a metal selected from the group consisting of Al, Ag, Au, and combinations thereof. In some examples, the plurality of metal particles can comprise a plurality of plasmonic particles.

The plurality of metal particles can, for example, further comprise a capping layer comprising a capping material such that the plurality of metal particles comprise a plurality of capped metal particles. Suitable capping materials for capping layers for metal particles are known in the art. "Capping" refers to the formation of an ionic or covalent bond of molecules to the surface atoms of a particle, this molecule is referred to as a capping agent. "Capping material" refers to a molecule possessing a functional group capable of binding to the surface

atoms of a particle by ionic or covalent bond. Such capping materials usually contain functional groups such as thiol (-SH), carboxyl (-COOH), or amine (-NH) groups. The capping materials can uniformly cover the surface of each of the plurality of metal particles, thereby forming the capping layer on the surface of each of the plurality of metal particles to form the plurality of

5   capped metal particles. The capping material can be used to stabilize the plurality of metal particles. The capping material can, for example, prevent the oxidation on the surface of the plurality of metal particles and/or to increase the dispersibility of the plurality of metal particles.

In some examples, the capping material can be attached to the surface of each of the plurality of metal particles, for example, by coordination bonds. The capping material can also

10   be associated with the plurality of metal particles via non-covalent interactions. In some examples, the capping material can individually be selected to be a hydrophilic, hydrophobic, or amphiphilic. In addition, the capping material can, in combination, be selected so as to provide a shell surrounding each of the plurality of metal particles which is hydrophilic, hydrophobic, or amphiphilic.

15   Examples of capping materials include, but are not limited to, citrate, tannic acid, lipoic acid, dodecane thiol, cetrimonium bromide (CTAB), cetrimonium chloride (CTAC), branched polyethylenimine (BPEI), polyethylene glycol (PEG), polyvinylpyrrolidone (PVP), sodium dodecyl sulfate (SDS), or combinations thereof. In some examples, the capping material is selected from the group consisting of cetrimonium bromide (CTAB), cetrimonium chloride

20   (CTAC), sodium dodecyl sulfate (SDS), and combinations thereof. In some examples, the capping materials and the surfactant are the same material.

The methods can further comprise, for example, generating a confinement region at a location in the liquid sample proximate to the first location of the plasmonic substrate, wherein at least a portion of the confinement region has a second temperature that is greater than the first

25   temperature such that the confinement region is bound by a temperature gradient. For example, the confinement region is located within at least a portion of the three-dimensional area within the liquid sample defined by the temperature gradient (e.g., the boundary of the confinement region can be defined by the temperature gradient). The confinement region can comprise a three dimensional area within the liquid sample where the balance of forces acting on the portion of

30   the plurality of metal particles substantially localizes the portion of the plurality of metal particles. In some examples, the method further comprises repulsing at least a portion of the surfactant from the confinement region such that the concentration of the surfactant within the confinement region is lower than the concentration of the surfactant outside the confinement

region. In some examples, the method further comprises repulsing at least a portion of the plurality of surfactant micelles from the confinement region such that the concentration of the plurality of surfactant micelles within the confinement region is lower than the concentration of the plurality of surfactant micelles outside the confinement region.

The second temperature can be, for example, of 273 K or more (e.g., 275 K or more, 280 K or more, 285 K or more, 290 K or more, 295 K or more, 300 K or more, 305 K or more, 310 K or more, 315 K or more, 320 K or more, 325 K or more, 330 K or more, 335 K or more, 340 K or more, 345 K or more, 350 K or more, 355 K or more, or 360 K or more). In some examples, the second temperature can be 363 K or less (e.g., 360 K or less, 355 K or less, 350 K or less, 345 K or less, 340 K or less, 335 K or less, 330 K or less, 325 K or less, 320 K or less, 315 K or less, 310 K or less, 305 K or less, 300 K or less, 295 K or less, 290 K or less, 285 K or less, 280 K or less, or 275 K or less). The second temperature can range from any of the minimum values described above to any of the maximum values described above. For example, the second temperature can be from 273 K to 363 K (e.g., from 273 K to 315 K, from 315 K to 363 K, from 273 K to 290 K, from 290 K to 310 K, from 310 K to 330 K, from 330 K to 350 K, from 350 K to 363 K, or from 275 to 360 K).

In some examples, the second temperature can be greater than the first temperature by 3 K or more (e.g., 3.5 K or more, 4 K or more, 4.5 K or more, 5 K or more, 5.5 K or more, 6 K or more, 6.5 K or more, 7 K or more, 7.5 K or more, 8 K or more, 8.5 K or more, 9 K or more, or 9.5 K or more). In some examples, the second temperature can be greater than the first temperature by 10 K or less (e.g., 9.5 K or less, 9 K or less, 8.5 K or less, 8 K or less, 7.5 K or less, 7 K or less, 6.5 K or less, 6 K or less, 5.5 K or less, 5 K or less, 4.5 K or less, 4 K or less, or 3.5 K or less). The amount that the second temperature is greater than the first temperature by can range from any of the minimum values described above to any of the maximum values described above. For example, the second temperature can be greater than the first temperature by from 3 K to 10 K (e.g., from 3 K to 6.5 K, from 6.5 K to 10 K, from 3 K to 5 K, from 5 K to 7 K, from 7 K to 10 K, or from 4 K to 9 K).

In some examples, the confinement region is generated by plasmon-enhanced photothermal effects. The confinement region can, for example, have a diameter of 500 nm or more (e.g., 550 nm or more, 600 nm or more, 650 nm or more, 700 nm or more, 750 nm or more, 800 nm or more, 850 nm or more, 900 nm or more, 950 nm or more, 1 μm or more, 2 μm or more, 3 μm or more, 4 μm or more, 5 μm or more, 6 μm or more, 7 μm or more, 8 μm or more, or 9 μm or more). In some examples, the confinement region can have a diameter of 10 μm or

26

less (e.g., 9 μm or less, 8 μm or less, 7 μm or less, 6 μm or less, 5 μm or less, 4 μm or less, 3 μm or less, 2 μm or less, 1 μm or less, 950 nm or less, 900 nm or less, 850 nm or less, 800 nm or less, 750 nm or less, 700 nm or less, 650 nm or less, 600 nm or less, or 550 nm or less). The diameter of the confinement region can range from any of the minimum values described above

5   to any of the maximum values described above. For example, the confinement region can have a diameter of from 500 nm to 10 μm (e.g., from 500 nm to 5 μm, from 5 μm to 10 μm, from 500 nm to 2 μm, from 2 μm to 4 μm, from 4 μm to 6 μm, from 6 μm to 8 μm, from 8 μm to 10 μm, or from 600 nm to 9 μm). The diameter of the confinement region can, for example, be controlled by the power density of the electromagnetic radiation used to illuminate the plasmonic substrate.

10   The diameter of the confinement region can be selected in view of a number of factors. In some examples, the diameter of the confinement region can be selected relative to the average particle size of the plurality of metal particles in the liquid sample.

        The methods can further comprise, for example, trapping at least a portion of the plurality of metal particles within the confinement region. The portion of the plurality of metal

15   particles trapped within the confinement region can be trapped, for example, by an electrostatic force, a thermophoretic force, van der Waals force, or combinations thereof. In some examples, the portion of the plurality of metal particles are not damaged during the trapping. In some examples, the portion of the plurality of metal particles trapped is one metal particle. In other words, also disclosed herein are methods for single-particle trapping.

20   The portion of the plurality of metal particles can be trapped, for example, at a trapping speed of 200 nm/s or more (e.g., 300 nm/s or more, 400 nm/s or more, 500 nm/s or more, 600 nm/s or more, 700 nm/s or more, 800 nm/s or more, 900 nm/s or more, 1 μm/s or more, 2 μm/s or more, 3 μm/s or more, 4 μm/s or more, 5 μm/s or more, 6 μm/s or more, 7 μm/s or more, 8 μm/s or more, 9 μm/s or more, 10 μm/s or more, 15 μm/s or more, 20 μm/s or more, 25 μm/s or

25   more, 30 μm/s or more, 35 μm/s or more, 40 μm/s or more, or 45 μm/s or more). In some examples, the portion of the plurality of metal particles can be trapped at a trapping speed of 50 μm/s or less (e.g., 45 μm/s or less, 40 μm/s or less, 35 μm/s or less, 30 μm/s or less, 25 μm/s or less, 20 μm/s or less, 15 μm/s or less, 10 μm/s or less, 9 μm/s or less, 8 μm/s or less, 7 μm/s or less, 6 μm/s or less, 5 μm/s or less, 4 μm/s or less, 3 μm/s or less, 2 μm/s or less, 1 μm/s or less,

30   900 nm/s or less, 800 nm/s or less, 700 nm/s or less, 600 nm/s or less, 500 nm/s or less, 400 nm/s or less, or 300 nm/s or less). The trapping speed at which the portion of the plurality of metal particles is trapped can range from any of the minimum values described above to any of the maximum values described above. For example, the portion of the plurality of metal particles

can be trapped at a trapping speed of from 200 nm/s to 50 μm/s (e.g., from 200 nm/s to 25 μm/s, from 25 μm/s to 50 μm/s, from 200 nm/s to 10 μm/s, from 10 μm/s to 20 μm/s, from 20 μm/s to 30 μm/s, from 30 μm/s to 40 μm/s, from 40 μm/s to 50 μm/s, or from 300 nm/s to 45 μm/s).

5   The methods can further comprise, for example, illuminating a second location of the plasmonic substrate thereby: generating a second confinement region at a location in the liquid sample proximate to the second location of the plasmonic substrate, wherein at least a portion of the second confinement region has a third temperature that is greater than the first temperature such that the second confinement region is bound by a temperature gradient; and translocating the trapped portion of the plurality of metal particles from the first confinement region to the

10   second confinement region, trapping at least a second portion of the plurality of metal particles within the second confinement region, or a combination thereof. As used herein, "a second location" and "the second location" are meant to include any number of locations in any arrangement on the plasmonic substrate. Thus, for example "a second location" includes one or more second locations. In some embodiments, the second location can comprise a plurality of

15   locations. In some embodiments, the second location can comprise a plurality of locations arranged in an ordered array. In some examples, the plasmonic substrate, the light source, the mirror, or a combination thereof can be translocated to illuminate the second location. As used herein translocating refers to any type of movement about any axis (e.g., rotation, translation, etc.) In other words, as used herein, translocation refers to a change in position and/or

20   orientation.

          In some examples, the plasmonic substrate comprises a portion of a substrate, the substrate further comprising a non-plasmonic portion and wherein the substrate is in thermal contact with the liquid sample. The non-plasmonic portion of the substrate can, for example, comprise a transparent non-plasmonic material. As used herein, a "transparent non-plasmonic

25   material" is meant to include any material that is not plasmonic and is transparent at the wavelength or wavelength region of interest. In some examples, the non-plasmonic portion of the substrate can comprise glass, quartz, silicon dioxide, a polymer, and combinations thereof.

          In certain examples, wherein the plasmonic substrate comprises a portion of a substrate, the substrate further comprising a non-plasmonic portion and wherein the substrate is in thermal

30   contact with the liquid sample, the methods can further comprise illuminating a location of the non-plasmonic portion of the substrate, thereby: generating a second confinement region at a location in the liquid sample proximate to the location of the non-plasmonic portion of the substrate, wherein at least a portion of the second confinement region has a third temperature

that is greater than the first temperature such that the second confinement region is bound by a temperature gradient; and translocating the trapped portion of the plurality of metal particles from the first confinement region to the second confinement region. In some examples, the substrate can be translocated to illuminate the location of the non-plasmonic portion of the

5   substrate. In some examples, wherein the electromagnetic radiation is provided by a light source, the light source can be translocated to illuminate the location of the non-plasmonic portion of the substrate. In some examples, wherein the electromagnetic radiation is provided by a light source, the light source being configured to illuminate a mirror and the mirror is configured to reflect the electromagnetic radiation from the artificial light source to illuminate the substrate, the mirror

10   can be translocated to illuminate the location of the non-plasmonic portion of the substrate.

Also disclosed herein are patterned sample made using the methods described herein. Also disclosed herein are methods of use of patterned sample made using the methods described herein, for example using the patterned samples for single-particle sensing, functional optical devices, or combinations thereof. In some examples, the patterned sample can be used for

15   surface-enhanced Raman spectroscopy (SERS).

Also disclosed herein are systems for performing the methods described herein. Referring now to Figure 1, the systems **100** can comprise a plasmonic substrate **102** in thermal contact with a liquid sample **104** comprising a plurality of metal particles **106** and a surfactant **107**; and a light source **108** configured to illuminate the plasmonic substrate **102** at a first

20   location **110**. In some examples, the system **100** can include a single light source **108**. In other examples, more than one light source **108** can be included in the system **100**.

In some examples, the systems **100** can further comprise a means for translocating the plasmonic substrate **102** and/or the light source **108**.

Referring now to Figure 2, the system **110** can, in some examples, further comprise a

25   mirror **111**, wherein the system **110** can be aligned such that the light source **108** is configured to illuminate the mirror **111** and the mirror **111** is configured to reflect the electromagnetic radiation from the light source **108** to illuminate the first location **110** of the plasmonic substrate **102**. In some examples, the systems **100** can further comprise a means for translocating the mirror **111**.

30   Referring now to Figure 3, the system **110** can, in some examples, further comprise an instrument **112** configured to capture an electromagnetic signal from the plasmonic substrate **102**.

In some examples, the system **110** can further comprise a first lens **114**. In some examples, the system **110** can further comprise a second lens **116**. The lenses may independently be any type of lens, such as a simple lens, a compound lens, a spherical lens, a toric lens, a biconvex lens, a plano-convex lens, a plano-concave lens, a negative meniscus lens, a positive

5   meniscus lens, a biconcave lens, a converging lens, a diverging lens, a cylindrical lens, a Fresnel lens, a lenticular lens, or a gradient index lens.

Referring now to Figure 4, in some examples, the system **110** can be configured such that the light source **108** is below the first lens **114** and the plasmonic substrate **102** is above the first lens **114**.

10   Referring now to Figure 5, in some examples, the system **110** is aligned such that the light source **108** is below the first lens **114**, the plasmonic substrate **102** is above the first lens **114**, the second lens **116** is above the plasmonic substrate **102**, and the instrument **112** is above the second lens **116**.

In some examples, the systems **110** can further comprise a computing device **118**

15   configured to receive and process electromagnetic signals from the instrument **112**, for example as shown in Figure 6.

Figure 7 illustrates an example computing device **118** upon which examples disclosed herein may be implemented. The computing device **118** can include a bus or other communication mechanism for communicating information among various components of the

20   computing device **118**. In its most basic configuration, computing device **118** typically includes at least one processing unit **120** (a processor) and system memory **122**. Depending on the exact configuration and type of computing device, system memory **122** may be volatile (such as random access memory (RAM)), non-volatile (such as read-only memory (ROM), flash memory, etc.), or some combination of the two. This most basic configuration is illustrated in

25   Figure 7 by a dashed line **124**. The processing unit **120** may be a standard programmable processor that performs arithmetic and logic operations necessary for operation of the computing device **118**.

The computing device **118** can have additional features/functionality. For example, computing device **118** may include additional storage such as removable storage **126** and non-

30   removable storage **128** including, but not limited to, magnetic or optical disks or tapes. The computing device **118** can also contain network connection(s) **134** that allow the device to communicate with other devices. The computing device **118** can also have input device(s) **132** such as a keyboard, mouse, touch screen, antenna or other systems configured to communicate

with the camera in the system described above, etc. Output device(s) **130** such as a display, speakers, printer, etc. may also be included. The additional devices can be connected to the bus in order to facilitate communication of data among the components of the computing device **118**.

The processing unit **120** can be configured to execute program code encoded in tangible,
5   computer-readable media. Computer-readable media refers to any media that is capable of providing data that causes the computing device **118** (*i.e.*, a machine) to operate in a particular fashion. Various computer-readable media can be utilized to provide instructions to the processing unit **120** for execution. Common forms of computer-readable media include, for example, magnetic media, optical media, physical media, memory chips or cartridges, a carrier
10   wave, or any other medium from which a computer can read. Example computer-readable media can include, but is not limited to, volatile media, non-volatile media and transmission media. Volatile and non-volatile media can be implemented in any method or technology for storage of information such as computer readable instructions, data structures, program modules or other data and common forms are discussed in detail below. Transmission media can include coaxial
15   cables, copper wires and/or fiber optic cables, as well as acoustic or light waves, such as those generated during radio-wave and infra-red data communication. Example tangible, computer-readable recording media include, but are not limited to, an integrated circuit (*e.g.*, field-programmable gate array or application-specific IC), a hard disk, an optical disk, a magneto-optical disk, a floppy disk, a magnetic tape, a holographic storage medium, a solid-state device,
20   RAM, ROM, electrically erasable program read-only memory (EEPROM), flash memory or other memory technology, CD-ROM, digital versatile disks (DVD) or other optical storage, magnetic cassettes, magnetic tape, magnetic disk storage or other magnetic storage devices.

In an example implementation, the processing unit **120** can execute program code stored in the system memory **122**. For example, the bus can carry data to the system memory **122**, from
25   which the processing unit **120** receives and executes instructions. The data received by the system memory **122** can optionally be stored on the removable storage **126** or the non-removable storage **128** before or after execution by the processing unit **120**.

The computing device **118** typically includes a variety of computer-readable media. Computer-readable media can be any available media that can be accessed by device **118** and
30   includes both volatile and non-volatile media, removable and non-removable media. Computer storage media include volatile and non-volatile, and removable and non-removable media implemented in any method or technology for storage of information such as computer readable instructions, data structures, program modules or other data. System memory **122**, removable

storage **126**, and non-removable storage **128** are all examples of computer storage media. Computer storage media include, but are not limited to, RAM, ROM, electrically erasable program read-only memory (EEPROM), flash memory or other memory technology, CD-ROM, digital versatile disks (DVD) or other optical storage, magnetic cassettes, magnetic tape,

5   magnetic disk storage or other magnetic storage devices, or any other medium which can be used to store the desired information and which can be accessed by computing device **118**. Any such computer storage media can be part of computing device **118**.

It should be understood that the various techniques described herein can be implemented in connection with hardware or software or, where appropriate, with a combination thereof.

10   Thus, the methods, systems, and associated signal processing of the presently disclosed subject matter, or certain aspects or portions thereof, can take the form of program code (*i.e.*, instructions) embodied in tangible media, such as floppy diskettes, CD-ROMs, hard drives, or any other machine-readable storage medium wherein, when the program code is loaded into and executed by a machine, such as a computing device, the machine becomes an apparatus for

15   practicing the presently disclosed subject matter. In the case of program code execution on programmable computers, the computing device generally includes a processor, a storage medium readable by the processor (including volatile and non-volatile memory and/or storage elements), at least one input device, and at least one output device. One or more programs can implement or utilize the processes described in connection with the presently disclosed subject

20   matter, *e.g.*, through the use of an application programming interface (API), reusable controls, or the like. Such programs can be implemented in a high level procedural or object-oriented programming language to communicate with a computer system. However, the program(s) can be implemented in assembly or machine language, if desired. In any case, the language can be a compiled or interpreted language and it may be combined with hardware implementations.

25   In certain examples, system memory **122** comprises computer-executable instructions stored thereon that, when executed by the processor **120**, cause the processor **120** to receive an electromagnetic signal from the instrument **112**, process the electromagnetic signal to obtain a characteristic of the plasmonic substrate **102**; and output the characteristic of the plasmonic substrate **102**.

30   The analysis of signals captured by the instrument can be carried out in whole or in part on one or more computing device. For example, the system may comprise one or more additional computing device.

The instrument can comprise, for example, a camera, an optical microscope, an electron microscope, a spectrometer, or combinations thereof. Examples of spectrometers include, but are not limited to, Raman spectrometers, UV-vis absorption spectrometers, IR absorption spectrometers, fluorescence spectrometers, and combinations thereof.

5   In some examples, the electromagnetic signal received by the processor from the instrument can comprise an image, a spectrum (e.g., Raman, UV-vis, IR, fluorescence), a micrograph, or combinations thereof. The characteristic of the plasmonic substrate can comprise, for example, the presence, location, size, shape, and/or quantity of a portion of the plurality of metal particles trapped within the confinement region; the presence, location,

10 composition, size, shape, and/or quantity of plasmonic particles comprising the plasmonic substrate; or combinations thereof. In some examples, the characteristic of the plasmonic substrate can be monitored over time, for example, to identify the effect of trapping the portion of the plurality of metal particles within the confinement region.

       A number of embodiments of the invention have been described. Nevertheless, it will be

15 understood that various modifications may be made without departing from the spirit and scope of the invention. Accordingly, other embodiments are within the scope of the following claims.

       The examples below are intended to further illustrate certain aspects of the systems and methods described herein, and are not intended to limit the scope of the claims.

EXAMPLES

20   The following examples are set forth below to illustrate the methods and results according to the disclosed subject matter. These examples are not intended to be inclusive of all aspects of the subject matter disclosed herein, but rather to illustrate representative methods and results. These examples are not intended to exclude equivalents and variations of the present invention which are apparent to one skilled in the art.

25   Efforts have been made to ensure accuracy with respect to numbers (e.g., amounts, temperature, etc.) but some errors and deviations should be accounted for. Unless indicated otherwise, parts are parts by weight, temperature is in °C or is at ambient temperature, and pressure is at or near atmospheric. There are numerous variations and combinations of measurement conditions, e.g., component concentrations, temperatures, pressures and other

30 measurement ranges and conditions that can be used to optimize the described process.

Example 1

Reversible assembly of plasmonic nanoparticles can be associated with significant modulation of structural, electrical and optical properties. Despite their versatility in nanoparticle manipulation and assembly, current optical tweezers require tightly focused and high-power laser beams (10-100 mW/μm^2) with precise optical alignment, which has significantly limited their applications.

Based on the temperature-gradient field in solution, thermophoresis has proven effective in low-energy and non-invasive trapping of particles (Braun M et al. *ACS Nano* **2013**, 7, 11200-11208; Braun M et al. *Phys. Chem. Chem. Phys.* **2014**, 16, 15207-15213; Ilic O et al. *ACS Photonics* **2016**, 3, 197-202) and biomolecules (e.g., DNA) (Thamdrup LH et al. *Nano Lett.* **2010**, 10, 826-832; Reichl M et al. *Phys. Rev. Lett.* **2014**, 112, 198101; Braun M et al. *Nano Lett.* **2015**, 15, 5499-5505).

Herein, a versatile optical technique that uses the plasmon-enhanced thermophoresis for the light-directed assembly of general plasmonic nanoparticles with dynamic control of assembly sizes and patterns at a low optical power (e.g., power intensity lower than 0.1 mW/μm^2) is discussed. By introducing a non-photoresponsive cationic surfactant, e.g., cetrimonium chloride (CTAC), into the plasmonic nanoparticle suspension, the surface-modified positively charged nanoparticles can be directed towards the laser spot at the interface between a plasmonic substrate and suspension. The experiments and simulations discussed herein reveal that the low-power assembly is enabled by the thermophoretic migration of nanoparticles due to the plasmon-enhanced photothermal effect and the associated local electric field over a plasmonic substrate. By employing a holographic optical system to control the laser beam, the parallel and dynamic manipulation of multiple nanoparticle assemblies was achieved. The assemblies formed over plasmonic substrates can further be transported to non-plasmonic substrates. The nanoparticle assemblies with dynamically controlled electromagnetic "hot spots" were also employed for surface-enhanced Raman spectroscopy (SERS) with controlled sensitivity, which can analyze molecules in their native liquid environments. Using Rhodamine 6G and methyl orange as model molecules, the effects of nanoparticle compositions and geometries on the SERS performances was investigated. By taking advantage of the parallel manipulation of multiple nanoparticle assemblies, "multiplex" SERS with enhanced sensitivity was demonstrated. With the advantages of low-power reversible nanoparticle assembly, applicability to general nanoparticles and simple optics, the plasmon-enhanced thermophoretic technique discussed herein is paving a new way

towards the further development and applications of dynamic nanoparticle assemblies, including biomolecular analysis in their native environments and smart drug delivery.

Figure 8 illustrates the basic concept of the light-directed reversible assembly of plasmonic nanoparticles based on the plasmon-enhanced thermophoresis. Herein, Au

5   nanotriangles (AuNTs) are used as an illustrative example. Other nanoparticles such as Au nanospheres (AuNSs) and Ag nanospheres (AgNSs) have also been used to demonstrate the generality of this technique.

Au nanotriangles in a CTAC solution (10 mM in DI water) were prepared with previously established synthetic protocols (Nedev S et al. *Nano Lett.* **2011**, 11, 5066-5070). The

10   Au nanotriangles feature a side length of ~150 nm (Figure 9) and plasmon resonance wavelength of 720 nm, which exhibit significantly enhanced electromagnetic fields at their tips (Scarabelli L et al. *ACS Nano* **2014**, 8, 5833-5842; Jin R et al. *Science* **2001**, 294, 1901-1903). Sixty microliters (60 µL) of the as-prepared Au nanotriangle solution was centrifuged for 10 min (4500 rpm) and the Au nanotriangles were re-dispersed in 20 µL CTAC solution (10 mM) with

15   sonication for 10 min. As displayed in the inset of Figure 8, the positive head group of CTAC is attached preferentially to the particle surface due to the electrostatic attraction (i.e., negative charge on the original Au surface). Above the critical micelle concentration (CMC, 0.13-0.16 mM) (Pignolet C et al. *J. Colloid Interface Sci.* **2010**, 349, 41-48), a second layer of CTA^+ is formed on the particle surface with the head group pointing outward due to hydrophobic

20   interaction between the tails of CTA^+ molecules, leading to a positive and hydrophilic surface of the nanoparticle that is surrounded by Cl^- ions.

Au nanospheres 100 nm in diameter in PBS (0.1 mM) were purchased from Sigma–Aldrich. Sixty microliters (60 µL) of the as-purchased Au nanosphere solution (0.0389 mg/mL) was centrifuged for 10 min (4500 rpm) and the Au nanospheres were re-dispersed in 20 µL

25   CTAC solutions with concentrations of 5, 10, 20, 50, 75, 100 and 150 mM, respectively.

Ag nanospheres 100 nm in diameter (0.02 mg/mL) with citrate-functionalized surfaces was purchased from nanoComposix. Two hundred microliters (200 µL) of the as-purchased Ag nanosphere solution was centrifuged for 10 min (4500 rpm) and the Ag nanospheres were re-dispersed in 20 µL CTAC solution (20 mM) with sonication for 10 min.

30   Figure 10 shows the normalized optical transmission spectra of three types of plasmonic nanoparticle suspensions used in this work: Au nanotriangles (AuNTs), Ag nanospheres (AgNSs) and Au nanospheres (AuNSs). The Au nanospheres, Au nanotriangles and Ag nanospheres show plasmon resonance peaks at 570 nm, 720 nm and 480 nm, respectively.

Optical transmission spectra of the plasmonic nanoparticle solutions were taken using an Ocean Optics spectrometer (HR4000CG-UV-NIR).

A plasmonic substrate consisting of Au nanoislands (AuNIs) was employed to induce plasmon-enhanced photothermal effect. The Au nanoisland plasmonic substrate was prepared by depositing a 4.5 nm Au thin film on a glass coverslip with thermal evaporation (Denton thermal evaporator) at a base pressure of 9×10^{-6} Torr. The Au thin film was annealed in air at 550°C for 2 h to obtain the Au nanoislands on the coverslip. Figure 11 shows a scanning electron microscopy (SEM) image of the Au nanoislands as a plasmonic substrate. The substrate features Au nanoislands with diameters of 20-40 nm and inter-particle distances of 5-10 nm. Figure 12 shows an optical transmission spectrum of the Au nanoislands with a transmission dip at ~580 nm, which arises from the plasmon resonances of the Au nanoparticles. The transmission spectrum was taken with the substrate covered by water. Optical transmission spectra of the plasmonic substrates were taken using an Ocean Optics spectrometer (HR4000CG-UV-NIR).

The induced plasmon-enhanced photothermal effect from the Au nanoisland plasmonic substrate allows for the use of low optical power to create an appropriate temperature-gradient field for the thermophoretic assembly of nanoparticles. To optically assemble plasmonic nanoparticles, a 532 nm diode-pumped solid-state (DPSS) laser (Coherent, Genesis MX STM-1 W) was expanded with a 5× beam expander and focused onto the plasmonic substrate through a 60× objective (Newport, NA 0.85). When the plasmonic substrate is illuminated with the low-power laser beam, the plasmonic heating of the Au nanoislands on the substrate increases temperature of the surrounding nanoparticle suspensions. The thermophoresis that arises from the temperature gradient enables the rapid formation of the Au nanotriangle assembly at the laser spot near the substrate-solution interface (Figure 13). The *in-situ* optical imaging was achieved through a customized upright Nikon microscope with 10× (NA: 0.30) and 100× (NA: 0.90) objectives. The successive optical images of the light-directed assembling process are shown in Figure 13, which reveals that a stable Au nanotriangle assembly formed at $t_4 = 10$ s. The assembly is reversible. The Au nanotriangles re-dispersed into the solution once the laser was turned off (Figure 14).

The assembly of the Au nanotriangles can be caused by the particle migration in the thermal-induced local electric field, i.e., thermoelectric effect (Reichl M et al. *Phys. Rev. Lett.* **2014**, 112, 198101; Würger A. *Phys. Rev. Lett.* **2008**, 101, 108302). As illustrated in Figure 15, a light-induced local temperature gradient can impose a non-uniform concentration of the CTA^+ molecules as per the following equation:

$$\nabla \ln c = -\alpha \nabla \ln T \qquad (1)$$

where c is the molecule concentration, α is the diffusion coefficient, and T is the local temperature. A positive α drives the CTA^+ molecules to accumulate in the regime with the lower temperature (i.e., the cold regime). The orientation of the local electric field is determined by the separation of the positive CTA^+ molecules and the negative Cl^- ions, which can be calculated by the relative Soret coefficient:

$$\delta S_T = S_T{}^+ - S_T{}^- \qquad (2)$$

where $S_T{}^+$ and $S_T{}^-$ denote the Soret coefficient of the positive molecules and the negative ions, respectively. Although a positive $S_T{}^-$ can also drive the Cl^- ions towards the cold regime, the small Soret coefficient of Cl^- ions (7.18×10^{-4} 1/K) gives a positive δS_T, which induces a local electric field E along the temperature gradient that points from cold to hot regime.

The electric force on a positive Au nanotriangle is described as $F = qE$, where q is the surface charge of the Au nanotriangle with a CTA^+ bilayer. The electric force F induced by the local electric field from the accumulation of the CTA^+ molecules in the cold regime drives the Au nanotriangles towards the hot regime (i.e., laser beam spot) to rapidly form the nanoparticle assembly. The speed of the formation of the nanoparticle assembly can be controlled by the incident optical power.

When the nanoparticles are in close contact in the assembly, the van der Waals attraction becomes strong enough to stabilize the assembly. However, the electrostatic repulsive force between the positive CTA^+ molecules on the nanoparticle surfaces has a negative effect on the assembly stability, which can lead to the disassembling process. Therefore, a balance among the thermal-induced electric force, van der Waals attraction, and electrostatic repulsive force enables the reversible assembly of the nanoparticles. When the laser is turned off, the temperature-gradient field disappears and the nanoparticles in the aggregate separate from each other due to the electrostatic repulsive force (Figure 16), leading to the re-dispersion of the nanoparticles and thus the disassembly of the aggregates.

To estimate the plasmon-enhanced photothermal effect and its role in the assembly of the plasmonic nanoparticles, the temperature-gradient profiles at the substrate-solution interfaces upon the illumination of a laser beam were simulated using computational fluid dynamic (CFD) simulations. Finite-element method-based numerical simulations (by COMSOL Multiphysics) were employed to analyze the temperature distribution around the laser beam focused at the substrate-water interface. For simplicity, a 2D axisymmetric model comprising of glass substrate, Au nanotriangle assembly and water was established. Since the physics involved is the

heat transfer in solids (glass substrate and Au nanotriangles assembly) and the fluid, the pre-defined model Conjugate Heat Transfer was used. A Gaussian-beam-form heat source was given at the substrate-fluid interface to model the heating from the laser beam. For cases with Au nanotriangles sandwiched between the substrate and the fluid layer, a highly conductive layer

5   was set to consider the heat transfer in the Au nanotriangle layer. Room temperature was set for other boundaries.

       The results of the computational fluid dynamic (CFD) simulations are displayed in Figure 17- Figure 19. When a 532 nm laser beam (power: 0.1 mW, diameter: 2 μm) is illuminated on the plasmonic substrate, a moderate temperature gradient of ~0.6 K/μm is

10   obtained on top of the substrate. The rapid migration of the Au nanotriangles to the hot regime at the interface between the substrate and solution leads to the growth of the assembly. The Au nanotriangles assembled on top of the plasmonic substrate absorb the light that would otherwise transmit through the substrate, which further increases the photothermal effect and temperature gradient. As displayed in Figure 18, when an Au nanotriangle assembly with a diameter of 2 μm

15   forms on top of the plasmonic substrate, the transmitted light through the substrate is completely absorbed by the Au nanotriangle assembly, which leads to a temperature gradient of ~0.7 K/μm.

       The optical power density used herein (~0.03 mW/μm^2) is at least 3 orders of magnitude lower than that used in optical tweezers for nanoparticle assembly (Tong L et al. *Lab Chip* **2009**, 9, 193-195; Messina E et al. *J. Phys. Chem. C* **2011**, 115, 5115-5122; Yoshikawa H et al. *Phys.*

20   *Rev. E* **2004**, 70, 061406).

       The formation of a stable Au nanotriangle assembly depends on the optical power. If the optical power is too low (e.g., < 0.03 mW/μm^2 for the examples herein), it cannot create a sufficiently strong local electric field to trap the nanoparticles as required for the assembling process. However, if the optical power is too high, it will induce strong thermal convection and

25   Brownian motion of the plasmonic nanoparticles, causing the instability of the particle assembly. For example, as shown in Figure 20, a stable Au nanotriangle assembly (t_1) was achieved by a 532 nm laser beam with an optical power of 0.2 mW and a diameter of 1 μm, but an increase of the optical power from 0.2 mW to 0.5 mW induced the stronger thermal convection, which disassembled the Au nanotriangle aggregate (t_2–t_4).

30   Further, it was found that, while the Au nanoislands-based plasmonic substrate is required to initialize the light-directed assembly of nanoparticles via the plasmon-enhanced photothermal effect, it is not essential to maintain and to dynamically manipulate the nanoparticle assemblies once formed. The nanoparticle assembly itself becomes a heating source

sufficient to maintain the force balance. As shown in Figure 19, the light absorption by an Au

nanotriangle assembly on a plain glass substrate can generate a temperature gradient of ~0.8

K/μm, which is even higher than that on the plasmonic substrate. Unlike the plasmonic substrate

where the incident light is partially reflected at the interface between Au nanoislands and glass

5   substrate, the plain glass substrate exhibits significantly reduced reflection loss. The self-

sustainability of the heating source lays the foundation for delivering a stable nanoparticle

assembly over a non-plasmonic substrate. As experimentally demonstrated in Figure 21, a stable

Au nanotriangle assembly with a diameter of 4 μm was generated over the plasmonic substrate at

t_1, and transported across the Au nanoisland/glass boundary at t_2 - t_4 and over the glass substrate

10   at t_5. The transport was achieved by translating the sample stage. The substrate-independent

optical manipulation of nanoparticle assemblies promises a myriad of new opportunities for

optofluidic applications.

The contribution of optical tweezing effect was excluded from the light-directed

assembly of nanoparticles discussed herein. Experiments revealed that the initial light-directed

15   assembly nanoparticles only occurred over the plasmonic substrate. Focusing the same laser

beam at the interface of glass substrate and nanoparticle suspensions could not initiate the

assembly of the nanoparticles, indicating that the optical force from the focused laser beam alone

cannot trap and assemble the nanoparticles in this case. In fact, the transmitted laser beam

through the non-plasmonic substrate exerts a scattering force on the nanoparticles, which pushes

20   the nanoparticles away from the substrate and thus prevents the trapping and assembly. One may

argue that the plasmon-enhanced optical force on the plasmonic substrate can improve the

trapping and assembling capability of nanoparticles. However, the Au nanoislands as plasmonic

substrate exhibit weak electromagnetic filed enhancement under the light illumination, which is

far away from the condition for the maximum optical gradient force that is strong enough for the

25   particle assembly (Lin L et al. *Nano Lett.* **2016**, 16, 701-708). As a further test, the same laser

beam was irradiated at the interface of Au nanoislands substrate and nanoparticle suspensions

without CTAC surfactant, and no assembly of the nanoparticles occurred due to the absence of

the thermoelectric effect.

Taking advantage of flexible light management via holographic optics, versatile

30   manipulation of multiple nanoparticle assemblies was also achieved. The optical setup for the

parallel and dynamic manipulation of multiple nanoparticle assemblies is displayed

schematically in Figure 22. To optically assemble multiple nanoparticle assemblies, a spatial

light modulator (SLM) (Boulder Nonlinear Systems, Model P512) and a 50× objective of long

working distance (Mitutoyo, NA: 0.55) were used. The spatial light modulator was applied to dynamically control the laser beam in an arbitrary manner. The desired optical patterns on the plasmonic substrate were obtained by focusing an expanded laser beam that is modulated by the spatial light modulator onto the substrate.

5   Through engineering the optical patterns on the plasmonic substrate, the simultaneous generation of 25 Au nanotriangle assemblies in a 5×5 square array was demonstrated (Figure 23). Another example was forming 17 Au nanotriangle assemblies in an "Au" pattern (Figure 24). Despite an optical power fluctuation of ~20% among the different laser beams generated by the spatial light modulator, multiple Au nanotriangle assemblies were generated with high

10   uniformity and stability. Furthermore, dynamic manipulation of the Au nanotriangle assemblies was demonstrated, as shown in Figure 25. In the demonstration, 13 Au nanotriangle assemblies were generated in a "UT" pattern at t_1, as shown in Figure 25. A series of transport processes of selected assemblies was implemented to transform the pattern, as shown from t_1 to t_6 in Figure 25.

15   Since the formation of nanoparticle assemblies relies on the photothermal effect from the plasmonic substrate and the CTAC surfactant, this technique is also applicable to general metallic nanoparticles. Along this line, the light-directed assembly of metallic nanoparticles of different compositions, sizes, and shapes was also demonstrated. This versatile manipulation of the nanoparticle assemblies can be harnessed as dynamic lithography to form arbitrary patterns

20   of dispersed nanoparticles at the solid-liquid interfaces. With their reversible characteristics, the lithographic patterns can be "erased" and "rewritten" repeatedly. The minimum size of a single nanoparticle assembly can reach ~1 μm with the current optical setup described herein. The light-directed dynamic manipulation of multiple nanoparticle assemblies also allowed for the development of a "multiplex" *in-situ* surface-enhanced Raman spectroscopy (SERS) platform, as

25   also discussed herein.

Exploiting the plasmon-enhanced electromagnetic field at plasmonic nanostructures, surface-enhanced Raman spectroscopy (SERS) is an analytical technique that can detect molecules with a sensitivity down to single-molecule level. A number of approaches have been implemented to enhance the localized electromagnetic field to improve the SERS sensitivity,

30   including tailoring the particle shape and inducing near-field coupling. In particular, the integration of optical tweezers with SERS (also known as SERS tweezers) paves the way towards analyzing biomolecules in their native environments and developing optofluidics-based lab on a chip (Tong L et al. *Lab Chip* **2009**, 9, 193-195; Messina E et al. *J. Phys. Chem. C* **2011**,

115, 5115-5122; Stetciura IY et al. *Analyst* **2015**, 140, 4981-4986; Svedberg F et al. *Nano Lett.* **2006**, 6, 2639-2641). However, the high optical power required for nanoparticle manipulation in optical tweezers can potentially damage the biomolecules (Fazio B et al. *Sci. Rep.* **2016**, 6, 26952), which limits the applications of the SERS tweezers.

5   With the low-power operation and reversible assembly of plasmonic nanoparticles, the plasmon-enhanced thermophoretic technique discussed herein has advantages for its use in SERS tweezers, as demonstrated in *in-situ* molecular sensing herein. Meanwhile, SERS measurements can also be applied to monitor the dynamics of the light-directed nanoparticle assembly. Considering the role of CTAC in the assembly of nanoparticles, the effects of CTAC

10   concentration on the performance of SERS based on the nanoparticle assemblies was investigated. For this study, Au nanosphere assemblies were used as the SERS substrates and rhodamine 6G as the targeted molecules.

        As-prepared rhodamine 6G solutions (2 mM) were diluted to a series of concentrations of 200 µM, 20 µM and 2 µM. As-prepared methyl orange solutions (10 mM) were diluted to a

15   series of concentrations of 1 mM, 100 µM and 10 µM. The different solutions of molecular analytes were mixed with plasmonic nanoparticle solutions of various concentrations in a 1:1 ratio. The mixtures were sonicated for 5 min. 10 µL mixed solutions were sandwiched between the Au nanoislands (as a plasmonic substrate) and a coverslip with a 120 µm spacer for SERS.

        A single laser beam was used for both the formation of nanoparticle assembly and the

20   Raman excitation. A typical Raman spectrum of rhodamine 6G recorded from a single Au nanosphere assembly (CTAC concentration: 10 mM) is shown in Figure 26. Raman spectra were recorded with an Andor Shamrock 303i spectrograph (grating: 1199 l/mm and slit width: 45 µm) and a Newton EMCCD integrated with an inverted Nikon microscope. For *in-situ* SERS on a single nanoparticle assembly, a 660 nm DPSS laser (Laser Quantum, OPS 1500-1.5 W) was

25   expanded with a 5× beam expander and focused onto the plasmonic substrate with a 40× objective (Nikon, NA 0.75) in the inverted microscope. The various vibration modes as indicated match those described elsewhere (Hildebrandt P et al. *J. Phys. Chem.* **1984**, 88, 5935-5944). To carry out the parametric study of SERS, two modes were chosen, i.e., C-C-C ring in-plane bending mode at 614 cm^{-1} and aromatic C-C stretching mode at 1510 cm^{-1}, for the detailed

30   analysis.

        As shown in Figure 27, Raman intensities at 614 cm^{-1} (C-C-C ring in-plane bending mode) and 1510 cm^{-1} (aromatic C-C stretching mode) (Hildebrandt P et al. *J. Phys. Chem.* **1984**, 88, 5935-5944) are highly sensitive to the CTAC concentrations. Specifically, both modes

experience an increase and then a decrease in the intensity when the CTAC concentration was increased from 2.5 to 75 mM. There is an optimal CTAC concentration of 10-25 mM for the highest Raman intensities, which arises from the opposite dependency of two factors on the concentration of CTAC molecules. On one hand, the increased concentration of CTAC

5   molecules leads to the stable nanoparticle assemblies with the stronger localized electromagnetic field and thus SERS signals. On the other hand, the increased concentration of CTAC reduces the interaction between the plasmonic nanoparticles and the targeted molecules, leading to the weaker Raman enhancement.

The near-field coupling between the plasmonic substrates and the plasmonic nanoparticle

10   assemblies were further exploited to improve the SERS performance. Figure 28 and Figure 29 summarize the assembly-size-dependent Raman intensities (of modes at 614 cm^{-1} and 1510 cm^{-1}) measured when the Au nanotriangle assemblies were over plasmonic substrate and glass substrate, respectively. In both cases, the Raman intensities increase with the assembly size, which can be attributed to the increased number of plasmonic "hot spots" and targeted molecules

15   in the larger assemblies. Significant improvement of SERS performance is observed for assemblies over the plasmonic substrate due to the assembly-substrate coupling. In addition, the SERS sensitivity of Au nanotriangle assemblies is almost an order of magnitude higher than that of Au nanosphere assemblies because the Au nanotriangles exhibit enhanced electromagnetic field at their tips. The Raman exposure time in Figure 27 is ten-fold longer than that in Figure 28

20   and Figure 29.

The technique was also extended to reversibly assemble Ag nanospheres and apply the Ag nanosphere assemblies for SERS of rhodamine 6G. Figure 30 shows the dependence of the Raman intensities for the two modes (i.e., 614 cm^{-1} and 1510 cm^{-1}) on the assembly size. The Ag nanospheres with a diameter of ~100 nm exhibit a plasmon resonance wavelength of 480 nm

25   (Figure 10), which is much shorter than the wavelength of the working laser beam (i.e., 660 nm). Compared with the Au nanotriangles, the Ag nanospheres exhibit smaller maximum assembly size because of the stronger Brownian motion of the smaller Ag nanospheres and the weaker photothermal effect at the Ag nanosphere assembly. Still, Ag nanosphere assemblies exhibit higher SERS sensitivity than Au nanotriangle assemblies, with an enhancement of one order of

30   magnitude. This observation is consistent with the previous studies that revealed better SERS performance from Ag nanoparticles (Kreibig U and Vollmer M. *Optical Properties of Metal Clusters*. Springer: Berlin, 1995).

To evaluate the ultimate sensitivity of SERS, the dependence of Raman signals on the concentration of rhodamine 6G with a single Ag nanosphere assembly as a SERS substrate was studied. As shown in Figure 31, a detection limit of ~1 μM for an acquisition time of 10 seconds was obtained. Two strategies were developed to further enhance the SERS sensitivity. One

5   strategy was to dry the nanoparticle assemblies. The hydrophobic interaction between the CTA^+ tails maintains the CTA^+ double layers, which exert the electrostatic repulsive force on the nanoparticles to maintain a certain inter-particle distance. The solvent removal would eliminate the hydrophobic interaction and damage the CTA^+ double layers, reducing the repulsive force. Therefore, it is expected that a dried nanoparticle assembly can become more compact with

10   smaller inter-particle distance due to the stronger van der Waals interaction and the weaker electrostatic repulsive force. The more compact assemblies can enhance the localized electromagnetic field or "hot spots" that amplify the Raman signals of the molecules. Figure 32 shows the time-evolved Raman spectra of rhodamine 6G recorded from a single Ag nanosphere assembly during the solvent evaporation. It can be seen from Figure 32 that the solvent

15   evaporation increases the SERS.

The other strategy was to use multiple nanoparticle assemblies for "multiplex" SERS. To demonstrate this concept, one, two and three nanoparticle assemblies were generated for the SERS of rhodamine 6G. For *in-situ* SERS on multiple nanoparticle assemblies, a spatial light modulator (SLM) (Hamamatsu, X13138-01) was added in the original optical path to create

20   multiple beams for the "multiplex" SERS. Figure 33 show the Raman spectra of rhodamine 6G from one Ag nanosphere assembly, two Ag nanosphere assemblies and three Ag nanosphere assemblies, respectively. A significant improvement of the SERS performance is observed when the assembly number is increased. The power variation of ~20% among individual beams generated by spatial light modulator could limit the uniformity of multiple assemblies.

25   The assembly-based SERS for detection of methyl orange with the concentration ranging from 5 μM to 500 μM was also demonstrated, as summarized in Figure 34 and Figure 35. For the Au nanotriangle assembly, Raman signals of methyl orange cannot be identified when the concentration is below 5 μM (Figure 34). Using the Ag nanosphere assembly as SERS substrate, Raman signals (with low signal-to-noise ratio) from methyl orange were identified when the

30   concentration is below 5 μM (Figure 35). The SERS sensitivity can be further improved by employing plasmonic nanoparticles with optimized sizes and shapes.

A method for the light-directed reversible assembly of general plasmonic nanoparticles using the plasmon-enhanced thermophoresis was discussed herein. The non-photoresponsive

CTAC surfactant forms a double layer to create a hydrophilic and positive nanoparticle surface. Such surface-functionalized nanoparticles can be driven to the hot regime on top of a plasmonic substrate under the plasmon-enhanced temperature-gradient field. The coordinated action from the thermophoretic force, electrostatic repulsive force, and van der Waals attraction enable the

5   reversible assembly of plasmonic nanoparticles independent of their compositions, sizes, and shapes. Using a holographic optical system, parallel manipulation of multiple particle assemblies was achieved. Compared with optical tweezers, this thermophoretic method features lower optical power and higher assembly efficiency with simpler optics. Furthermore, these plasmonic nanoparticle assemblies can be applied for "multiplex" SERS. With their low-power and parallel

10   operation, reversible nanoparticle assembly, and applicability to general nanoparticles, this technique can open up a new window of opportunities for trapping, manipulation, patterning and sensing of nanoparticles for various applications.

Example 2

15   Optical manipulation of plasmonic nanoparticles offers the possibility of dynamic control of light-matter interactions at the nanoscale, which is of interest for various applications in nanophotonics, materials science, and life sciences. Optical tweezers have been shown to trap metal nanoparticles at highly focused laser beams with strong light intensity, since they provide a sufficient optical gradient force (Lehmuskero A et al. *ACS Nano* **2015**, *9*, 3453-3469).

20   Although the use of optical tweezers succeeded in trapping Au and Ag nanoparticles with different sizes and shapes, the use of optical tweezer suffers from certain technical obstacles. First, upon excitation of localized surface plasmons (LSPs) of the metal nanoparticles by the trapping laser beam, enhanced light absorption and scattering result in optical heating of the particles and strong optical radiation forces, thereby significantly reducing the trapping stability

25   (Lehmuskero A et al. *ACS Nano* **2015**, *9*, 3453-3469; Ruijgrok PV et al. *Phys. Rev. Lett.* **2011**, *107*, 037401; Shao L et al. *ACS Nano* **2015**, *9*, 12542-12551). As a result, optical trapping is limited to near-infrared (NIR) lasers with wavelengths far away from the localized surface plasmon resonance of the metal nanoparticles (Selhuber-Unkel C et al. *Nano Lett.* **2008**, *8*, 2998-3003; Bosanac L et al. *Nano Lett.* **2008**, *8*, 1486-1491; Ruijgrok PV et al. *Phys. Rev. Lett.* **2011**,

30   *107*, 037401). Second, optical tweezers can only trap metal nanoparticles with sizes significantly smaller than the laser wavelength (i.e., in the Rayleigh regime) where the nanoparticle can be treated as a dipole. Optical trapping of larger particles with sizes comparable to or larger than the laser wavelength is challenging because the enhanced light-scattering cross section increases the

optical scattering force (Lehmuskero A et al. *ACS Nano* **2015**, *9*, 3453-3469; Min C et al. *Nat Commun* **2013**, *4*, 2891). Finally, high laser power is required to trap subwavelength metal nanoparticles, ranging from tens to hundreds of milliwatts. Such high optical powers can potentially damage the functional materials, surface molecules, and even the trapped metal
5   nanoparticles (Babynina A et al. *Nano Lett.* **2016**, *16*, 6485-6490).

By using plasmonic nanoantennas on substrates, plasmon-enhanced optical forces can be used for low-power optical trapping of dielectric nanoparticles (Tanaka Y et al. *Nano Lett.* **2013**, *13*, 2146-2150; Juan ML et al. *Nat. Phys.* **2009**, *5*, 915-919; Jensen RA et al. *ACS Photonics* **2016**, *3(3)*, 423-427). However, trapping metal nanoparticles in the vicinity of plasmonic
10   nanoantennas is still challenging due to strong near-field plasmon coupling between the trapped nanoparticles and the nanoantennas, such that the particle loses its intrinsic optical features in the trap (Zhang W et al. *Nano Lett.* **2010**, *10*, 1006-1011). Besides, plasmonic tweezers lack the ability to dynamically manipulate and transport the trapped particle (Zheng Y et al. *Nano Lett.* **2014**, *14*, 2971-2976; Ndukaife JC et al. *Nat. Nanotechnol.* **2016**, *11*, 53-59; Berthelot J et al.
15   *Nat. Nanotechnol.* **2014**, *9*, 295-299). Optical trapping of metal nanoparticles at their corresponding localized surface plasmons is expected to facilitate *in-situ* optical spectroscopy, leading to insights into plasmon coupling and its applications in sensing, imaging and optothermal therapy. By exploring the nanoparticle migration along a light-controlled thermoelectric field, an opto-thermoelectric nanotweezer (OTENT) method has been developed
20   that can capture and manipulate metal nanoparticles at single-particle resolution.

OTENT relies on the high optothermal conversion efficiency at the excitation of localized surface plasmons on a thermoplasmonic substrate (e.g., a porous Au film). The optothermal effect or Joule loss is often recognized as an intrinsic limitation for the use of metal plasmonic nanoparticles in nanophotonic devices (Govorov AO and Richardson HH. *Nano*
25   *Today* **2007**, *2*, 30-38; Baffou G and Quidant R. *Laser Photonics Rev.* **2013**, *7*, 171-187). Even though strategies have been developed to reduce losses (Kramer NJ et al. *Nano Lett.* **2015**, *15*, 5597-5603; Regmi R et al. *Nano Lett.* **2016**, *16*, 5143-5151; Boltasseva A and Atwater HA. *Science* **2011**, *331*, 290-291), the Joule loss can also be turned into advantage in applications such as optothermal therapy (Ayala-Orozco C et al. *ACS Nano* **2014**, *8*, 6372-6381; Cheng X et
30   al. *Adv. Mater.* **2017**, *29*, 1604894). The generated heat can also benefit optical trapping by creating a electrothermoplasmonic flow that can deliver nanoparticles to the trapping site (Ndukaife JC et al. *Nat. Nanotechnol.* **2016**, *11*, 53-59). However, it has been elusive to apply

the thermoelectric effect as a general mechanism for manipulation at the single-nanoparticle level.

The development and application of OTENT to achieve single-nanoparticle manipulation under in-situ monitoring by optical spectroscopy is described herein. Thermoplasmonic

5   substrates were prepared by depositing Au thin films on glass slides (Denton thermal evaporator, base pressure: 9×10^{-6} Torr), followed by thermal annealing at 550°C in air for 2 hours. Two different thicknesses of Au films were deposited, 4.5 nm and 6.5 nm, which were used for excitation with the 532 nm laser and 633 nm laser, respectively (Figure 36-Figure 38).

Using a laser beam matching the localized surface plasmon of the thermoplasmonic

10 substrate, a thermal hot spot is created at an optical power that is 2-3 orders of magnitude lower than that in optical tweezers, to trap and dynamically manipulate gold and silver nanoparticles of various sizes and shapes. Since the optical force arising from the light-nanoparticle coupling is weak at such a low optical power, both resonant and non-resonant laser wavelengths to the localized surface plasmons of metal nanoparticles can be used in the OTENT.

15   Colloidal particles or molecules can undergo thermophoretic migration under a thermoelectric field, which can arise from a temperature gradient field in a solvent with dissolved salts (Lin L et al. *ACS Nano* **2016**, *10*, 9659-9668; Piazza R and Parola A. *J. Phys.: Condens. Matter* **2008**, *20*, 153102; Würger A. *Phys. Rev. Lett.* **2008**, *101*, 108302; Würger A. *Rep. Prog. Phys.* **2010**, *73*, 126601; Reichl M et al. *Phys. Rev. Lett.* **2014**, *112*, 198101). The

20 resulting thermophoretic velocity is determined by the Soret coefficients of different ion species and the surface charge of the colloidal particles. For example, negatively charged particles migrate from a hot to a cold region in NaCl solution, but migrate from a cold to a hot region in NaOH solution (Würger A. *Rep. Prog. Phys.* **2010**, *73*, 126601). Although it has been demonstrated that optical confinement of single nanoparticles or macromolecules in the cold

25 regions can be achieved by means of a dynamic temperature field (Braun M and Cichos F. *ACS Nano* **2013**, *7*, 11200-11208; Braun M et al. *Nano Lett.* **2015**, *15*, 5499-5505), stable trapping and even tweezing has not been achieved. To enable OTENT, a cationic surfactant, cetyltrimethylammonium chloride (CTAC), was added to the nanoparticle colloid. The CTAC molecules adsorb on the particle surface and form a positively charged molecular double layer

30 (Figure 39). Simultaneously, CTAC molecules self-assemble into micelles when above its critical micelle concentration (cmc, 0.13-0.16 mM). With high charge density and nanoscale size, CTAC micelles act as macro cations (known as micellar ions, Figure 40), which, together with the Cl⁻ counter-ions (Figure 41) provide the thermoelectric field in OTENT.

Without optical heating, both the ions and the metal particles are randomly dispersed in the solution, without a preferred migration direction (Figure 42). To generate an optically controllable temperature gradient field, a laser beam was directed onto a thermoplasmonic substrate, i.e., a porous Au film which was fabricated by simply deposition of an Au layer

5   followed by thermal annealing. The porous Au film can be replaced by other opto-thermal responsive substrates, e.g., a continuous Au film or an indium tin oxide thin film. However, the porous Au film is chosen since it features high opto-thermal conversion efficiency due to the excitation of a high-density of "hot spots" and low thermal conductivity because of the spatially isolated nanoparticles on the substrate, which lead to a high temperature gradient with a low-

10   power light illumination and temperature increment.

The finite elements method (COMSOL Multiphysics) was used to simulate both the temperature gradient distribution and temperature distribution around the laser beam focused at the substrate-solution interface. A two-dimensional axisymmetric model comprised of a glass substrate, an Au thin film, and solvent was built. Both the pre-defined conjugate heat transfer

15   and Laminar flow models were used to include the heat transfer in solids and fluids. A Gaussian-distributed heating source was placed at the substrate-solution interface to model the optical heating from the laser beam. Room temperature was set at all other boundaries.

A cross-sectional view of the simulated temperature distribution (embedded in the scheme) at the substrate-solution interface is shown in Figure 43. Both the micellar ions and Cl⁻

20   ions undergo thermal diffusion, migrating from a hot to a cold region. The migration of ions under the temperature gradient is associated to the heat transfer between the ions and the surrounding environment, i.e. the heat will be absorbed from the reservoir at T, and given out at the temperature $T+\Delta T$, which provides the ability to maintain a temperature gradient during ionic transport (Eastman ED. *J. Am. Chem. Soc.* **1928**, *50*, 283-291). The quantity of heat absorbed

25   from the surroundings when one mole of ions is transferred is the ionic heat of transport Q^*, which creates a current along the temperature gradient (Würger A. *Rep. Prog. Phys.* **2010**, *73*, 126601):

$$J(Cl^-) = -D_{Cl^-}\left(\nabla n_{Cl^-} + n_{Cl^-}\frac{Q^*_{Cl^-}}{k_B T^2}\nabla T - n_{Cl^-}\frac{Z_{Cl^-}eE_0}{k_B T}\right) \qquad (3)$$

where D_{Cl^-} is the diffusion coefficient of Cl⁻ ions, n_{Cl^-} is the concentration of Cl⁻ ions, T is the

30   environmental temperature, Z_{Cl^-} is the charge number of the Cl⁻ ion, e is the elemental charge, E_0 is the electric field, ∇n_{Cl^-} is the concentration gradient of Cl⁻ ions, $Q^*_{Cl^-}$ is the heat of transport of Cl⁻ ions, k_B is the Boltzmann constant and ∇T is the temperature gradient . The Soret coefficient

of the Cl⁻ ions S_T (Cl⁻) is given as 7.18×10^{-4} K⁻¹. Meanwhile, the CTAC micelles are driven along the temperature gradient by thermoosmosis (Vigolo D et al. *Langmuir* **2010**, *26*, 7792-7801), which arises from the osmotic imbalance in the electric double layers, with the Soret coefficient (Bregulla AP et al. *Phys. Rev. Lett.* **2016**, *116*, 188303):

5
$$S_T(micelle) = \frac{\varepsilon \zeta_{mic}^2}{8\eta T D_{mic}} \tag{4}$$

where ε is the dielectric constant of the solvent, η is the viscosity of the solvent, D_{mic} is the diffusion coefficient of the CTAC micelles, and ζ_{mic} is the surface potential of CTAC micelles. At a steady state, the spatial redistribution of both CTAC micelles and Cl⁻ ions generates an electric field, which is given by (Reichl M et al. *Phys. Rev. Lett.* **2014**, *112*, 198101):

10
$$E_T = \frac{k_B T \nabla T}{e} \frac{\sum_i Z_i n_i S_{Ti}}{\sum_i Z_i^2 n_i} \tag{5}$$

where i indicates the ionic species, i.e. CTAC micellar ions or Cl⁻ ions. Since the CTAC micelle has a higher molecular mass and a larger Soret coefficient, i.e. S_T (micelle)> S_T (Cl⁻), an electric field E_T pointing towards the laser beam is obtained from spatial redistribution of both the CTAC micelles and the Cl⁻ ions (Lin L et al. *ACS Nano* **2016**, *10*, 9659-9668), which can trap the

15 positively charged metal nanoparticle at the laser spot, as shown in Figure 44. The corresponding in-plane and out-of-plane temperature gradient and trapping force $F_T = qE_T$ are schematically presented in Figure 45 and Figure 46, where q is the charge of the metal nanoparticles. This trapping electric field is balanced by the repulsive electric field E_r arising from the positive charge of the thermoplasmonic substrate. Different from optical tweezers, where the particle is

20 trapped with the optical gradient force from a highly focused laser beam, the trapping electric field in OTENT arises from optical heating, which can relax the rigorous optics requirements of optical tweezers. Based on this general concept, the trapping and dynamic manipulation of various types of metal nanoparticles, including Au nanospheres (AuNSs), Ag nanospheres (AgNSs), Au nanotriangles (AuNTs), Au nanorods (AuNRs) and Ag nanowires (AgNWs), with

25 *in-situ* optical spectroscopy at single-particle resolution is demonstrated herein.

The 200 nm Au nanospheres, 100 nm Au nanospheres (in PBS, 0.1 mM) and Au nanorods with nominal absorption peak at 700 nm were purchased from Sigma–Aldrich. The 100 nm Ag nanospheres with citrate-functionalized surfaces were purchased from nanoComposix. The nanoparticle suspension was centrifuged for 5 min (4500 rpm) and re-

30 dispersed in CTAC solutions with the desired concentration. Au nanotriangles in 10 mM CTAC solution were prepared using previously reported synthesis protocols (Scarabelli L et al. *ACS Nano* **2014**, *8*, 5833-5842). Silver nanowires were synthesized using the polyol method,

according to a procedure reported elsewhere (Coskun S et al. *Cryst. Growth Des.* **2011**, *11*, 4963-4969). At the end of the synthesis, silver nanowires were purified through multiple centrifugation steps in acetone and ethanol. Following purification, the final product was dispersed in ethanol for storage. The Ag nanowire suspensions were diluted with CTAC solution to the targeted concentration for trapping experiments.

Sharing the same concept, other ionic surfactants such as cetyltrimethylammonium bromide (CTAB) and sodium dodecyl sulfate (SDS) also work for OTENT. SDS has a negative charge and thus reverses both the trapping electric field and the sign of surface charge of the metal nanoparticles to enable the opto-thermoelectric trapping. However, a similar trapping effect cannot be achieved using non-ionic surfactants such as Triton X-100, which further verifies the working mechanism of OTENT.

First, the use of OTENT for trapping and manipulating single Au nanospheres and Ag nanospheres is demonstrated. Due to their strong light scattering at the localized surface plasmon resonance wavelengths, Au nanospheres and Ag nanospheres were tracked with *in-situ* dark-field optical imaging.

The optical set up for OTENTS included a 532 nm diode-pumped solid-state laser was expanded with a 5× beam expander and projected onto a digital micromirror device (DMD). The optical images were reflected by the DMD and focused onto the thermoplasmonic substrate for optical heating. The size of the beam was reduced by 200 times after being relayed by a 1000 mm doublet lens, a 200 mm doublet lens, an infinity-corrected tube lens and a 40× objective (Nikon, NA 0.75) in a Nikon inverted microscope.

Figure 47 shows the trapping process of a single 100 nm Ag nanosphere using a low-power 532 nm laser beam. Different from the plasmon-enhanced optical force on plasmonic nanoantennas, which is limited by the delay length of localized surface plasmons, the temperature gradient field has a much larger working range (Figure 45 and Figure 46). Thus, OTENT can effectively deliver the metal nanoparticles to the trapping center within a surrounding region of 5-10 µm in radius. OTENT can also overcome another limitation of plasmonic tweezers, namely the lack of dynamic manipulation of the trapped nanoparticles (Zheng Y et al. *Nano Lett.* **2014**, *14*, 2971-2976; Ndukaife JC et al. *Nat. Nanotechnol.* **2016**, *11*, 53-59). The substrate used herein in the OTENT is optically continuous and the optically generated temperature gradient field is uniform, which allows the trapped particle to be dynamically transported at will by directing the laser beam. As shown in Figure 48, a trapped Ag nanosphere was delivered over a distance of ~110 µm in 9 s. The trapped particle was released as

soon as the heating laser was turned off and the temperature gradient field disappeared (Figure 49).

The trapping efficiency was evaluated by measuring escape velocities of the trapped nanoparticles. To measure the escape velocity of trapped particles, a single 532 nm laser beam

5   with a diameter of 2 μm was created on the thermoplasmonic substrate to capture a single metal nanoparticle. A motorized sample stage with a given moving velocity was used to introduce a Stokes drag force from the fluid on the trapped particle. The escape velocity was defined as the critical velocity when the trapping force of the particle was balanced by the drag force.

Figure 50 summarizes the measured escape velocities of different metal nanoparticles

10   (200 nm Au nanospheres, 100 nm Au nanospheres and 100 nm Ag nanospheres) at different optical power (see Figure 51 for the escape velocity measurement of a single 200 nm Au nanosphere in SDS solution). The faster escape velocities indicate stronger trapping capabilities. The escape velocities were found to increase almost linearly with the optical power for all particles, because of the increased temperature gradient. Surprisingly, the escape velocities of the

15   100 nm Au nanospheres were consistently faster than those for the 200 nm Au nanospheres, in contrast to what has been observed in optical tweezers. To trap a smaller metal nanoparticle using optical tweezers, one needs to increase the optical power to obtain the sufficiently large optical gradient force. To explain the faster escape velocities of the smaller nanoparticles using OTENT, the in-plane temperature gradients were simulated at the planes that are 50 nm and 100

20   nm above the thermoplasmonic substrate (also see Figure 52 for the out-of-plane temperature gradients), which are around the spherical centers for 100 nm Au nanospheres and 200 nm Au nanospheres, respectively. An increased temperature gradient is observed at the plane that is 50 nm above the substrate, providing an enhanced thermoelectric field and in turn a larger trapping force. Therefore, compared with optical tweezers, OTENT is more efficient in trapping small

25   nanoparticles at low optical power. OTENT was also applied to trap 400 nm Au nanospheres. There is expected to be no upper limit for the size for metal nanoparticles that can be trapped using OTENT. This is because, despite its increase as a function of particle size, the optical scattering force that prevents trapping is limited at such a low optical power.

In the case of 100 nm Ag nanospheres, the escape velocities were much faster than those

30   for 100 nm Au nanospheres (Figure 50). This velocity difference can be attributed to the different optical gradient forces experienced by the two types of nanospheres. Specifically, upon excitation by the 532 nm laser beam, the 100 nm Au nanospheres and 100 nm Ag nanospheres exhibit different signs of polarizability and optical gradient force. The optical gradient force is

attractive for 100 nm Ag nanospheres with higher-frequency localized surface plasmons, thereby enhancing the trapping stability. In contrast, 100 nm Au nanospheres with lower-frequency localized surface plasmons experience a repulsive optical gradient force, leading to reduced trapping stability (Huang L and Martin OJF. *Opt. Lett.* **2008**, *33*, 3001-3003; Arias-González JR

5   and Nieto-Vesperinas M. *J. Opt. Soc. Am. A* **2003**, *20*, 1201-1209). Despite of not being dominant at such a low optical power in OTENT, the optical gradient force can still significantly change the trapping stability depending on the polarizability of the nanospheres, as shown in Figure 50.

The trapping stability of different nanoparticles as a function of CTAC concentration was

10   also investigated. According to the migration velocity of the particle under the electric field $v = -\frac{\varepsilon\zeta}{\eta}E_T$, the Helmholtz-Smoluchowski electrophoretic mobility $\frac{\varepsilon\zeta}{\eta}$ is linearly dependent on the zeta potential of the particle ζ. An increase of CTAC concentration leads to a higher zeta potential ζ and in turn to a higher trapping stability. Simultaneously, an increase of CTAC concentration also reduces the Soret coefficient of the micelles and thus the electric field

15   intensity, according to equation 5. In addition, the increase of CTAC concentration will also increase the viscosity of the CTAC solution and thus the Stokes drag force that tries to release the trapped particle. Due to the tradeoff between the CTAC-dependent trapping force and the drag force, a maximum escape velocity was obtained at ~1 mM CTAC for both 100 nm Au nanospheres and 200 nm Au nanospheres (Figure 53). However, for the 100 nm Ag nanospheres,

20   the escape velocity increased initially, then decreased and increased again when the CTAC concentration was continuously increased. The increased escape velocity above 2 mM CTAC can be attributes to the reduced particle-substrate gap that can lead to an enhanced hydrodynamic boundary effect (Würger A. *Phys. Rev. Lett.* **2016**, *116*, 138302). Both the plasmon-enhanced optical gradient force and reduced particle-substrate electrostatic interaction can significantly

25   reduce the gap between the trapped Ag nanosphere and the thermoplasmonic substrate, with the trapping efficiency increasing logarithmically as the Ag nanosphere approaches the substrate. For Au nanospheres, the plasmon-enhanced optical repulsive force arising from the coupling between the Au nanospheres and the incident laser reduces the trapping force from the incident laser, and the balance between the trapping force and the electrostatic repulsive force is achieved

30   at a larger particle-substrate gap, as compared with that observed in the trapping of Ag nanospheres. Thus, the hydrodynamic boundary effect is much weaker in the trapping of Au nanospheres.

To carry out *in-situ* optical spectroscopy of the trapped metal nanoparticles, a high-performance spectrometer was incorporated into the OTENT, as shown in Figure 54. For *in-situ* spectroscopy, the DMD was removed from the optics and a 100× oil objective (Nikon, NA 0.5-1.3) was used to focus the laser beam and to record the scattering signal. An oil condenser (NA 1.43-1.20) was used to focus the incident white light onto the sample from the top. The single-particle scattering spectra of both Ag nanospheres and Au nanospheres were taken when the particles were trapped by a 660 nm laser (without DMD), with a 650 nm shortpass filter inserted between the objective and the spectrometer to block the laser beam. The scattering signal from the trapped metal nanoparticles was directed to a two-dimensional detector in a spectrometer (Andor). Either the 500 nm grating or 860 nm grating was used for detection, depending on the spectral location of the trapped particles. Reference spectra were recorded when the trapped particles were released from the laser spots and the laser was on. The reference spectra were subtracted to get the scattering signal of the trapped particles. The spectra were finally normalized with the light source spectra.

Dark-field optical scattering images and spectra were thus recorded from single metal nanoparticles. In Figure 55, single Ag nanospheres were selectively trapped according to the scattered color from the particles and recorded their scattering spectra (Prikulis J et al. *Nano Lett.* **2004**, *4*, 115-118). By matching the experimental spectra with the simulated spectra, the sizes of the Ag nanospheres were verified.

The scattering spectra of plasmonic nanoparticles were simulated using FDTD methods (Lumerical FDTD). A refractive index of 1.33 was set for the water environment. A mesh size of 1 nm was applied to define the metal nanoparticles. The electric field distribution was recorded by excitation at the resonant wavelength of the localized surface plasmons.

The color of Ag nanospheres changes from violet to blue when the diameter increases from 80 nm to 100 nm, with an improved polarizability and reduced electric field enhancement factor. From the *in-situ* scattering imaging and spectroscopy of single Au nanospheres, it can be seen that the color changes from green to yellow when the diameter of the Au nanospheres increases from 80 nm to 100 nm (Figure 56), with the localized surface plasmon peak wavelength red-shifting from 556 nm to 578 nm. Optical trapping of metal nanoparticles has certain requirements on the laser wavelength. For example, it would be challenging to trap Au nanospheres with a 532 nm laser using optical tweezers, due to the enhanced repulsive optical force by excitation of the localized surface plasmon. However, with OTENT trapping can be achieved using lasers with working wavelengths either close to or far away from the resonance

wavelength of the metal nanoparticle. A 660 nm red laser was used to trap the particles for recording the full spectra in Figure 55 and Figure 56. The 532 nm laser can also be used to trap Ag nanospheres (Figure 57) and Au nanospheres (Figure 58), which have localized surface plasmons close to the laser wavelength.

5   The versatility of OTENT was explored by trapping nanoparticles with different morphologies. Shown in Figure 59 is the trapping of single anisotropic Au nanotriangles with side length of 140 nm, which display a scattering peak at 721 nm, with a red color observed by a camera. Even though smaller 60 nm Au nanotriangles, with a blue-shifted localized surface plasmon peak wavelength at 646 nm, were also expected to show a red color, the reduced

10   particle size was found to significantly decrease the polarizability and the scattering intensity. As a result, the trapped 60 nm Au nanotriangle shows a yellow color, which arises from a mixture of the red light scattered by the Au nanotriangle and the fluorescence and scattering light from the thermoplasmonic substrate (Figure 60). As a further demonstration of the capability of OTENT to trap small metal nanoparticles, stable trapping of single small Au nanorods was achieved

15   without increasing the incident optical power (Figure 61). The fluorescence light from the thermoplasmonic substrate dominated over the weak scattered light from the single Au nanorod, due to its small size. As a result, an overall green color was observed from the trapped Au nanorod (Figure 62 and Figure 63). To further verify that single metal nanoparticles were trapped, the particles were printed on the substrates by increasing the optical power after the

20   particles were trapped at the laser spot, which significantly increases the trapping force to lock the particles on the substrate. The samples were then imaged using scanning electron microscopy (SEM), after the samples were rinsed and dried (Figure 64-Figure 66).

       The arbitrary light manipulation by means of a digital micromirror device (DMD) allows multiple metal nanoparticles to be trapped and manipulated in parallel using OTENT. For the

25   imaging of parallel trapping of both Ag nanospheres and Au nanotriangles, an air condenser (NA 0.95-0.8) was used to focus the white light in the OTENT optical setup. As shown in Figure 67, six laser beams were created with the DMD to capture six 100 nm Ag nanospheres, with one nanosphere in each beam. The successive dark-field optical images show the six Ag nanospheres trapped into a circle pattern. As another example, six laser beams were created and arranged into

30   a triangular pattern, where each beam trapped a single 150 nm Au nanotriangle (Figure 68). Such a parallel nanoparticle manipulation represents an opportunity for dynamic lithography at single-particle resolution.

In-situ monitoring of the trapping dynamics was demonstrated by recording the time-dependent scattering intensity at a specific wavelength. A CTAC concentration of 1 mM was selected to avoid near-field coupling between the trapped particles, and the background from the thermoplasmonic substrate was removed. Once a single 100 Au nanosphere was captured by the

5   thermoelectric field, the scattering intensity at 580 nm increased immediately (Figure 69). The scattering intensity fell back to zero once the particle was released. Without significant near-field coupling between the trapped particles, the number of trapped particles can be estimated according to the photon counts. As shown in Figure 70, the photon counts increase linearly with the number of Au nanospheres in the trap, which also verifies that no obvious near-field

10   plasmonic coupling occurs to the trapped multiple Au nanospheres in the 1 mM CTAC solution.

One-dimensional (1D) metal nanostructures with high aspect ratio (e.g. metal nanowires) can confine surface plasmons on the metal surfaces with longitudinal propagation, which are also known as surface plasmon resonators (Ditlbacher H et al. *Phys. Rev. Lett.* **2005**, *95*, 257403). The multiple longitudinal plasmon resonances dramatically increase the absorption and

15   scattering of light, which amplify the optical scattering force and make optical trapping extremely challenging (Yan Z et al. *ACS Nano* **2013**, *7*, 8794-8800; Yan Z et al. *ACS Nano* **2012**, *6*, 8144-8155; Tong L et al. *Nano Lett.* **2010**, *10*, 268-273). With its low-power operation and versatility of light management, OTENT can trap metal nanowires with precise location and orientation control. As shown in Figure 71, a 1D optical image was created on the

20   thermoplasmonic substrate to trap a single Ag nanowire. Different from optical tweezers, which rely on highly focused laser beams, the generated thermoelectric field can be well controlled by rational design of the optical images projected on the substrate. The thermoelectric field exerts a trapping force on the Ag nanowire that tends to align it with the optical image. The alignment allows for further control of the nanowire orientation by rotating the optical image, as shown in

25   Figure 72. The scattering optical images of the trapped Ag nanowire excited with differently polarized light were also recorded. A linear visible polarizer (Thorlabs) was inserted between the white light source and the condenser to control the incident light polarization for the dark-field imaging of Ag nanowires. When the polarization was tuned along the Ag nanowire, the multiple longitudinal surface plasmons were excited (right panel in Figure 73), with a bright scattering

30   optical image observed. When the polarization was perpendicular to the Ag nanowire, only the transverse mode (λ=420 nm) can be excited, with the scattering intensity greatly suppressed (Figure 74).

Optical heating arising from light absorption and photon-to-phonon conversion is considered as an intrinsic loss in metal nanomaterials, which limits some applications based on plasmonics. In plasmon-enhanced optical trapping, various strategies have been developed to suppress optothermal effects and in turn reduce thermal convection and thermophoresis for improved trapping efficiency. Herein, these optothermal effects are taken advantage of, by developing a low-power optical tweezing technique, termed opto-thermoelectric nanotweezers (OTENT). This technique can be used to trap and manipulate diverse metal nanoparticles by optically heating a thermoplasmonic substrate. A light-directed thermoelectric field can be generated due to spatial separation of dissolved ions within the heating laser spot, which allows metal nanoparticles of a wide range of materials, sizes, and shapes to be confined with single-particle resolution. Dynamic manipulation of the trapped nanoparticles can be accomplished by steering the laser beam or engineering the beam profile. In combination with dark-field optical imaging, nanoparticles can be selectively trapped and their spectroscopic response can be resolved *in-situ*. Besides their conventional role in surface modification of metal nanoparticles, ionic surfactants were further exploited to act as micellar ions that create light-controlled thermoelectric fields. As a general tweezing technique, OTENT is applicable to a wide range of metal, semiconductor, polymer and dielectric nanostructures, using various ionic surfactants such as CTAB and SDS. With its simple and flexible optics, simple fabrication of the substrate, low-power and non-invasive operation, diverse options in the trapping wavelength, and generality in the size, shape, and composition of the trapped nanoparticles, OTENT can become a powerful tool in colloid science, life sciences and nanotechnology.

Other advantages which are obvious and which are inherent to the invention will be evident to one skilled in the art. It will be understood that certain features and sub-combinations are of utility and may be employed without reference to other features and sub-combinations. This is contemplated by and is within the scope of the claims. Since many possible embodiments may be made of the invention without departing from the scope thereof, it is to be understood that all matter herein set forth or shown in the accompanying drawings is to be interpreted as illustrative and not in a limiting sense.

The methods of the appended claims are not limited in scope by the specific methods described herein, which are intended as illustrations of a few aspects of the claims and any methods that are functionally equivalent are intended to fall within the scope of the claims. Various modifications of the methods in addition to those shown and described herein are

intended to fall within the scope of the appended claims. Further, while only certain representative method steps disclosed herein are specifically described, other combinations of the method steps also are intended to fall within the scope of the appended claims, even if not specifically recited. Thus, a combination of steps, elements, components, or constituents may be explicitly mentioned herein or less, however, other combinations of steps, elements, components, and constituents are included, even though not explicitly stated.

CLAIMS

What is claimed is:

1.   A method comprising:

illuminating a first location of a plasmonic substrate with electromagnetic

radiation at a power density of 0.1 mW/μm² or less;

wherein the electromagnetic radiation comprises a wavelength that

overlaps with at least a portion of the plasmon resonance

energy of the plasmonic substrate; and

wherein the plasmonic substrate is in thermal contact with a liquid

sample comprising a plurality of metal particles and a

surfactant, the liquid sample having a first temperature;

thereby:

generating a confinement region at a location in the liquid sample

proximate to the first location of the plasmonic substrate,

wherein at least a portion of the confinement region has a

second temperature that is greater than the first temperature

such that the confinement region is bound by a temperature

gradient; and

trapping at least a portion of the plurality of metal particles within the

confinement region.

2.   The method of claim 1, wherein the power density of the electromagnetic radiation is
0.05 mW/μm² or less.

3.   The method of claim 1 or 2, wherein the electromagnetic radiation is provided by a light
source and the light source is an artificial light source, preferably a laser.

4.   The method of claim 3, wherein the light source is configured to illuminate a mirror and
the mirror is configured to reflect the electromagnetic radiation from the light source to
illuminate the first location of the plasmonic substrate.

5.   The method of claim 4, wherein the mirror comprises a plurality of mirrors, preferably a
digital micromirror device.

6.   The method of any one of claims 1-5, wherein the plasmonic substrate comprises a
plurality of plasmonic particles.

7.   The method of claim 6, wherein the plurality of plasmonic particles comprise a plurality
        of metal particles.

8.   The method of claim 7, wherein the plurality of metal particles comprise a metal selected
        from the group consisting of Au, Ag, Al, and combinations thereof.

9.   The method of any one of claims 6-8, wherein the plurality of plasmonic particles have
        an average particle size of from 10 nm to 500 nm.

10.   The method of any one of claims 6-9, wherein the plurality of plasmonic particles are
        substantially spherical in shape.

11.   The method of any one of claims 6-10, wherein each plasmonic particle within the
        plurality of plasmonic particles on the substrate is separated from its neighboring
        plasmonic particles by an average distance of from 3 nm to 1500 nm.

12.   The method of any one of claims 6-11, wherein the density of the plurality of plasmonic
        particles on the plasmonic substrate is 10^{11} particles/cm^2 or less.

13.   The method of any one of claims 6-12, further comprising making the plasmonic
        substrate by depositing the plurality of plasmonic particles on a substrate.

14.   The method of claim 13, wherein depositing the plurality of plasmonic particles
        comprises printing, lithographic deposition, electron beam deposition, thermal
        deposition, spin coating, drop-casting, zone casting, dip coating, blade coating, spraying,
        vacuum filtration, or combinations thereof.

15.   The method of any one of claims 6-12, further comprising making the plasmonic
        substrate by thermally annealing a film of a plasmonic metal deposited on a substrate,
        thereby forming the plurality of plasmonic particles on the substrate.

16.   The method of claim 15, further comprising depositing the film of the plasmonic metal
        on the substrate.

17.   The method of claim 15 or claim 16, wherein the film of the plasmonic metal has a
        thickness of from 2 nm to 10 nm.

18.   The method of any one of claims 15-17, wherein thermally annealing the film comprises
        heating the film at a temperature of from 400°C to 600°C, preferably at a temperature of
        550°C.

19.   The method of any one of claims 15-18, wherein the film is thermally annealed for from 1 hour to 12 hours, preferably for 2 hours.

20.   The method of any one of claims 1-19, wherein the concentration of the plurality of metal particles in the liquid sample is from 10^{10} particle/mm^3 to 10^{12} particles/mm^3.

21.   The method of any one of claims 1-20, wherein the plurality of metal particles have an average particle size of from 60 nm to 1 μm.

22.   The method of any one of claims 1-21, wherein plurality of metal particles comprise a metal selected from the group consisting of Al, Ag, Au, and combinations thereof.

23.   The method of any one of claims 1-22, wherein the plurality of metal particles comprise a plurality of plasmonic particles.

24.   The method of any one of claims 1-23, wherein the plurality of metal particles comprises a plurality of capped metal particles.

25.   The method of claim 24, wherein the plurality of capped metal particles comprise a plurality of metal particles capped with a capping material, the capping material comprising cetrimonium bromide (CTAB), cetrimonium chloride (CTAC), sodium dodecyl sulfate (SDS), or combinations thereof.

26.   The method of claim 25, wherein capping material and the surfactant are the same material.

27.   The method of any one of claims 1-26, wherein the portion of the plurality of metal particles are not damaged during the trapping.

28.   The method of any one of claims 1-27, wherein the surfactant comprises a cationic surfactant or an anionic surfactant.

29.   The method of any one of claims 1-28, wherein the surfactant is selected from the group consisting of cetrimonium bromide (CTAB), cetrimonium chloride (CTAC), sodium dodecyl sulfate (SDS), and combinations thereof.

30.   The method of any one of claims 1-29, wherein the concentration of the surfactant in the liquid sample is from 1 mM to 75 mM.

31.   The method of any one of claims 1-30, wherein the concentration of the surfactant in the liquid sample is above the critical micelle concentration of the surfactant, such that the

59

surfactant forms a plurality of surfactant micelles in the liquid sample.

32.   The method of any one of claims 1-31, wherein the method further comprises repulsing at least a portion of the surfactant from the confinement region.

33.   The method of any one of claims 1-32, wherein the liquid sample further comprises an aqueous solvent.

34.   The method of any one of claims 1-33, wherein the confinement region has a diameter of from 500 nm to 10 μm.

35.   The method of any one of claims 1-34, wherein the portion of the plurality of metal particles trapped is one metal particle.

36.   The method of any one of claims 1-35, wherein the first temperature is from 273 K to 343 K.

37.   The method of any one of claims 1-36, wherein the second temperature is from 276 K to 363 K.

38.   The method of any one of claims 1-37, wherein the second temperature is greater than the first temperature by from 3 K to 10 K.

39.   The method of any one of claims 1-38, wherein the confinement region is generated by plasmon-enhanced photothermal effects.

40.   The method of any one of claims 1-39, wherein the portion of the plurality of metal particles are trapped by an electrostatic force, a thermophoretic force, van der Waals force, or combinations thereof.

41.   The method of any one of claims 1-40, further comprising illuminating a second location of the plasmonic substrate thereby:

          generating a second confinement region at a location in the liquid sample proximate to the second location of the plasmonic substrate, wherein at least a portion of the second confinement region has a third temperature that is greater than the first temperature such that the second confinement region is bound by a temperature gradient; and

          translocating the trapped portion of the plurality of metal particles from the first confinement region to the second confinement region, trapping at least a

second portion of the plurality of metal particles within the second confinement region, or a combination thereof.

42. The method of claim 41, wherein the plasmonic substrate is translocated to illuminate the second location.

43. The method of claim 41 or claim 42, wherein the electromagnetic radiation is provided by a light source, and the light source is translocated to illuminate the second location.

44. The method of any one of claims 41-43, wherein the electromagnetic radiation is provided by a light source, the light source being configured to illuminate a mirror and the mirror is configured to reflect the electromagnetic radiation from the artificial light source to illuminate the plasmonic substrate, and the mirror is translocated to illuminate the second location.

45. The method of any one of claims 1-44, wherein the plasmonic substrate comprises a portion of a substrate, the substrate further comprising a non-plasmonic portion and wherein the substrate is in thermal contact with the liquid sample, wherein the method further comprises illuminating a location of the non-plasmonic portion of the substrate, thereby:

generating a second confinement region at a location in the liquid sample proximate to the location of the non-plasmonic portion of the substrate, wherein at least a portion of the second confinement region has a third temperature that is greater than the first temperature such that the second confinement region is bound by a temperature gradient; and

translocating the trapped portion of the plurality of metal particles from the first confinement region to the second confinement region.

46. The method of claim 45, wherein the substrate is translocated to illuminate the location of the non-plasmonic portion of the substrate.

47. The method of claim 45 or claim 46, wherein the electromagnetic radiation is provided by a light source, and the light source is translocated to illuminate the location of the non-plasmonic portion of the substrate.

48. The method of any one of claims 45-47, wherein the electromagnetic radiation is provided by a light source, the light source being configured to illuminate a mirror and the mirror is configured to reflect the electromagnetic radiation from the artificial light

source to illuminate the substrate, and the mirror is translocated to illuminate the location of the non-plasmonic portion of the substrate.

49.   The method of any one of claims 45-48, wherein the non-plasmonic portion of the substrate comprises glass, quartz, silicon dioxide, a polymer, and combinations thereof.

50.   A patterned sample made using the methods of any one of claims 1-49.

51.   A method of use of the patterned sample of claim 50, wherein the patterned sample is used for single-particle sensing, functional optical devices, or combinations thereof.

52.   A method of use of the patterned sample of claim 50, wherein the patterned sample is used for surface-enhanced Raman spectroscopy (SERS).

53.   A system comprising:

a plasmonic substrate in thermal contact with a liquid sample comprising a plurality of metal particles and a surfactant, the liquid sample having a first temperature; and

a light source configured to illuminate the plasmonic substrate at a first location with electromagnetic radiation at a power density of 0.1 mW/μm^2 or less and at a wavelength that overlaps with at least a portion of the plasmon resonance energy of the plasmonic substrate;

thereby:

generating a confinement region at a location in the liquid sample proximate to the first location of the plasmonic substrate, wherein at least a portion of the confinement region has a second temperature that is greater than the first temperature such that the confinement region is bound by a temperature gradient; and

trapping at least a portion of the plurality of metal particles within the confinement region.

54.   The system of claim 53, further comprising an instrument configured to capture an electromagnetic signal from the plasmonic substrate.

55.   The system of claim 54, further comprising a first lens.

56.   The system of claim 55, wherein the system is configured such that the light source is

below the first lens and the plasmonic substrate is above the first lens.

57.   The system of claim 55 or claim 56, further comprising a second lens.

58.   The system of claim 57, wherein the system is aligned such that the light source is below the first lens, the plasmonic substrate is above the first lens, the second lens is above the plasmonic substrate, and the instrument is above the second lens.

59.   The system of any one of claims claim 54-58, further comprising a mirror.

60.   The system of claim 59, wherein the system is aligned such that the light source is configured to illuminate the mirror and the mirror is configured to reflect the electromagnetic radiation from the light source to illuminate the first location of the plasmonic substrate.

61.   The system of claim 59 or claim 60, wherein the mirror comprises a plurality of mirrors, preferably a digital micromirror device.

62.   The system of any one of claims 59-61, further comprising a means for translocating the mirror.

63.   The system of any one of claims 54-62, further comprising a computing device comprising a processor and a memory operably coupled to the processor, the memory having further computer-executable instructions stored thereon that, when executed by the processor, cause the processor to:

        receive an electromagnetic signal from the instrument

        process the electromagnetic signal to obtain a characteristic of the plasmonic
            substrate; and

        output the characteristic of the plasmonic substrate.

64.   The system of any one of claims 54-63, wherein the instrument comprises a camera, an optical microscope, an electron microscope, a spectrometer, or combinations thereof.

65.   The system of claim 64, wherein the spectrometer comprises a Raman spectrometer, a UV-vis absorption spectrometer, an IR absorption spectrometer, a fluorescence spectrometer, or combinations thereof.

66.   The system of any one of claims 53-65, wherein the light source comprises an artificial light source, preferably a laser.

67.   The system of any one of claims 53-66, wherein the plasmonic substrate comprises a portion of a substrate, the substrate further comprising a non-plasmonic portion and wherein the substrate is in thermal contact with the liquid sample.

68.   The system of any one of claims 53-67, further comprising a means for translocating the plasmonic substrate, the substrate, the light source, or a combination thereof.

69.   The system of any one of claims 53-68, wherein the power density of the electromagnetic radiation is 0.05 mW/μm^2 or less.

70.   The system of any one of claims 53-69, wherein the plasmonic substrate comprises a plurality of plasmonic particles.

71.   The system of claim 70, wherein the plurality of plasmonic particles comprise a plurality of metal particles.

72.   The system of claim 71, wherein the plurality of metal particles comprise a metal selected from the group consisting of Au, Ag, Al, and combinations thereof.

73.   The system of any one of claims 70-72, wherein the plurality of plasmonic particles have an average particle size of from 10 nm to 500 nm.

74.   The system of any one of claims 70-73, wherein the plurality of plasmonic particles are substantially spherical in shape.

75.   The system of any one of claims 70-74, wherein each plasmonic particle within the plurality of plasmonic particles on the substrate is separated from its neighboring plasmonic particles by an average distance of from 3 nm to 1500 nm.

76.   The system of any one of claims 70-75, wherein the density of the plurality of plasmonic particles on the plasmonic substrate is 10^{11} particles/cm^2 or less.

77.   The system of any one of claims 53-76, wherein the concentration of the plurality of metal particles in the liquid sample is from 10^{10} particle/mm^3 to 10^{12} particles/mm^3.

78.   The system of any one of claims 53-77, wherein the plurality of metal particles have an average particle size of from 60 nm to 1 μm.

79.   The system of any one of claims 53-78, wherein plurality of metal particles comprise a metal selected from the group consisting of Al, Ag, Au, and combinations thereof.

80. The system of any one of claims 53-79, wherein the plurality of metal particles comprise a plurality of plasmonic particles.

81. The system of any one of claims 53-80, wherein the plurality of metal particles comprise a plurality of capped metal particles.

82. The system of claim 81, wherein the plurality of capped metal particles comprise a plurality of metal particles capped with a capping material, the capping material comprising cetrimonium bromide (CTAB), cetrimonium chloride (CTAC), sodium dodecyl sulfate (SDS), or combinations thereof.

83. The system of claim 82, wherein the capping materials and the surfactant are the same material.

84. The system of any one of claims 53-83, wherein the portion of the plurality of metal particles are not damaged during the trapping.

85. The system of any one of claims 53-84, wherein the surfactant comprises a cationic surfactant or an anionic surfactant.

86. The system of any one of claims 53-85, wherein the surfactant is selected from the group consisting of cetrimonium bromide (CTAB), cetrimonium chloride (CTAC), benzalkonium chloride, sodium dodecyl sulfate (SDS), and combinations thereof.

87. The system of any one of claims 53-86, wherein the concentration of the surfactant in the liquid sample is from 1 mM to 75 mM.

88. The system of any one of claims 53-87, wherein the concentration of the surfactant in the liquid sample is above the critical micelle concentration of the surfactant, such that the surfactant forms a plurality of surfactant micelles in the liquid sample.

89. The system of any one of claims 53-88, wherein the liquid sample further comprises an aqueous solvent.

90. The system of any one of claims 53-89, wherein the confinement region has a diameter of from 500 nm to 10 μm.

91. The system of any one of claims 53-90, wherein the portion of the plurality of metal particles trapped is one metal particle.

92. The system of any one of claims 53-91, wherein the first temperature is from 273 K to

343 K.

93.   The system of any one of claims 53-92, wherein the second temperature is from 276 K to
       363 K.

94.   The system of any one of claims 53-93, wherein the second temperature is greater than
       the first temperature by from 3 K to 10 K.

95.   The system of any one of claims 53-94, wherein the confinement region is generated by
       plasmon-enhanced photothermal effects.

96.   The system of any one of claims 53-95, wherein the portion of the plurality of metal
       particles are trapped by an electrostatic force, a thermophoretic force, can der Waals
       force, or combinations thereof.

1/40
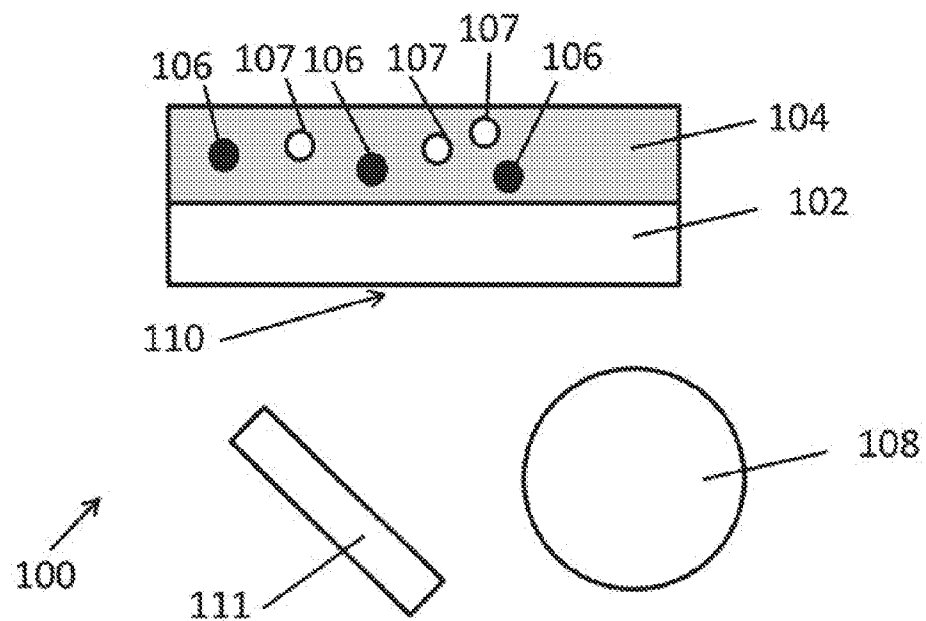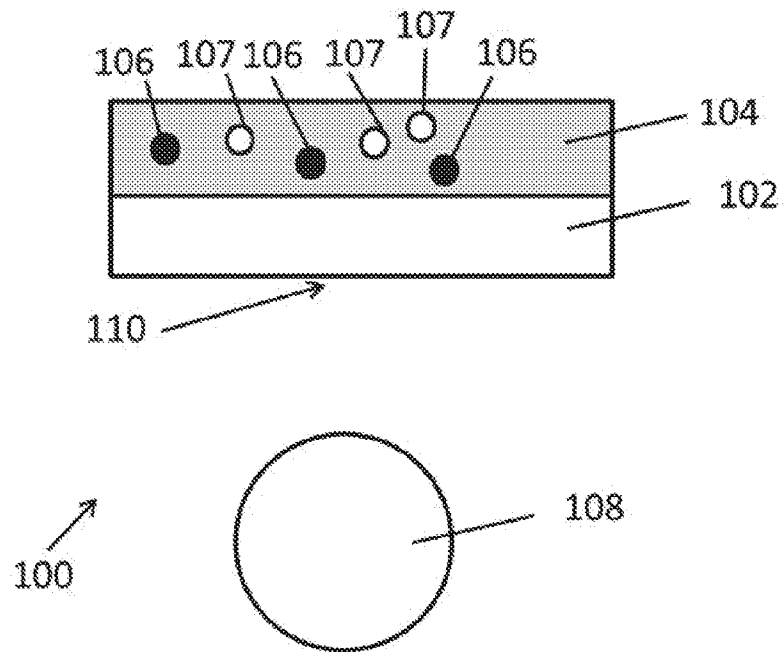
FIG. 1

FIG. 2

2/40
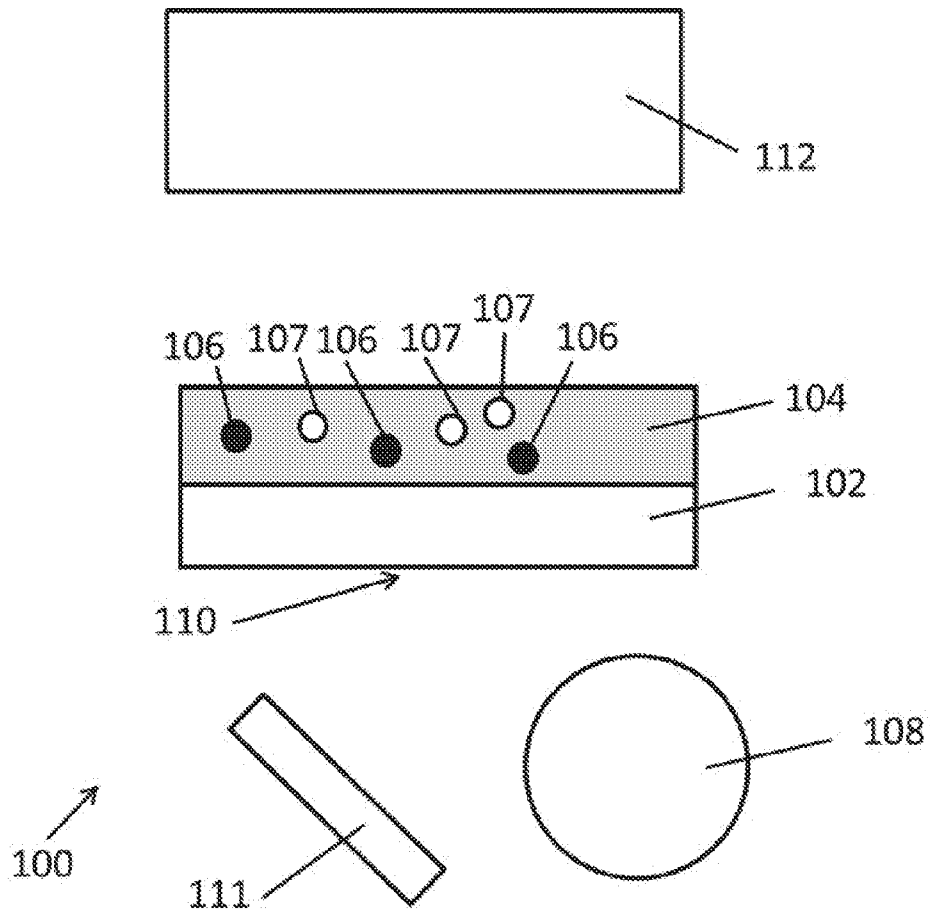
FIG. 3

3/40

FIG. 4

4/40

FIG. 5

5/40

106 107 106 107 107 106
104
102

110

111   108

100
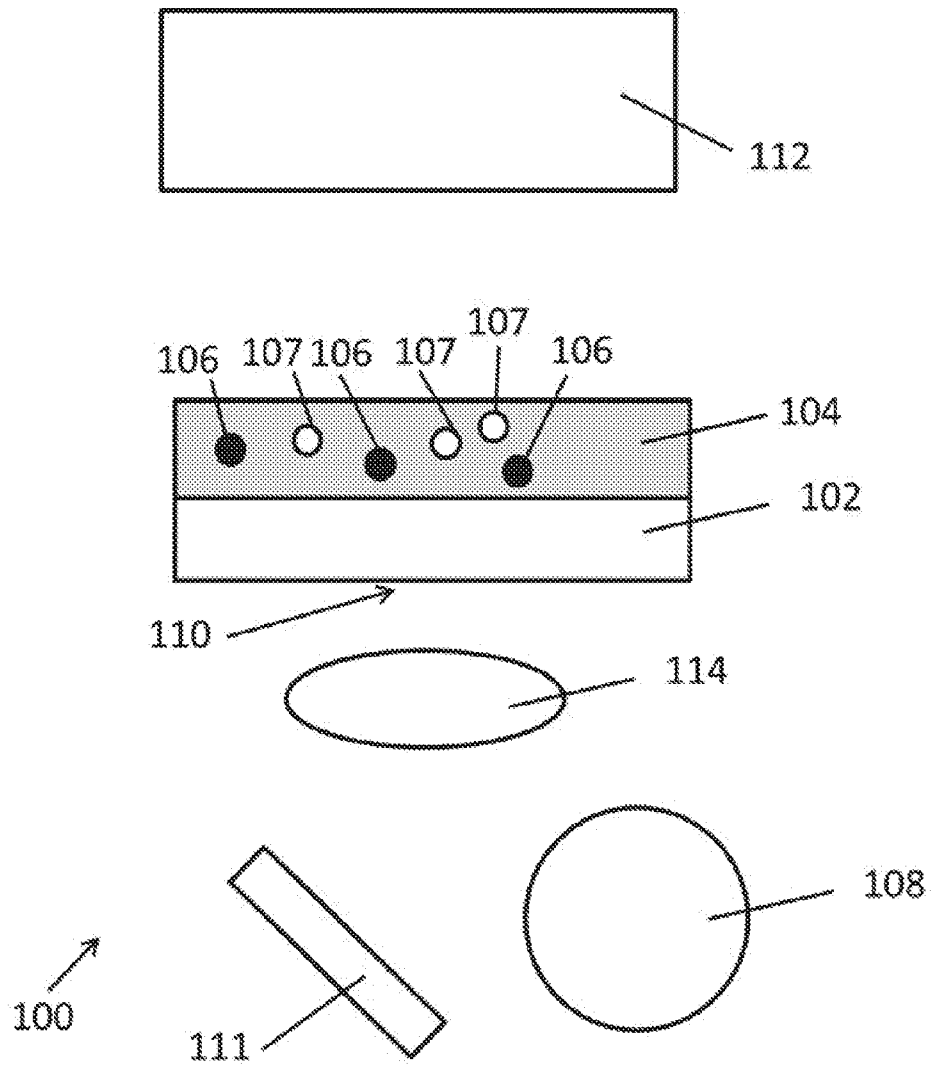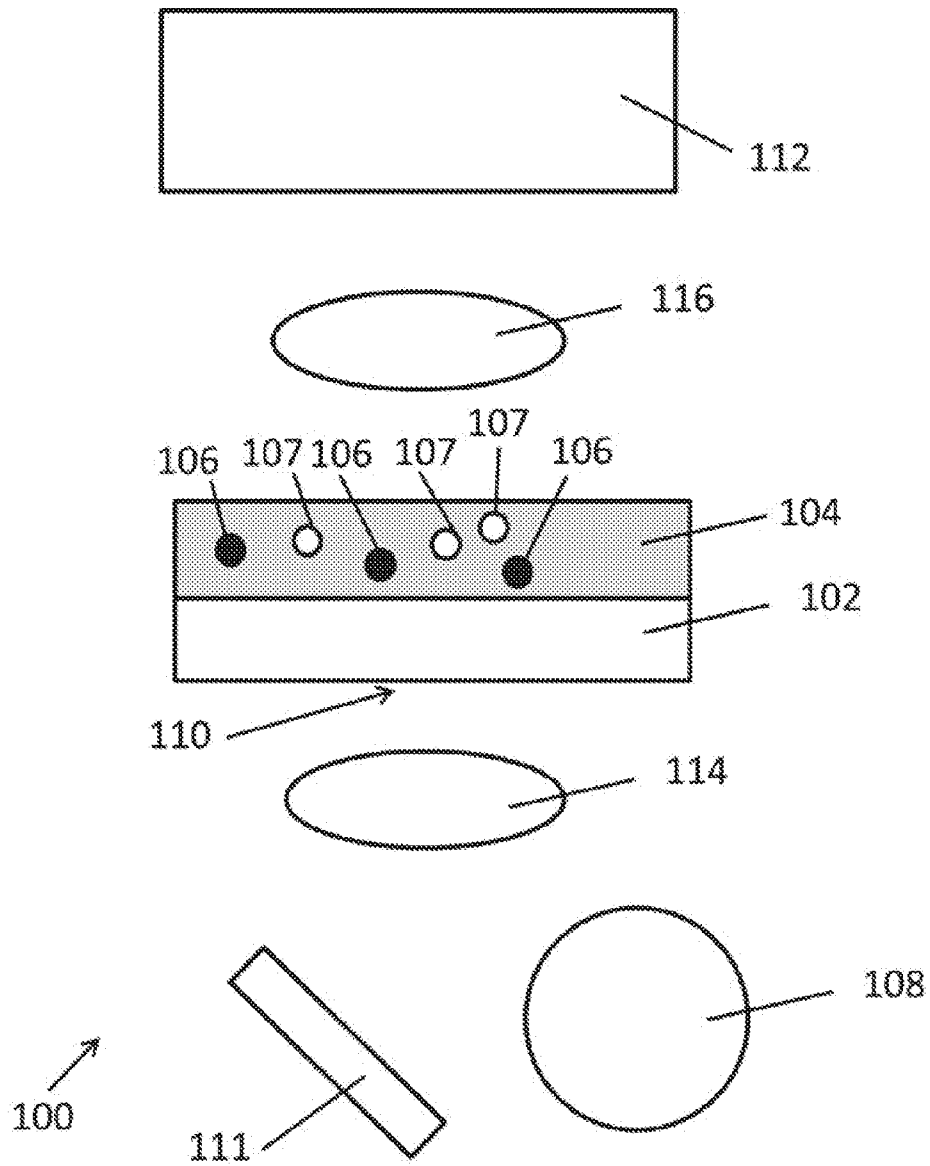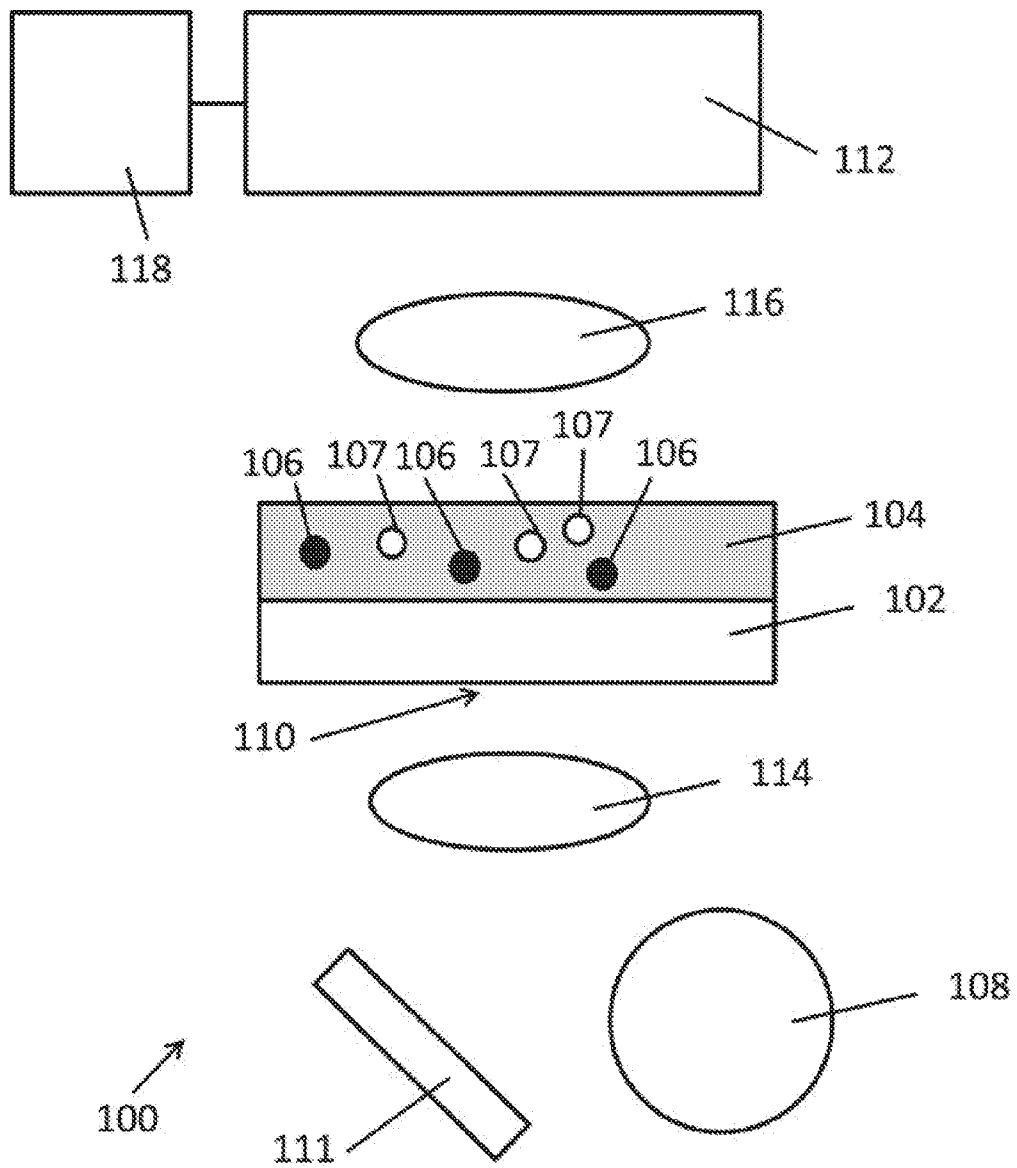
FIG. 6
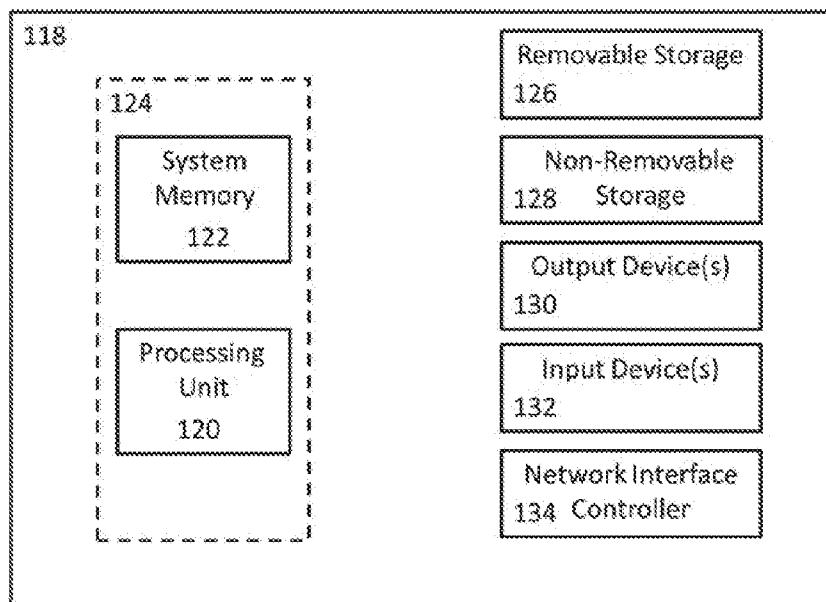
FIG. 7
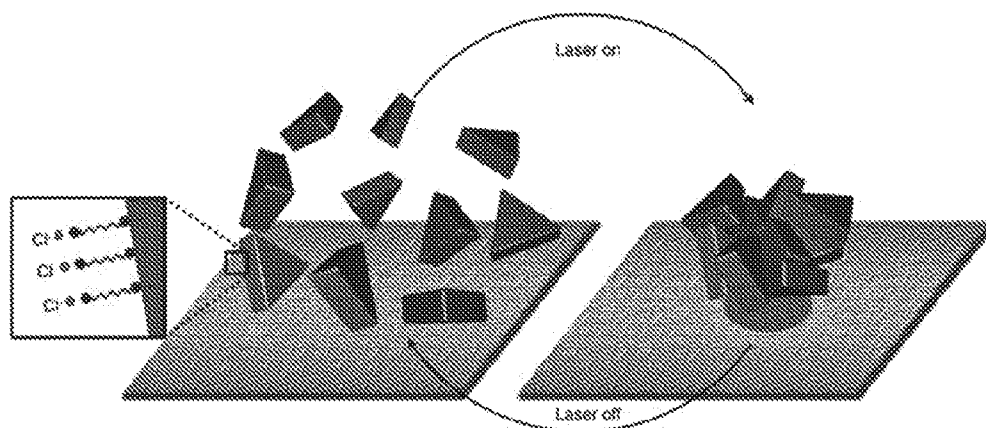
FIG. 8
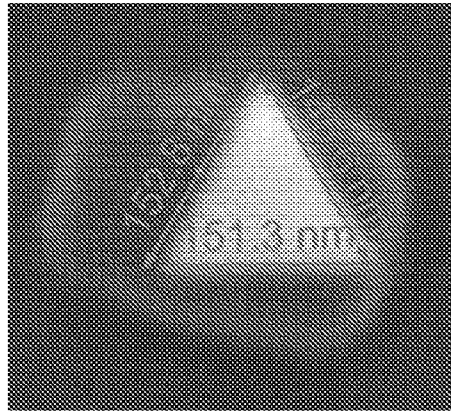
FIG. 9
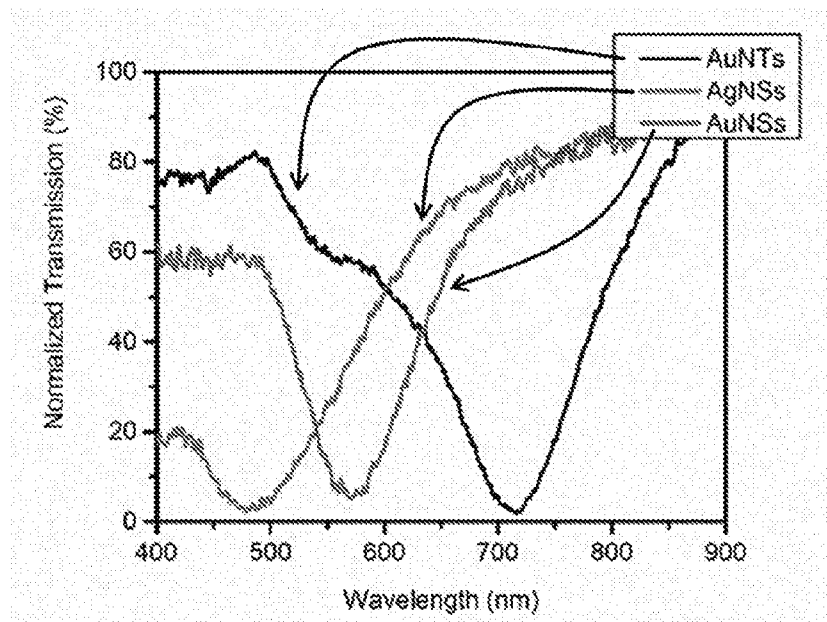
FIG. 10
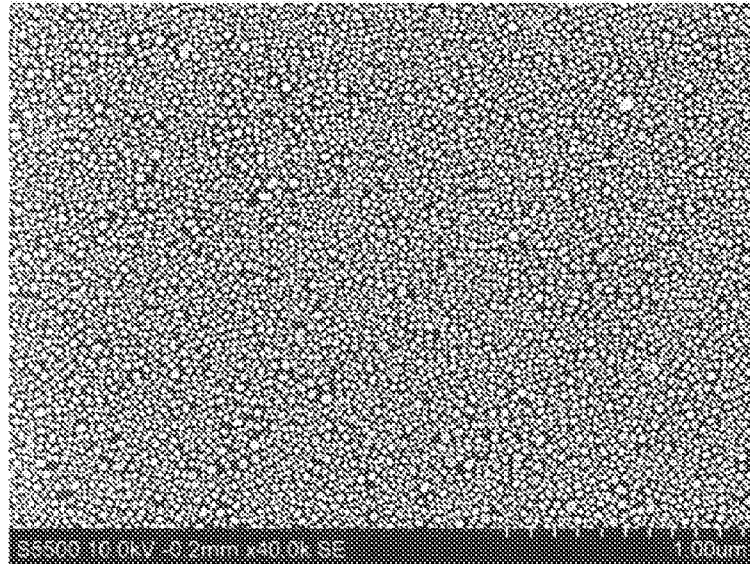
FIG. 11
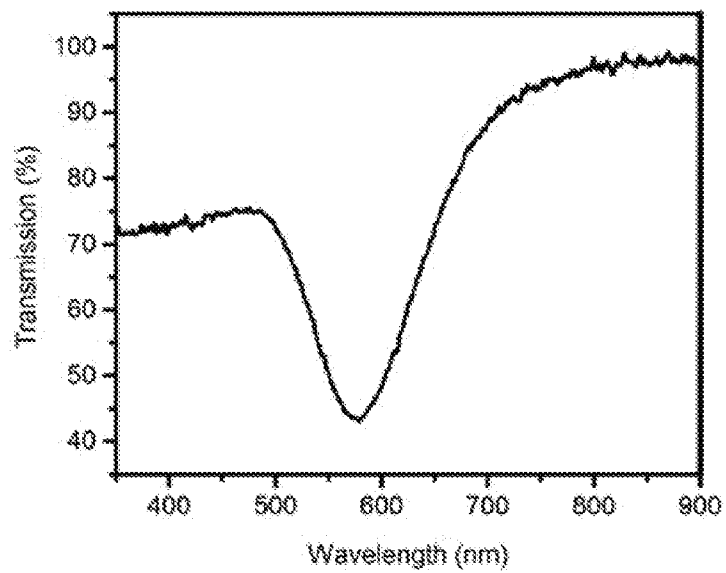
FIG. 12

9/40
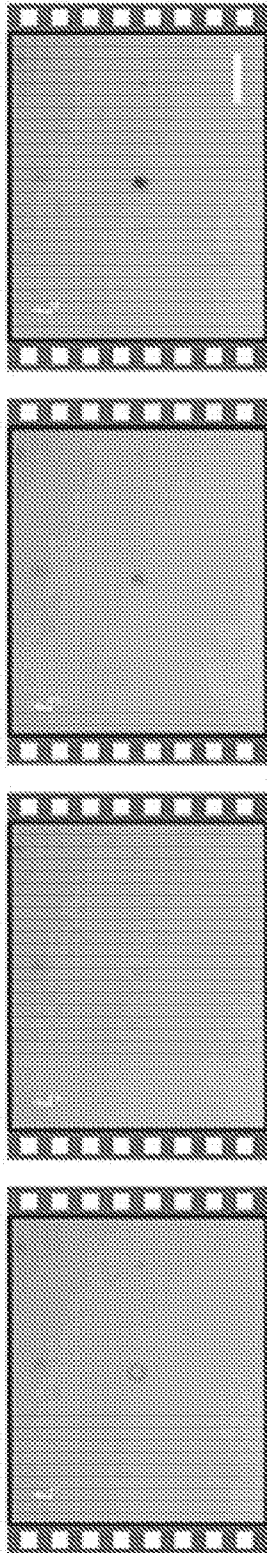
FIG. 13

FIG. 14

FIG. 15

FIG. 16

11/40

transmitted beam

T (K)

AuNT

296

295

294

plasmonic substrate

incident beam

FIG. 17

T (K)

297

296

AuNT assembly

295

294
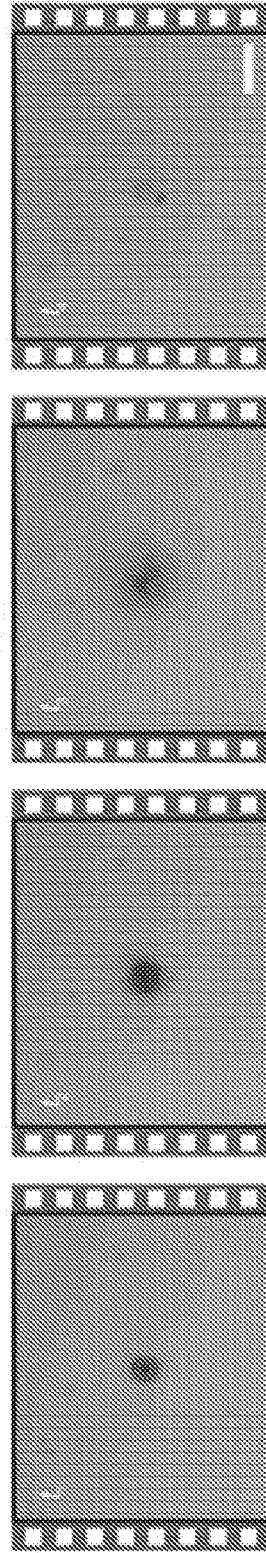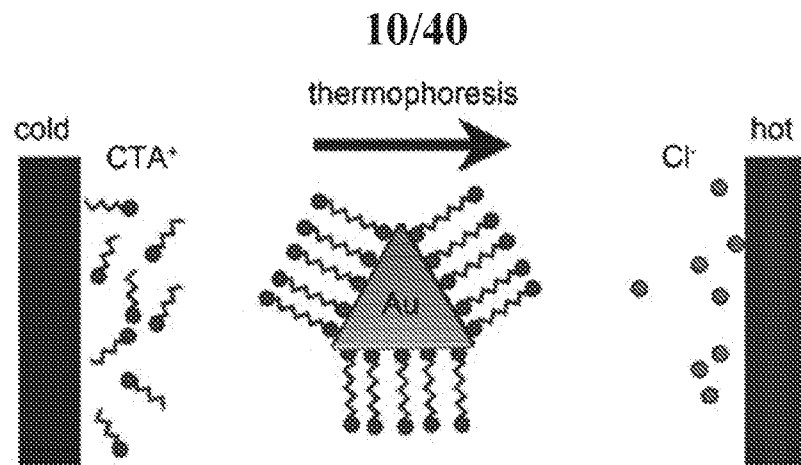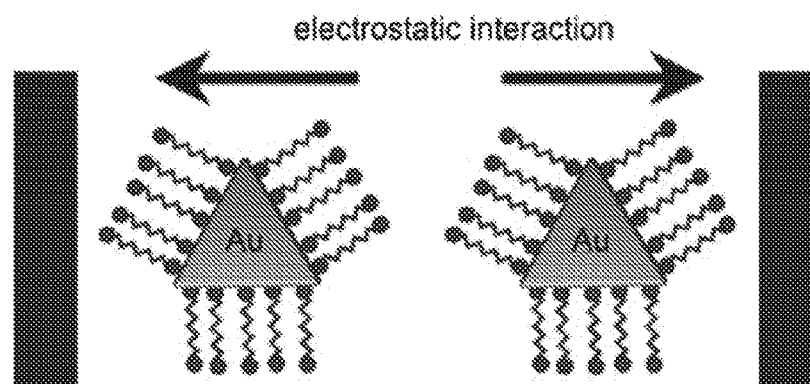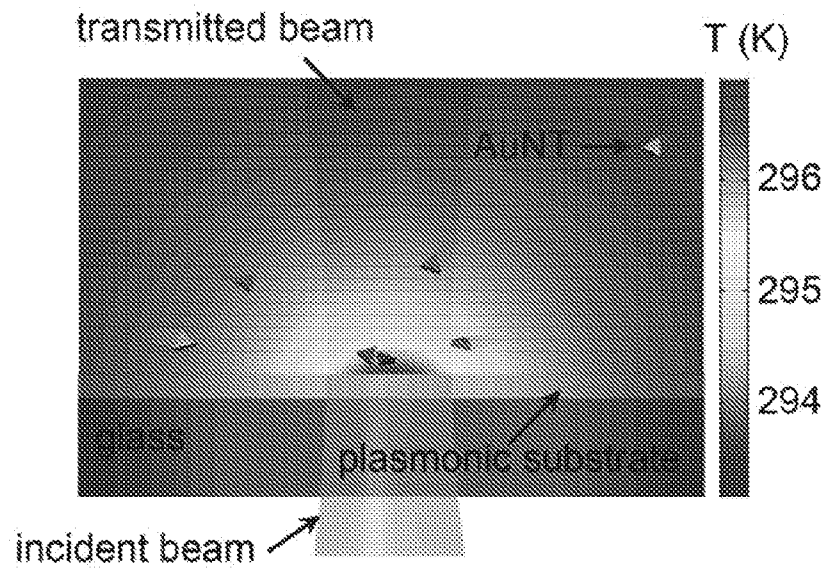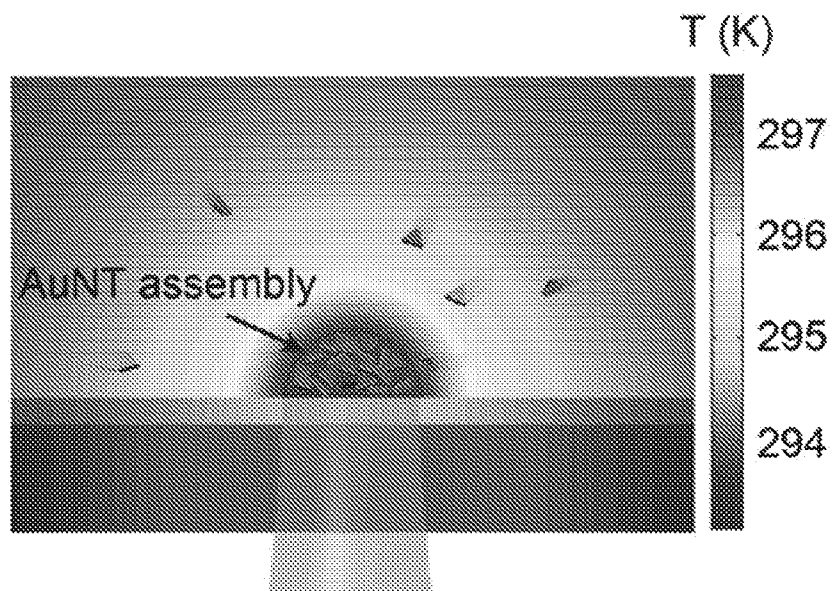
FIG. 18

12/40
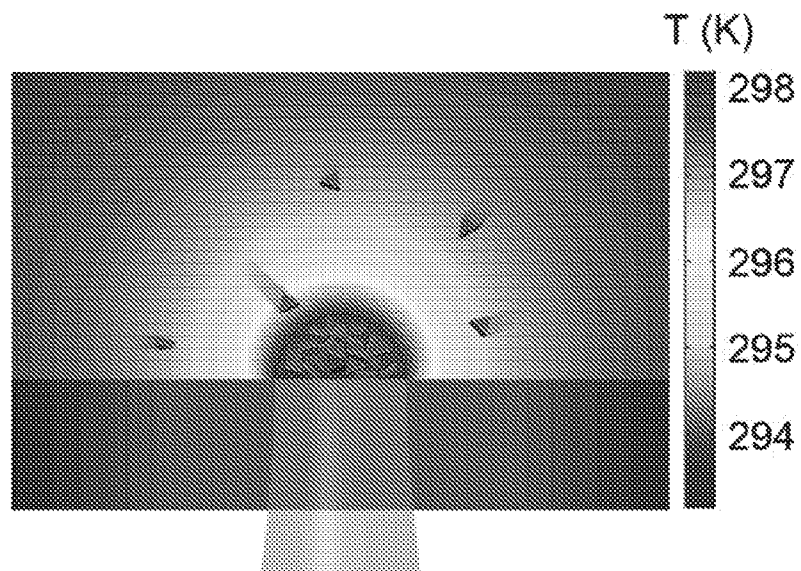
FIG. 19
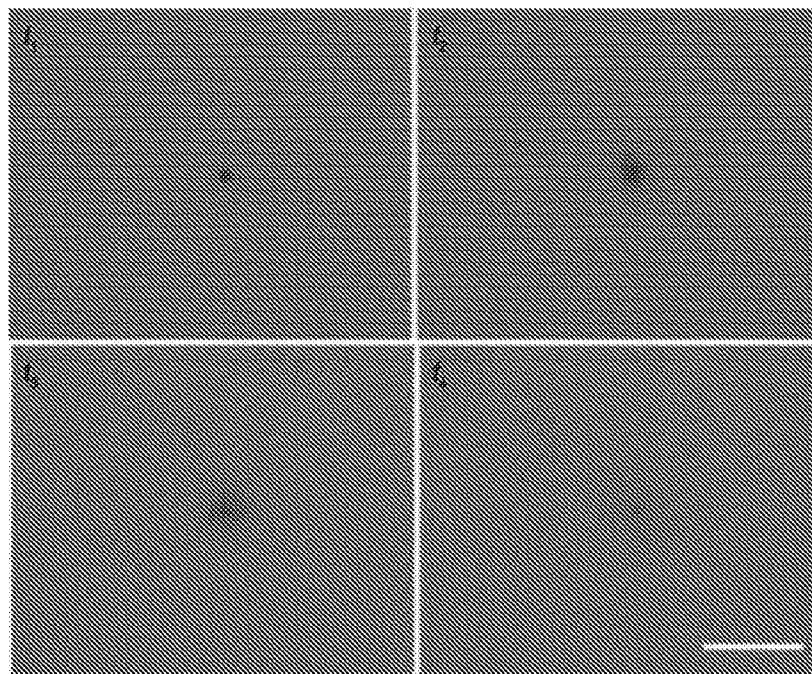
FIG. 20
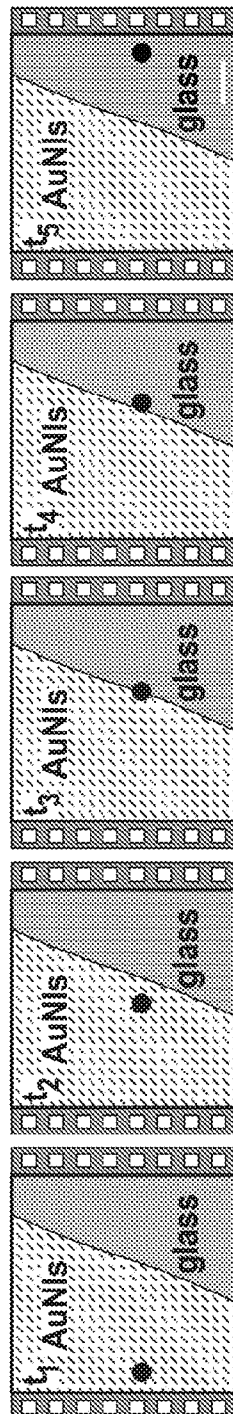
FIG. 21
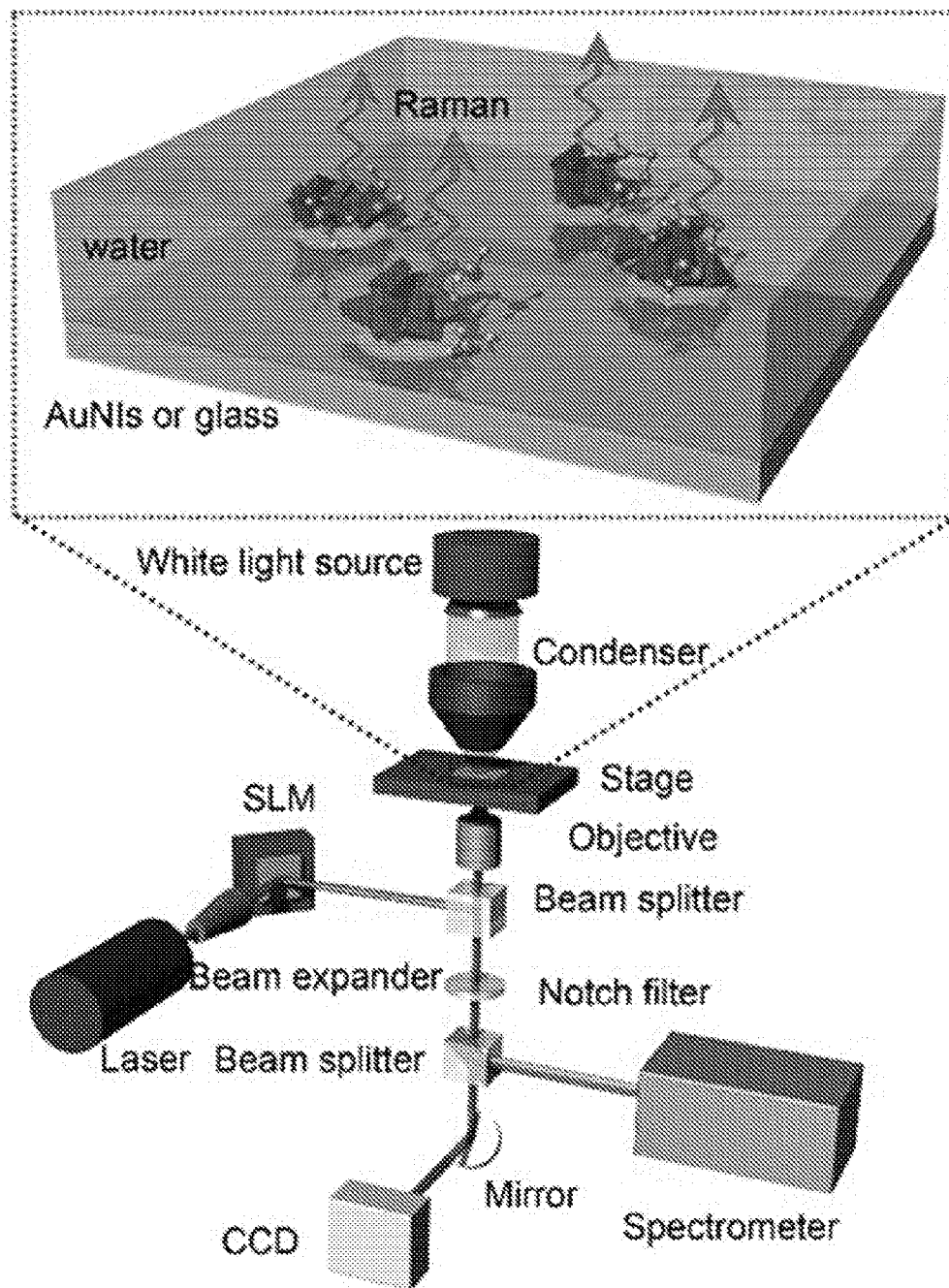
FIG. 22
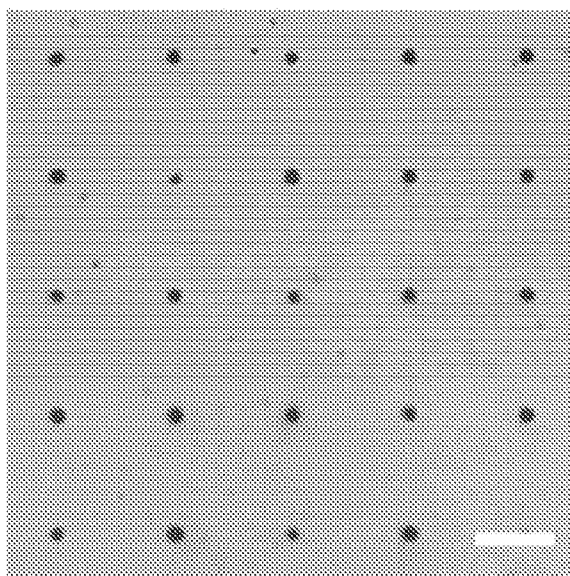
FIG. 23
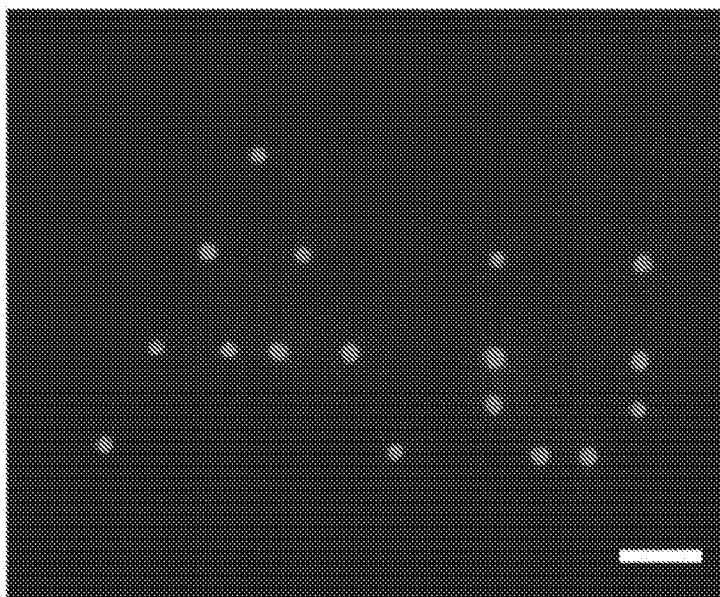
FIG. 24
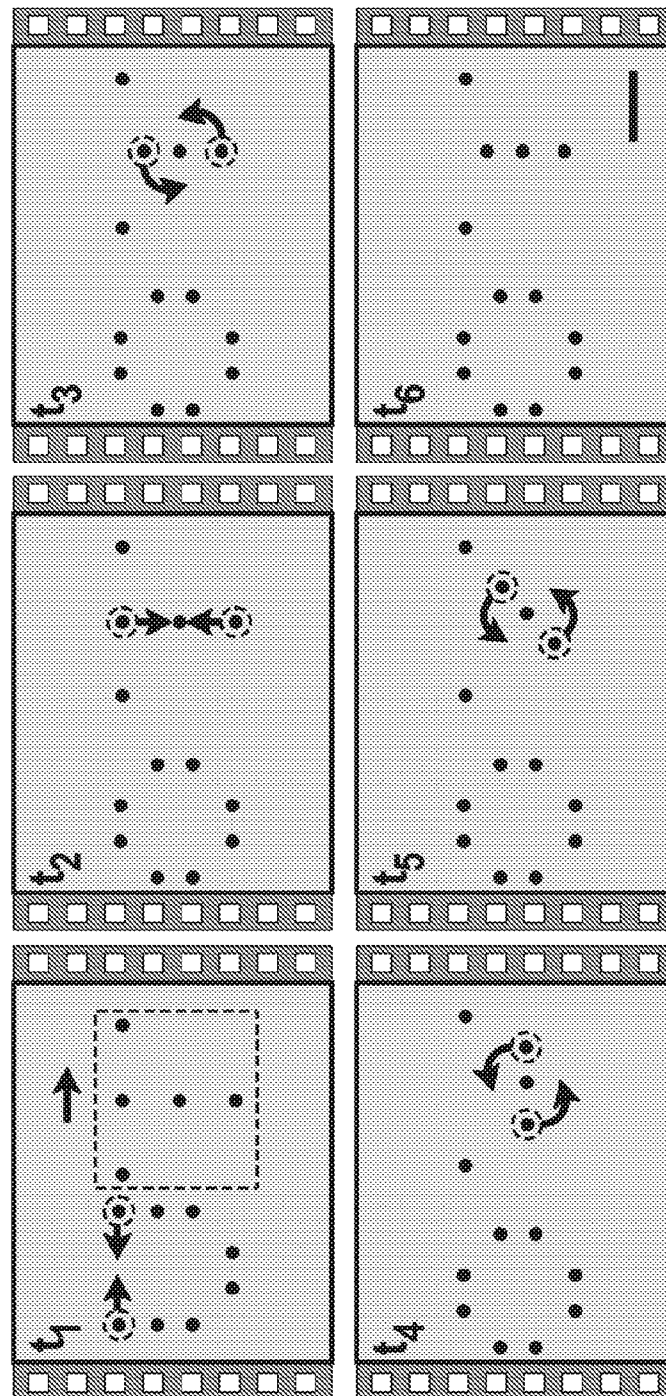
FIG. 25

17/40
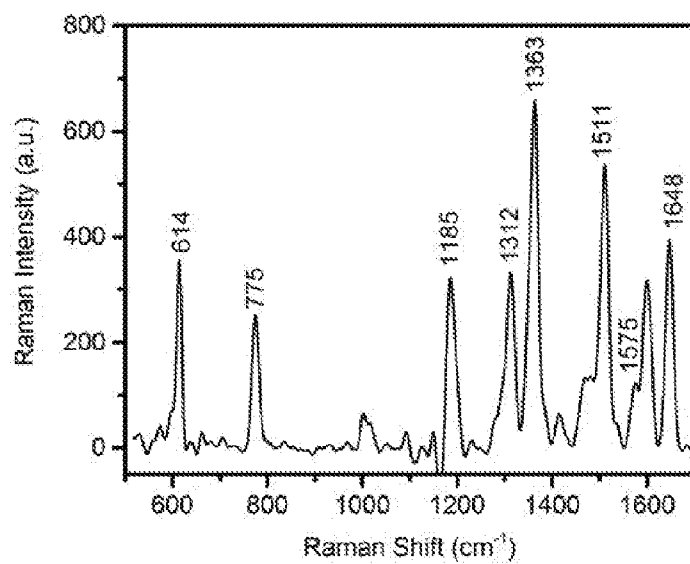
FIG. 26
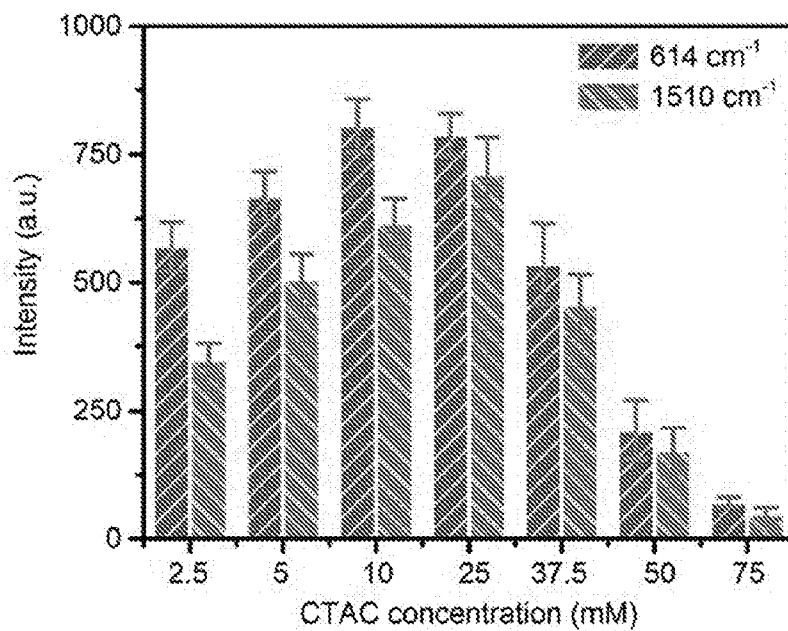
FIG. 27
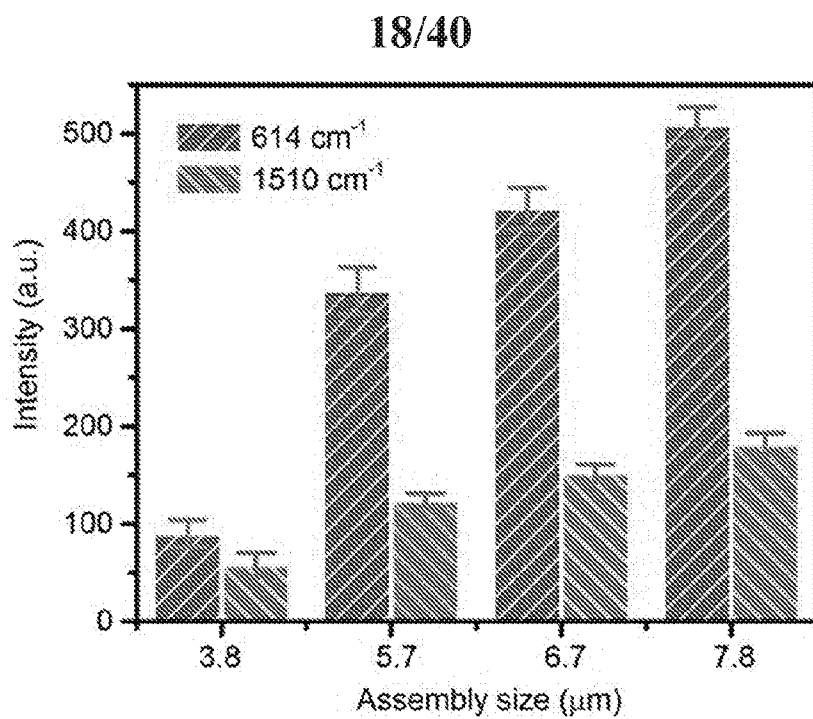
FIG. 28
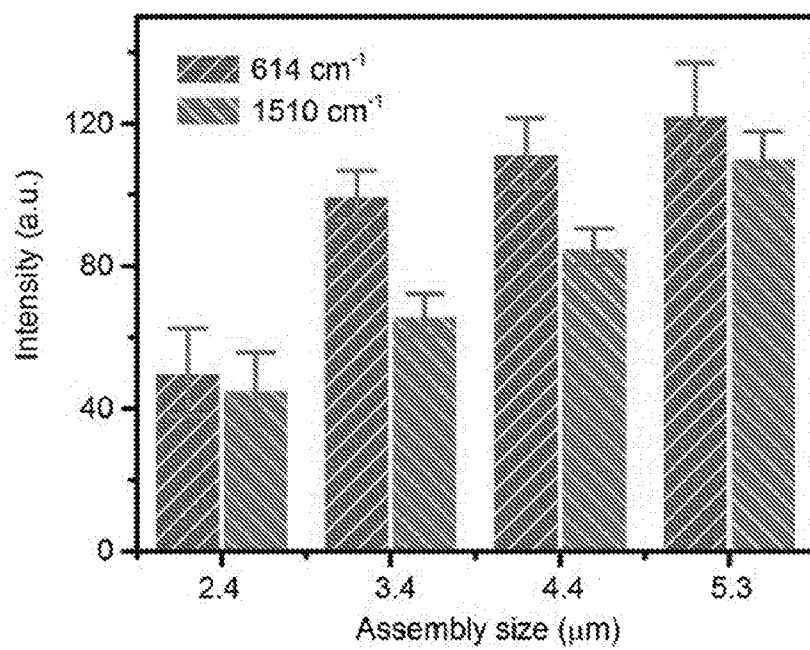
FIG. 29
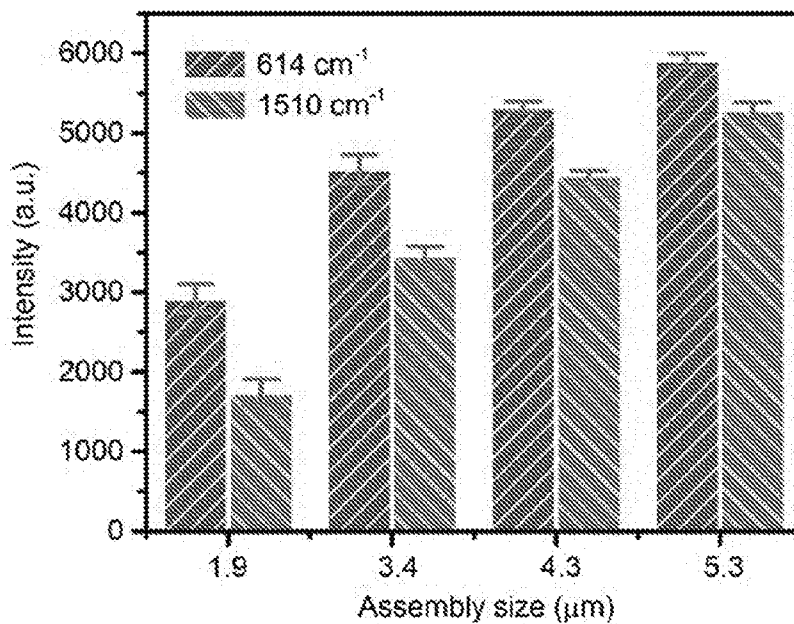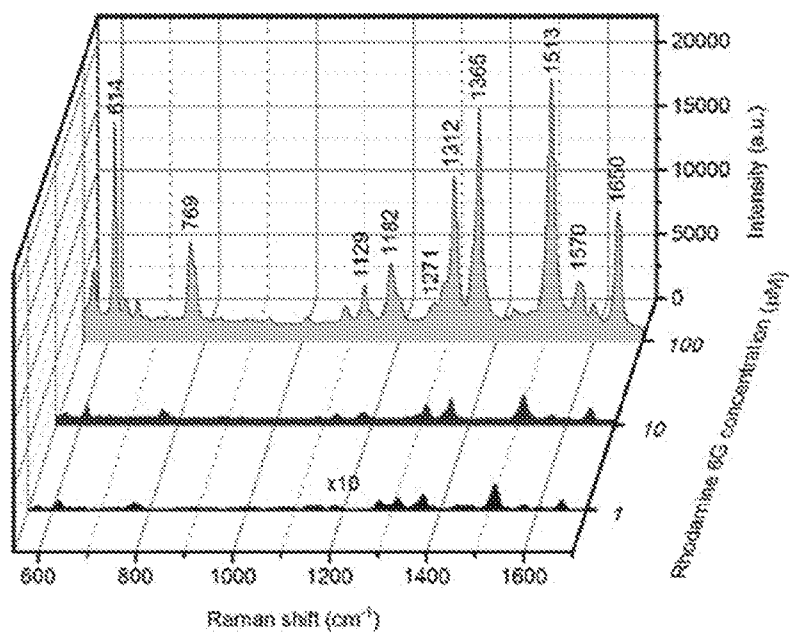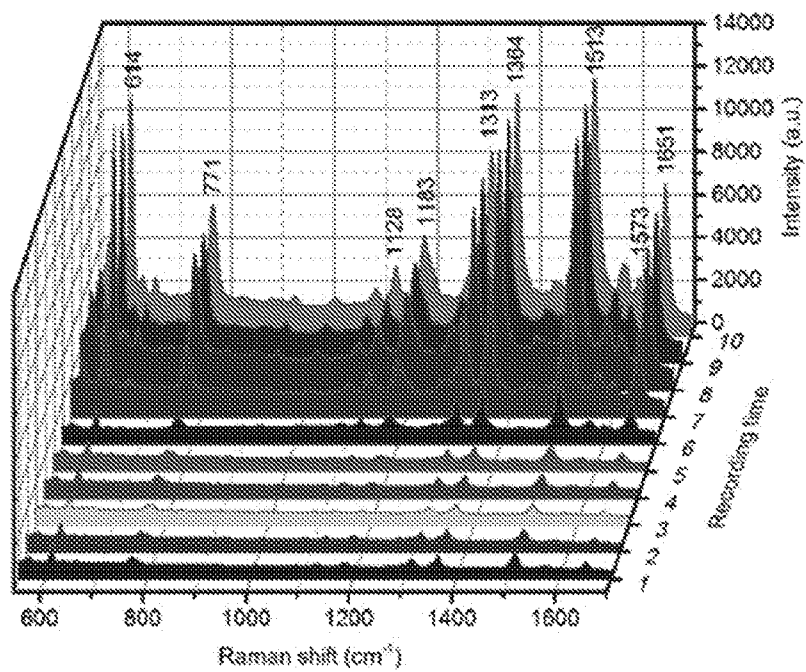
FIG. 30

FIG. 31

20/40

FIG. 32
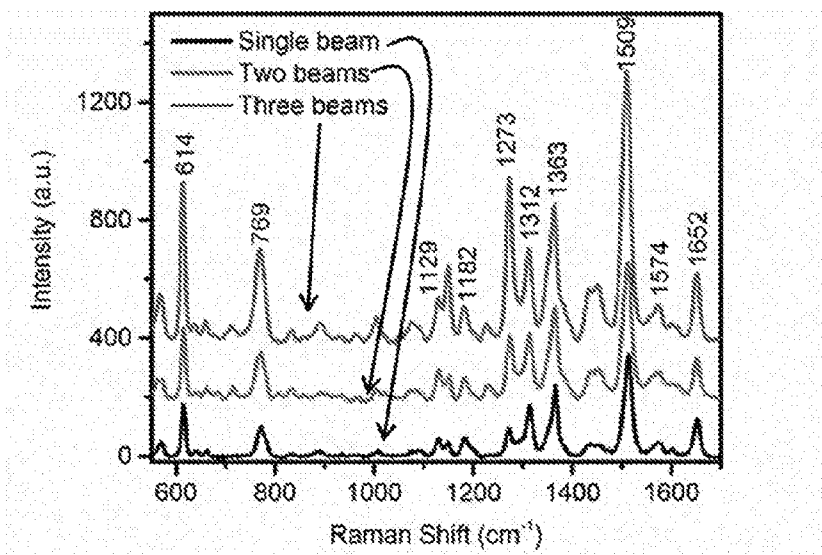
FIG. 33
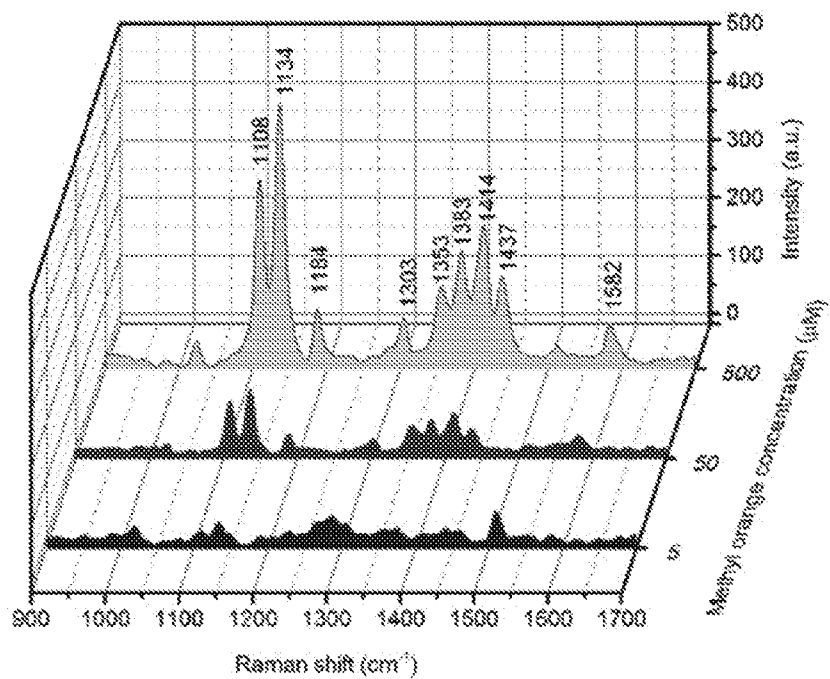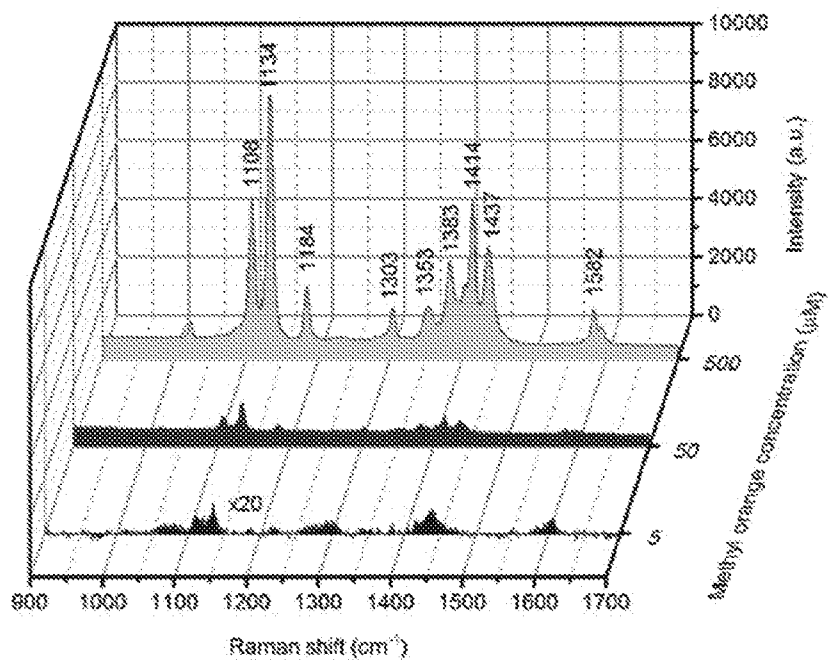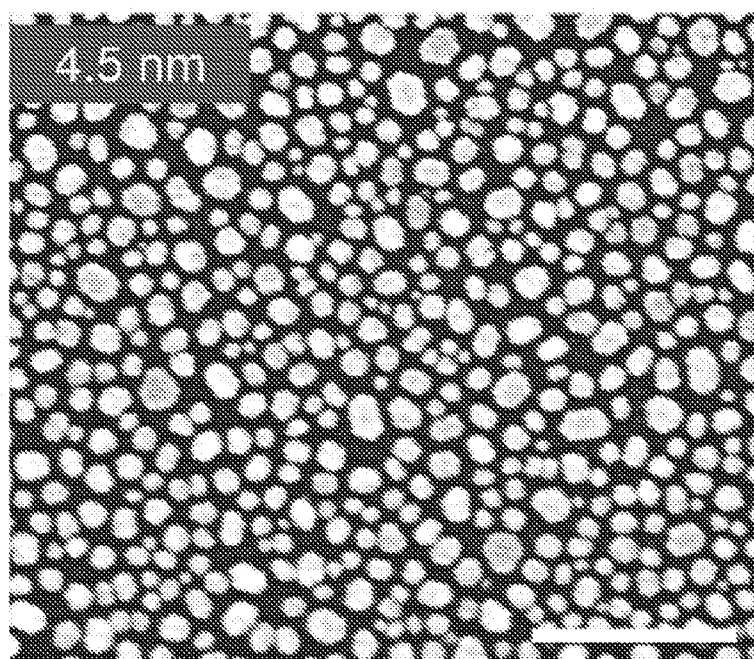
FIG. 34

FIG. 35

FIG. 36

FIG. 37

FIG. 38

FIG. 39

Positive micellar ion:

CTAC micelle

FIG. 40

Negative Cl⁻ ion:

FIG. 41

T (K)

306
304
302
300
298
296
294

FIG. 42

FIG. 43

FIG. 44

$\nabla T_r \ (\times 10^6 \ \text{K/m})$

-1

-3

-5

FIG. 45

$\nabla T_z \ (\times 10^7 \ \text{K/m})$

0

-0.5

-1
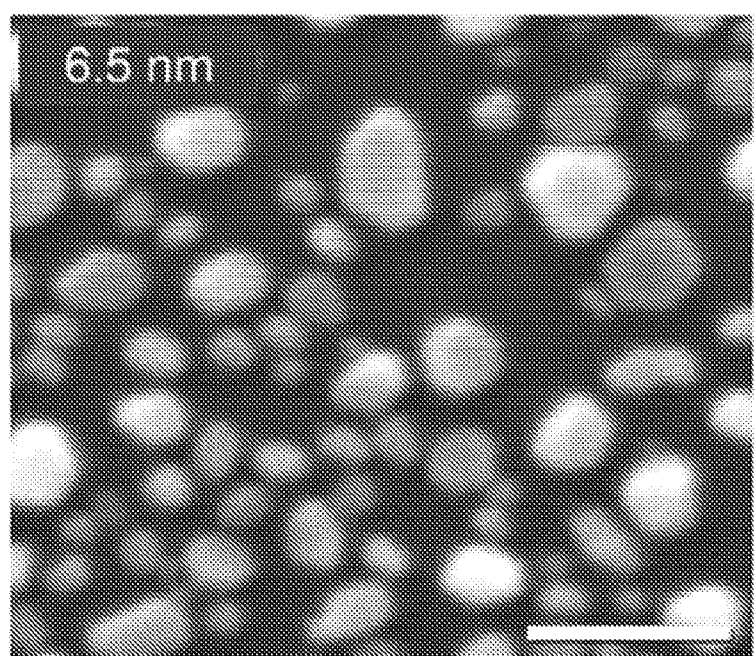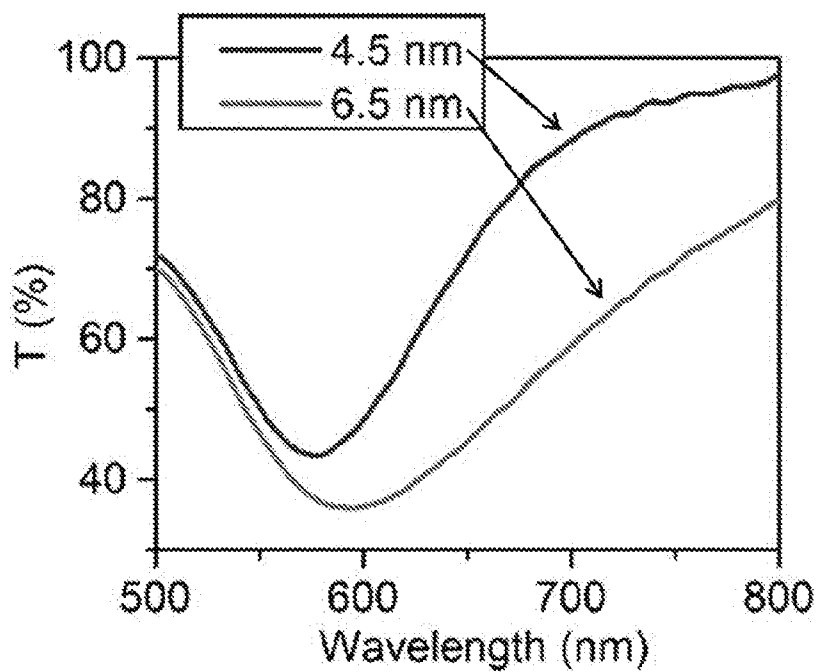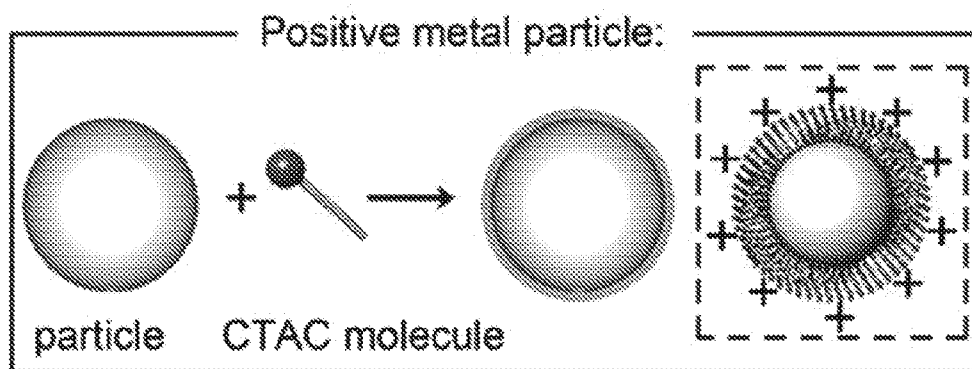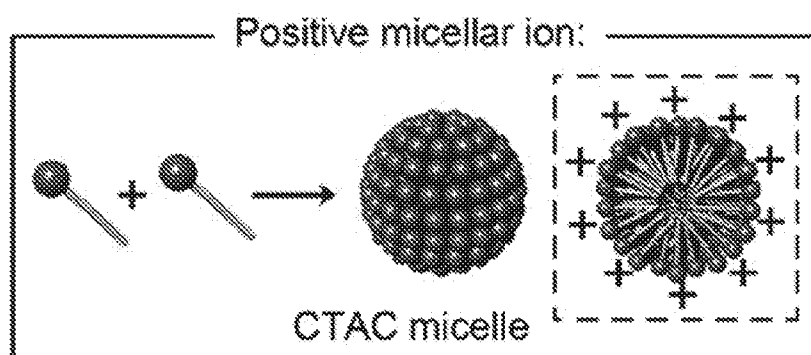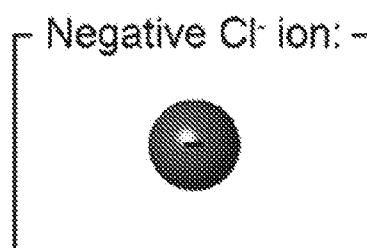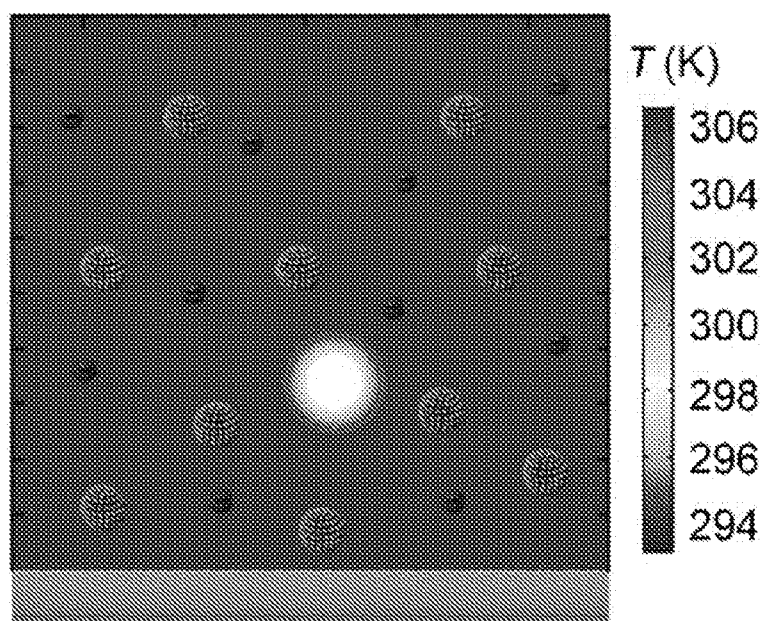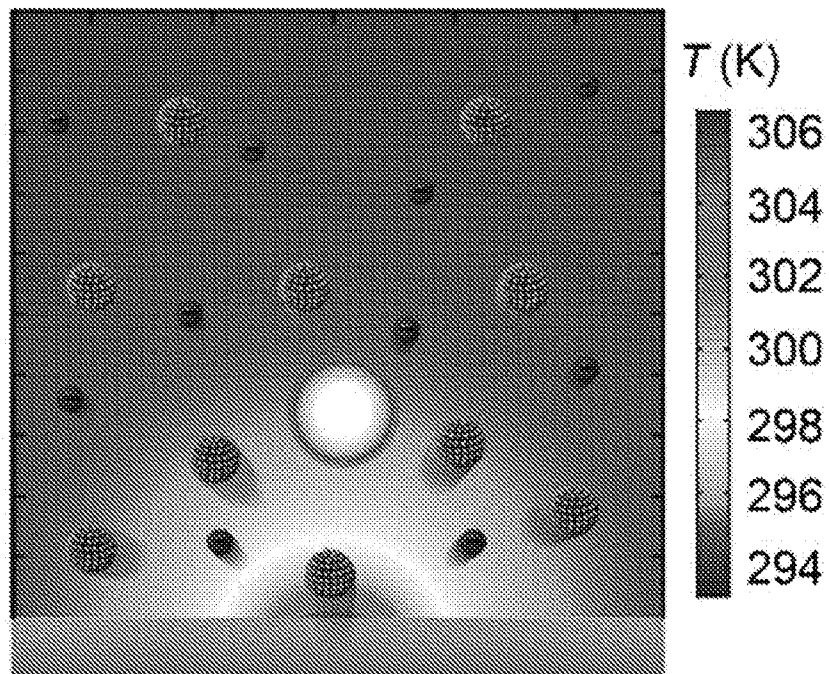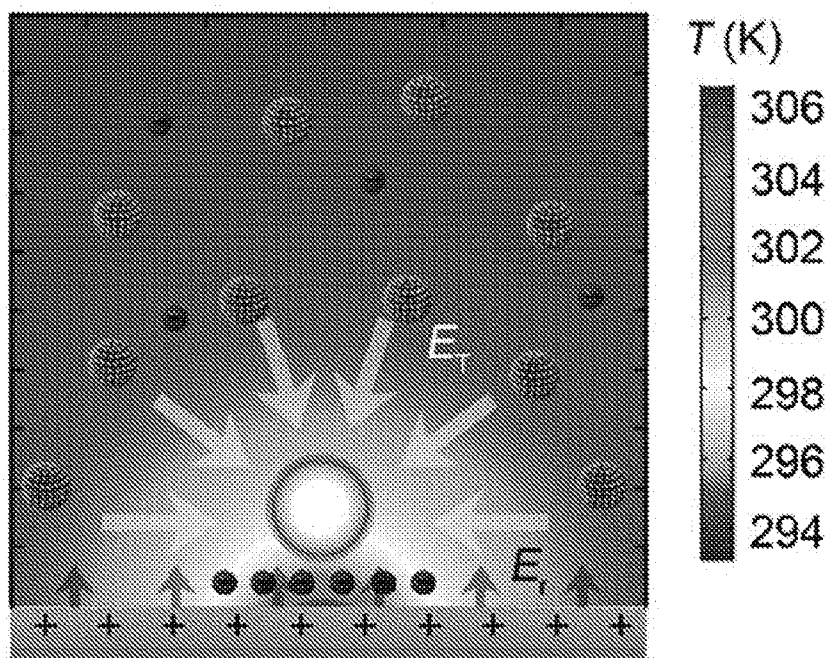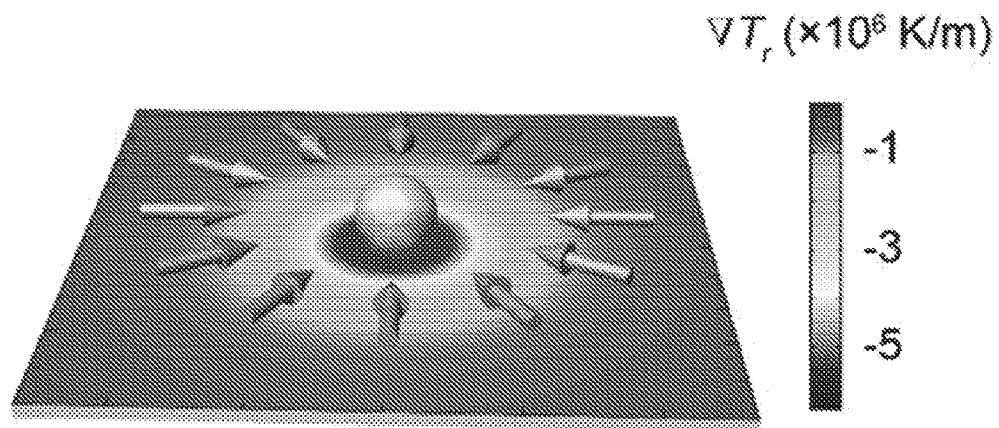
-1.5
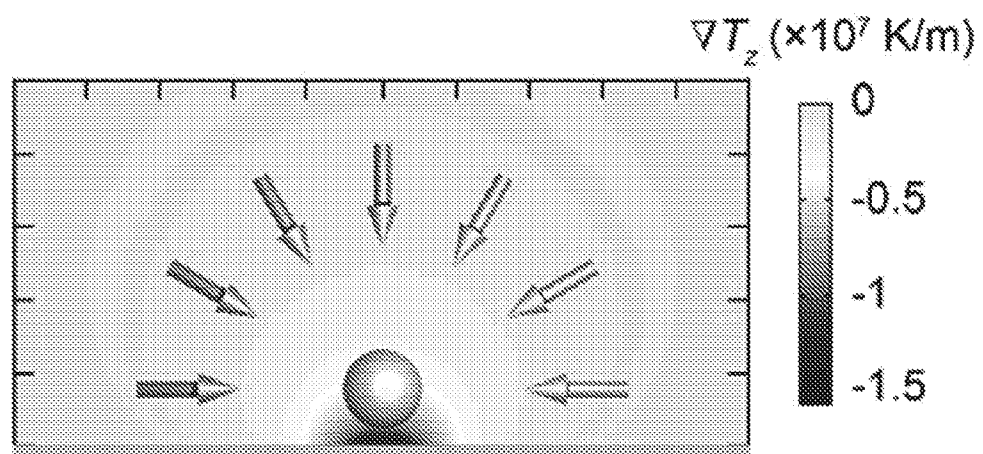
FIG. 46
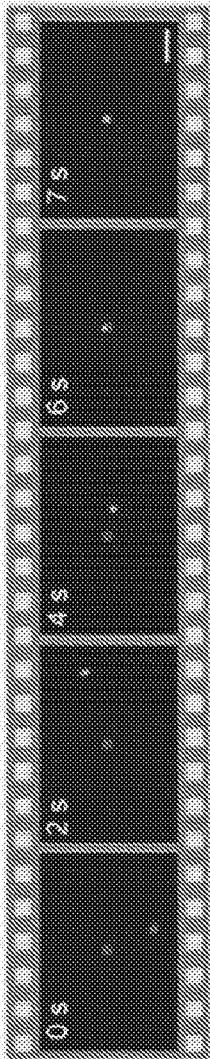
FIG. 47
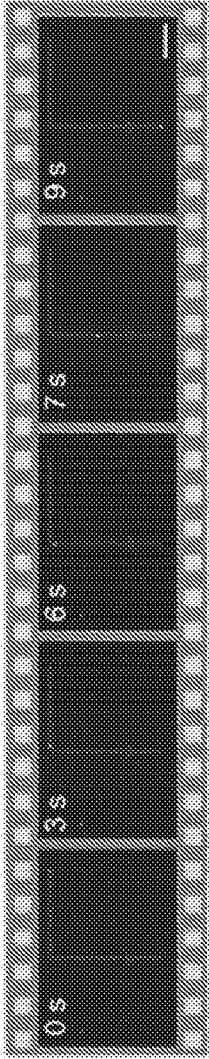
FIG. 48
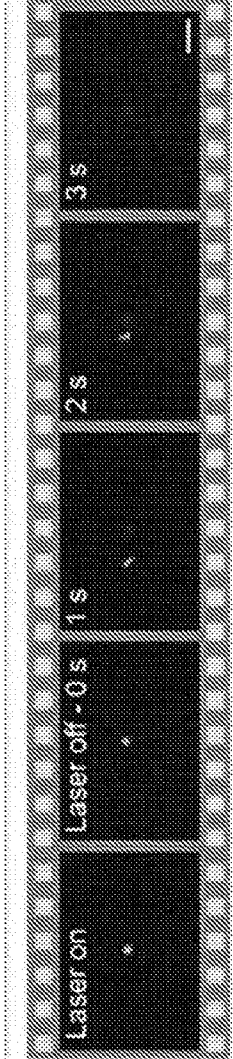
FIG. 49
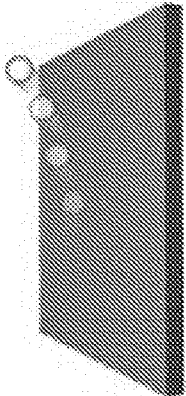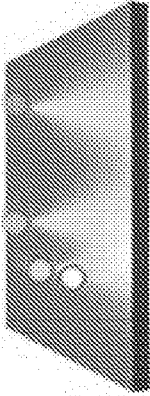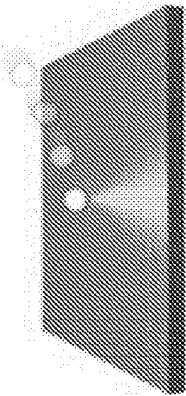
28/40
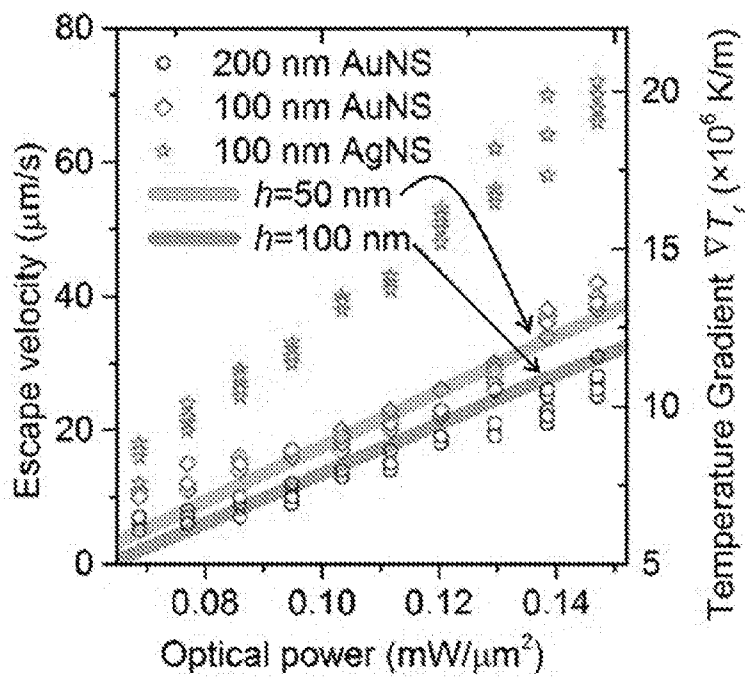
FIG. 50
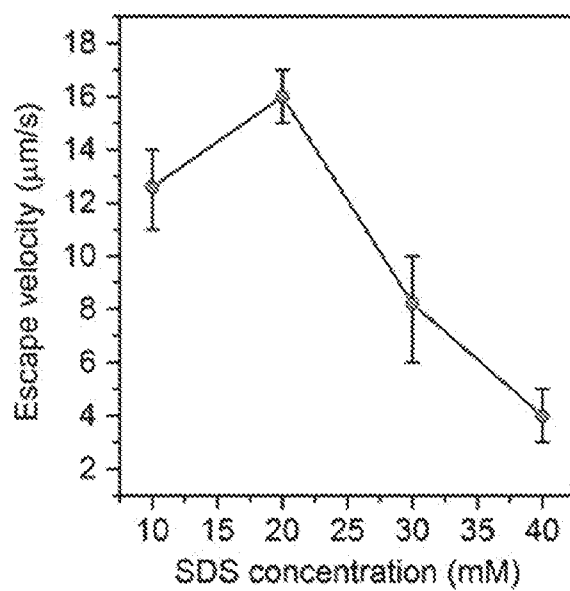
FIG. 51
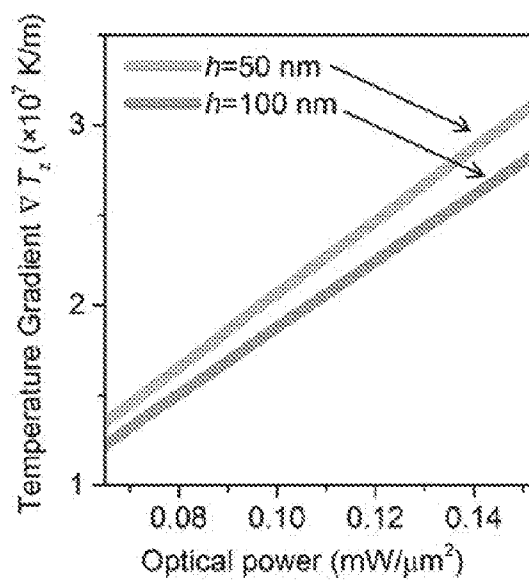
FIG. 52
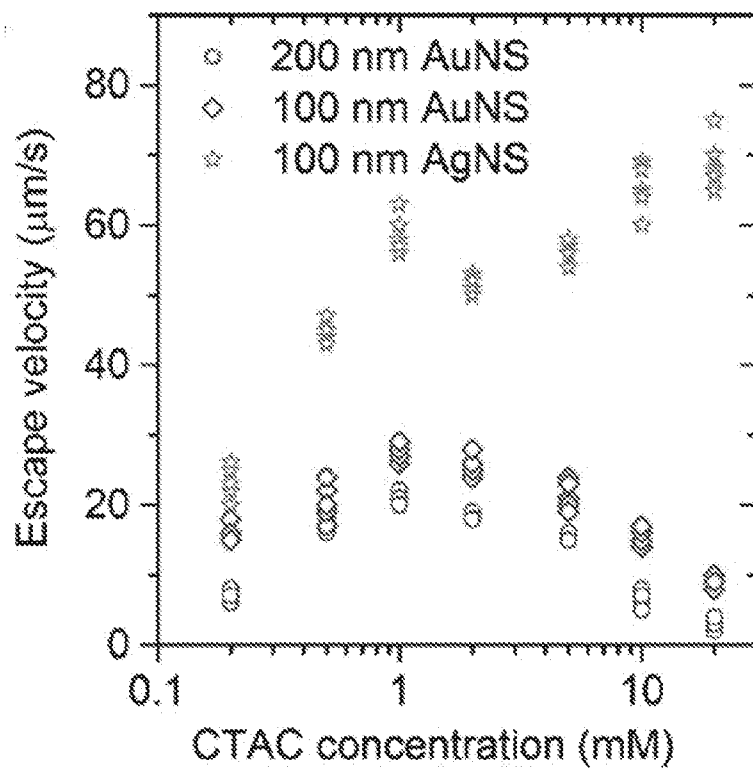
FIG. 53
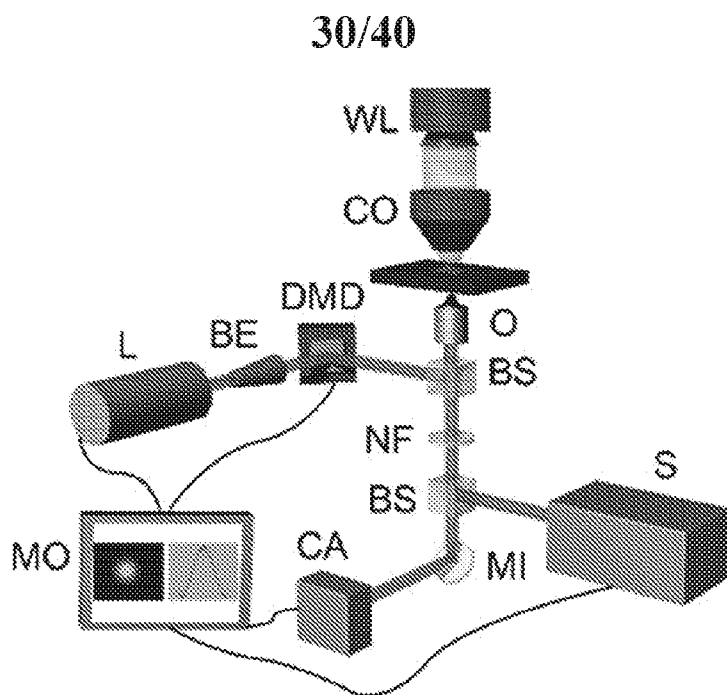
FIG. 54

FIG. 55
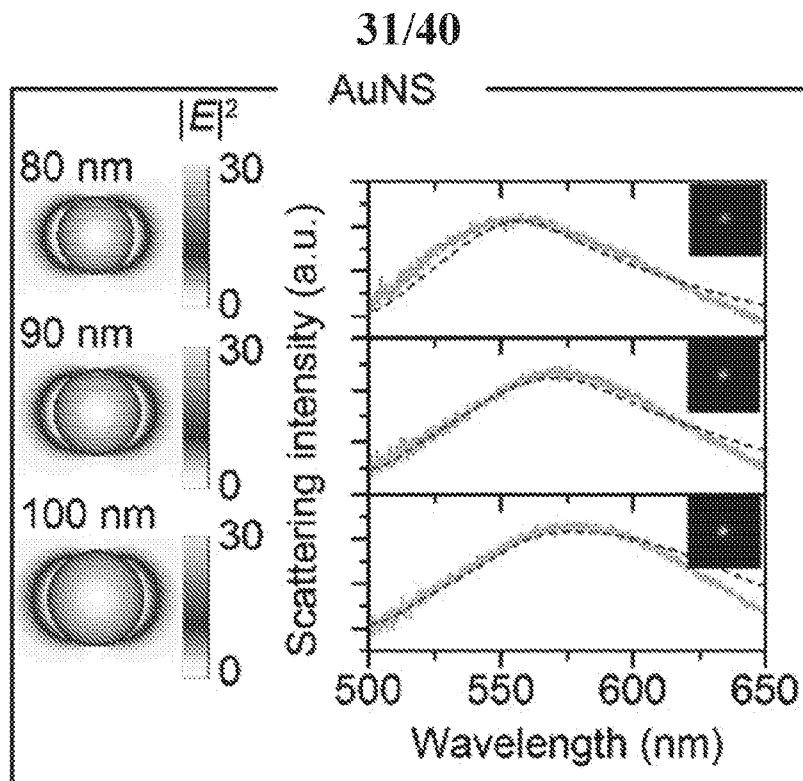
FIG. 56
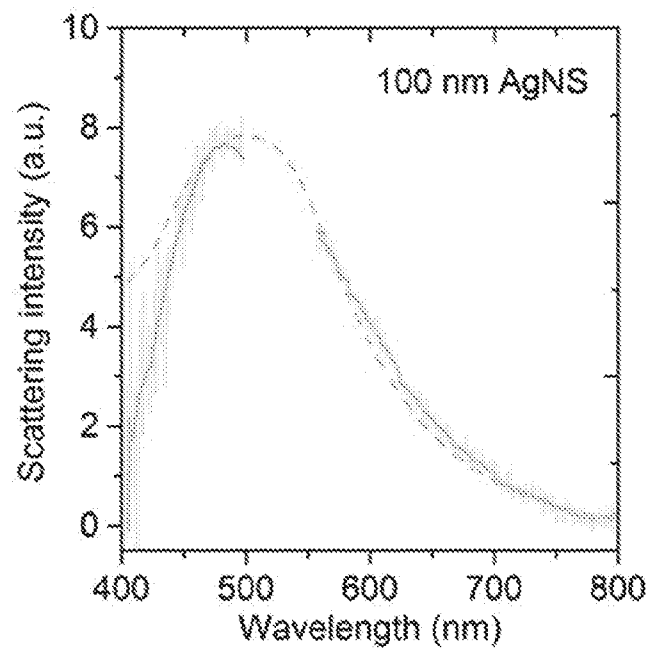
FIG. 57
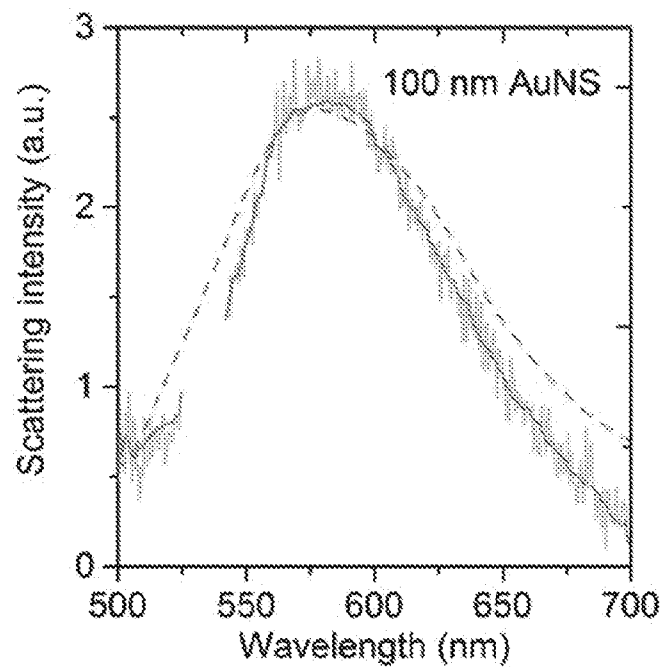
FIG. 58
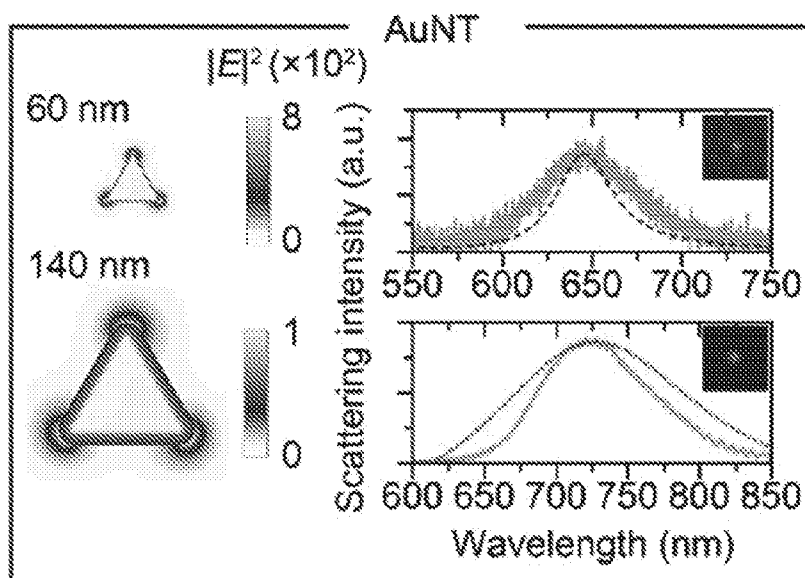
FIG. 59
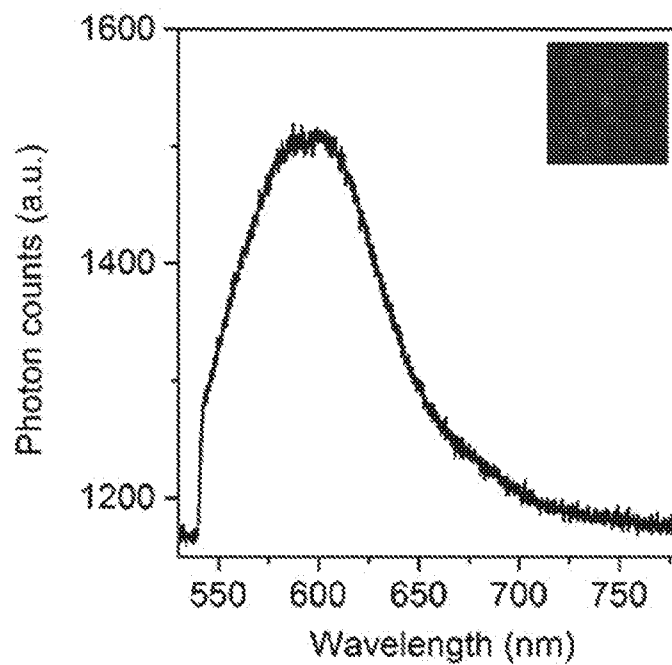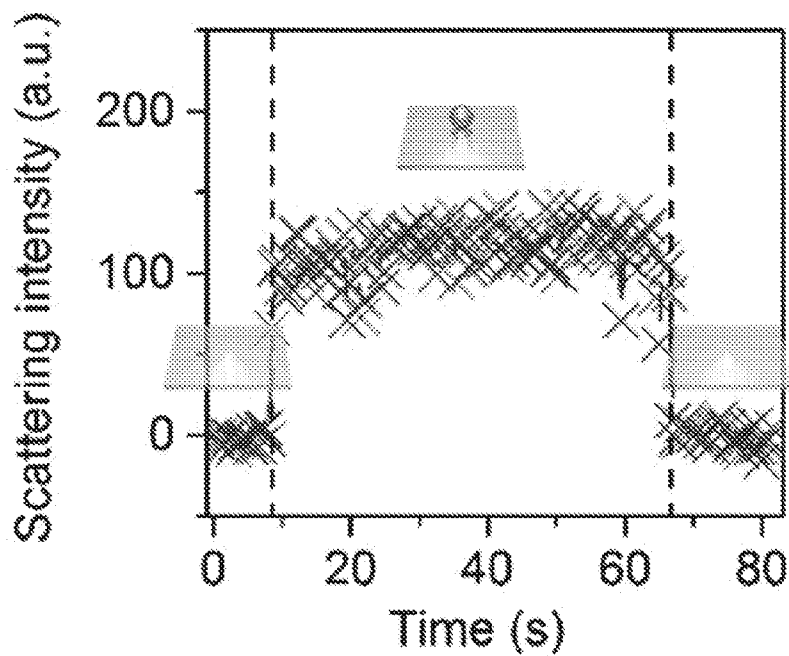
FIG. 60
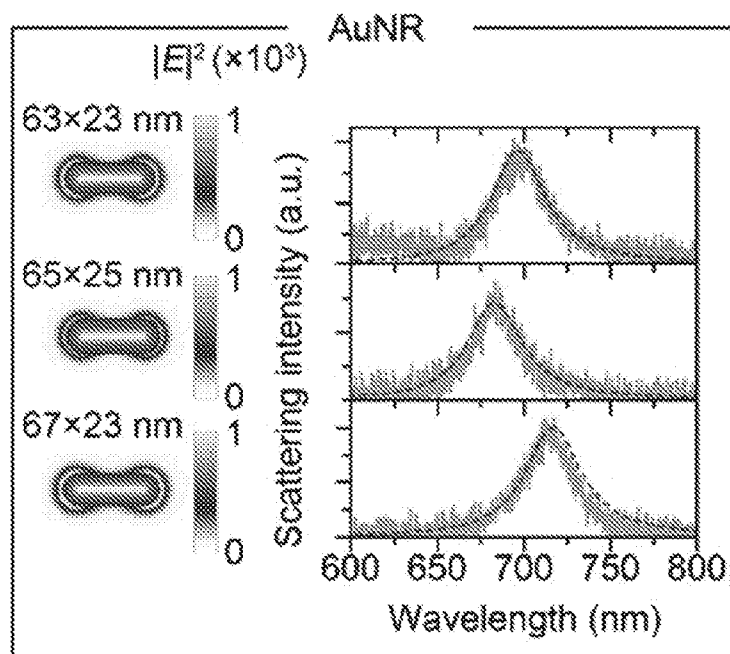
FIG. 61
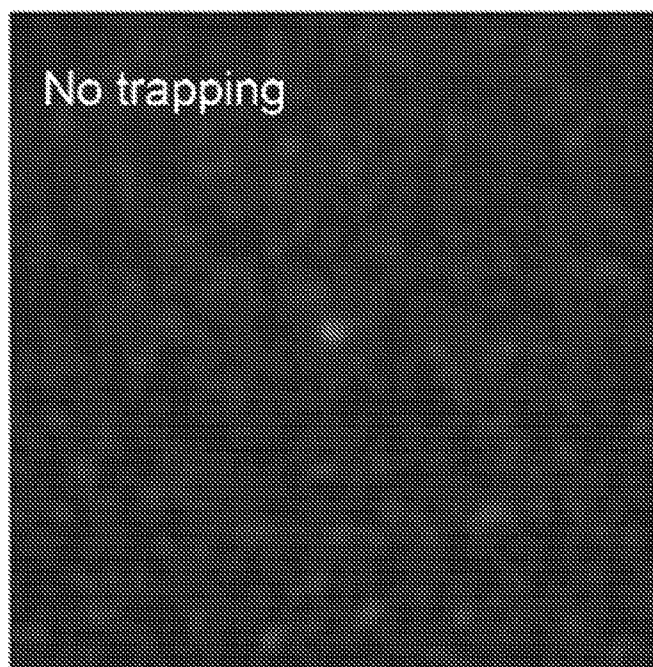
FIG. 62
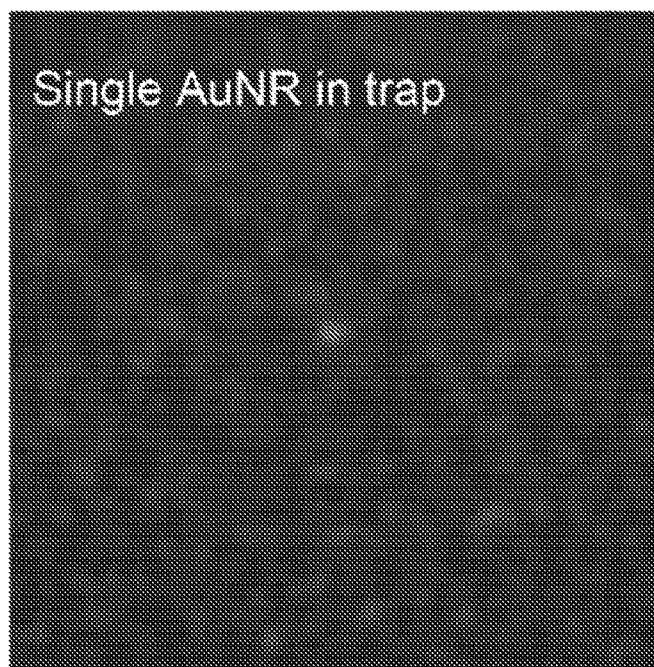
FIG. 63
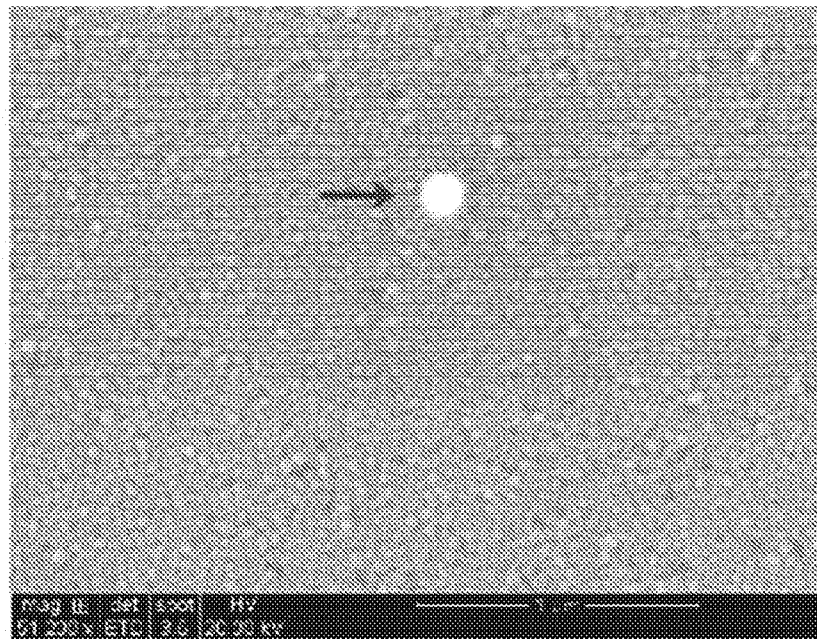
FIG. 64
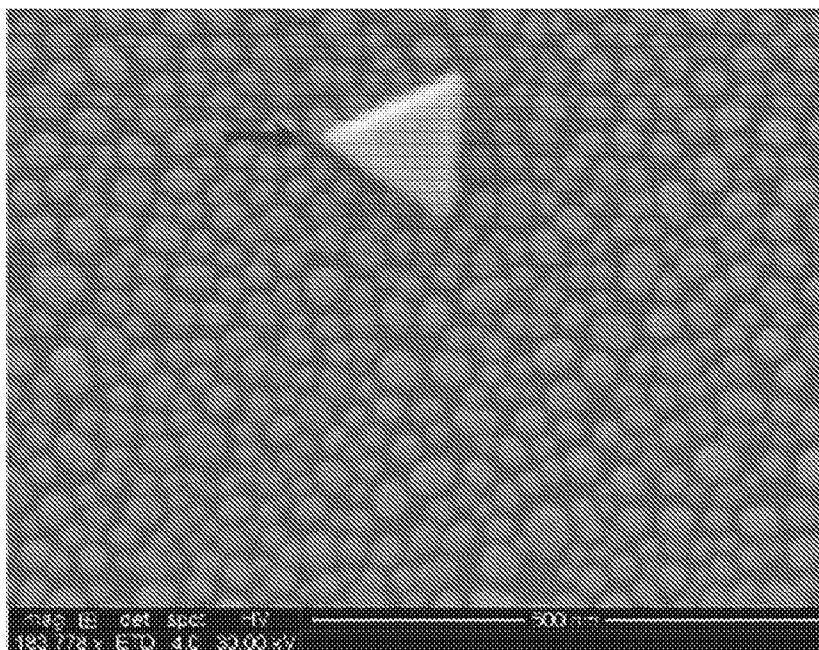
FIG. 65
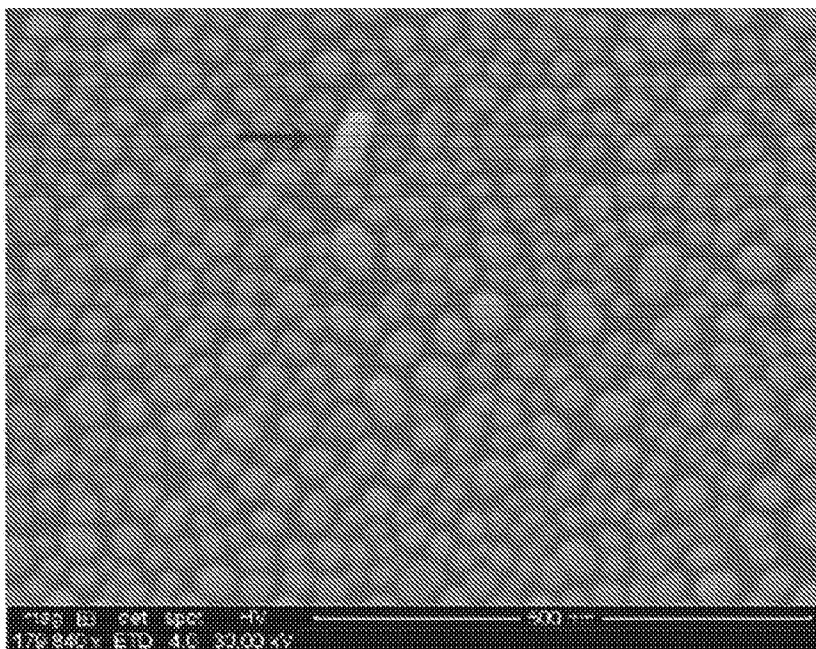
FIG. 66
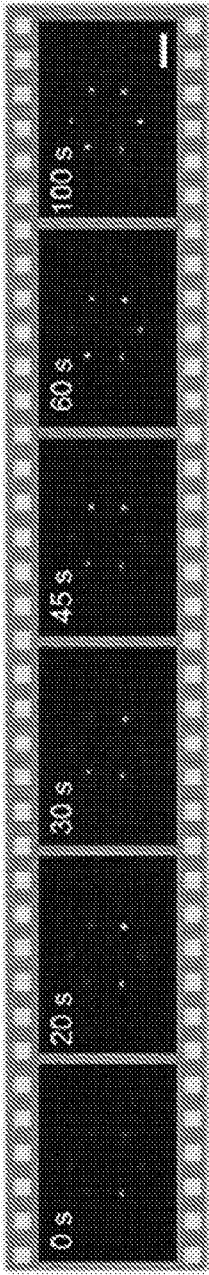
FIG. 67
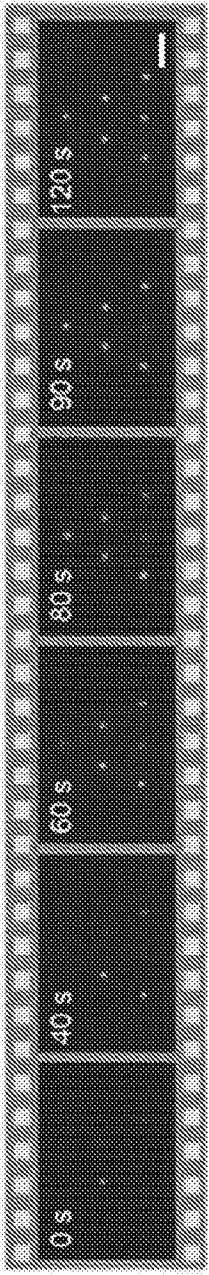
FIG. 68

38/40

FIG. 69
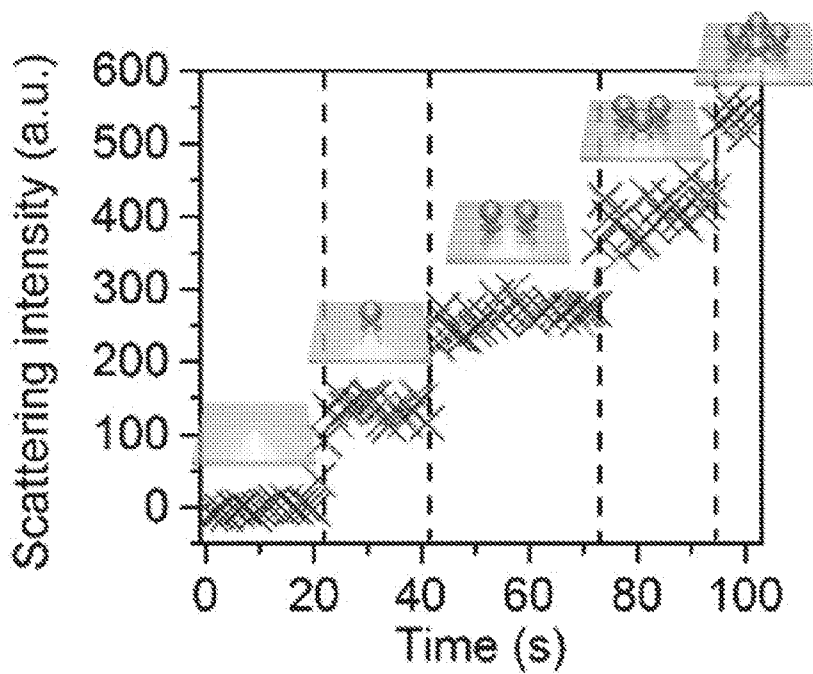
FIG. 70
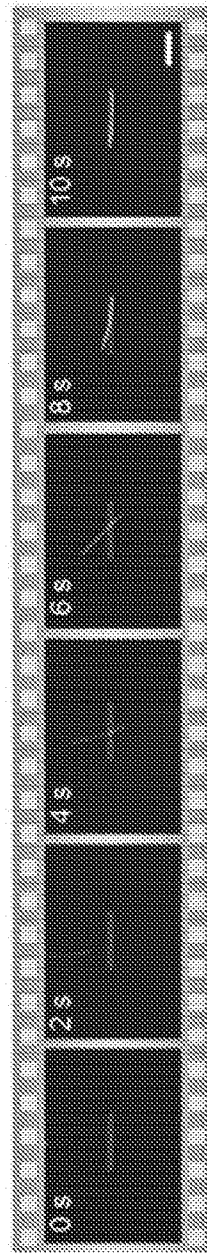
FIG. 71

FIG. 72

40/40

FIG. 73
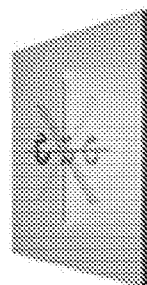

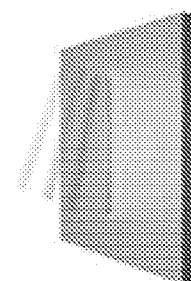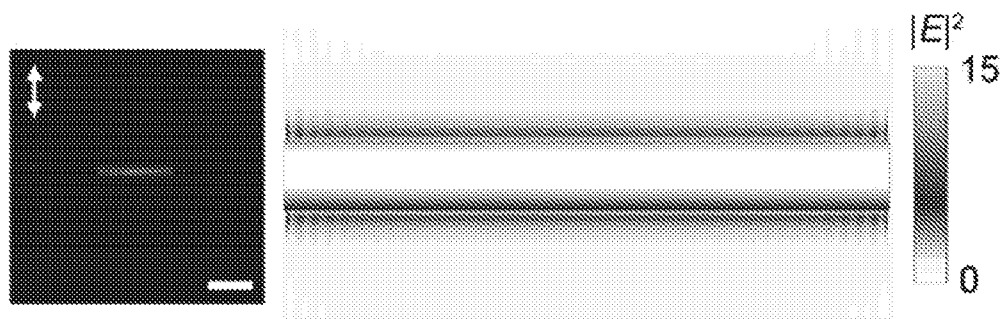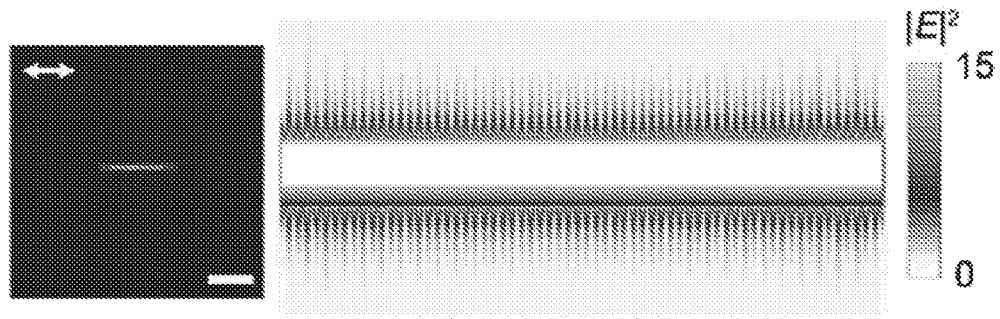FIG. 74
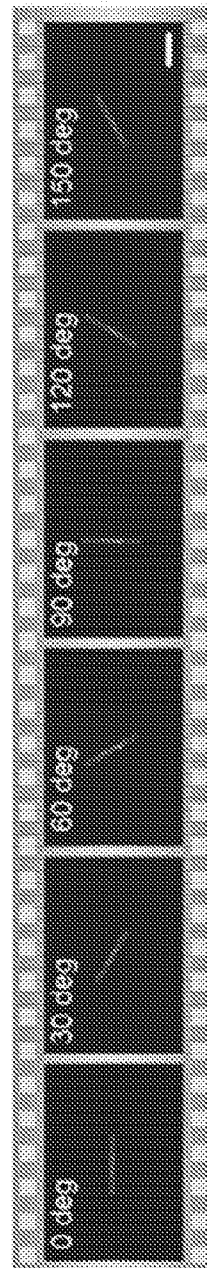
INTERNATIONAL SEARCH REPORT

International application No.

PCT/US2017/050605

A. CLASSIFICATION OF SUBJECT MATTER

IPC(8) - G01N 21/64; G01N 21/71; G02B 5/00; G21K 1/00 (2017.01)

CPC - G01N 21/645; G01N 21/6486; G01N 21/71; G02B 5/00; G02B 5/008; G21K 1/00; G21K 1/006 (2017.08)

According to International Patent Classification (IPC) or to both national classification and IPC

B. FIELDS SEARCHED

Minimum documentation searched (classification system followed by classification symbols)

See Search History document

Documentation searched other than minimum documentation to the extent that such documents are included in the fields searched

USPC - 250/458.1; 250/459.1 (keyword delimited)

Electronic data base consulted during the international search (name of data base and, where practicable, search terms used)

See Search History document

C. DOCUMENTS CONSIDERED TO BE RELEVANT

Category*	Citation of document, with indication, where appropriate, of the relevant passages	Relevant to claim No.
Y	US 2015/0380120 A1 (PURDUE RESEARCH FOUNDATION) 31 December 2015 (31.12.2015) entire document	1-5, 53-58
Y	US 4,425,261 A (STENIUS et al) 10 January 1984 (10.01.1984) entire document	1-5, 53-58
Y	US 2009/0034053 A1 (KING) 05 February 2009 (05.02.2009) entire document	4, 5
Y	US 6,016,226 A (ARISAWA) 18 January 2000 (18.01.2000) entire document	57, 58
A	US 2011/0084218 A1 (DUHR et al) 14 April 2011 (14.04.2011) entire document	1-5, 53-58
A	US 8,431,903 B2 (DUHR et al) 30 April 2013 (30.04.2013) entire document	1-5, 53-58
A	US 2015/0316480 A1 (NANOTEMPER TECHNOLOGIES GMBH) 05 November 2015 (05.11.2015) entire document	1-5, 53-58

☐ Further documents are listed in the continuation of Box C.   ☐ See patent family annex.

*	Special categories of cited documents:
"A"	document defining the general state of the art which is not considered to be of particular relevance
"E"	earlier application or patent but published on or after the international filing date
"L"	document which may throw doubts on priority claim(s) or which is cited to establish the publication date of another citation or other special reason (as specified)
"O"	document referring to an oral disclosure, use, exhibition or other means
"P"	document published prior to the international filing date but later than the priority date claimed

"T"	later document published after the international filing date or priority date and not in conflict with the application but cited to understand the principle or theory underlying the invention
"X"	document of particular relevance; the claimed invention cannot be considered novel or cannot be considered to involve an inventive step when the document is taken alone
"Y"	document of particular relevance; the claimed invention cannot be considered to involve an inventive step when the document is combined with one or more other such documents, such combination being obvious to a person skilled in the art
"&"	document member of the same patent family

Date of the actual completion of the international search	Date of mailing of the international search report
26 October 2017	**1 3 NOV 2017**

Name and mailing address of the ISA/US	Authorized officer
Mail Stop PCT, Attn: ISA/US, Commissioner for Patents P.O. Box 1450, Alexandria, VA 22313-1450	Blaine R. Copenheaver
Facsimile No. 571-273-8300	PCT Helpdesk: 571-272-4300 PCT OSP: 571-272-7774

Form PCT/ISA/210 (second sheet) (January 2015)

INTERNATIONAL SEARCH REPORT

International application No.

PCT/US2017/050605

Box No. II Observations where certain claims were found unsearchable (Continuation of item 2 of first sheet)

This international search report has not been established in respect of certain claims under Article 17(2)(a) for the following reasons:

1. ☐ Claims Nos.:
   because they relate to subject matter not required to be searched by this Authority, namely:

2. ☐ Claims Nos.:
   because they relate to parts of the international application that do not comply with the prescribed requirements to such an extent that no meaningful international search can be carried out, specifically:

3. ☒ Claims Nos.: 6-52, 59-96
   because they are dependent claims and are not drafted in accordance with the second and third sentences of Rule 6.4(a).

Box No. III Observations where unity of invention is lacking (Continuation of item 3 of first sheet)

This International Searching Authority found multiple inventions in this international application, as follows:

1. ☐ As all required additional search fees were timely paid by the applicant, this international search report covers all searchable claims.

2. ☐ As all searchable claims could be searched without effort justifying additional fees, this Authority did not invite payment of additional fees.

3. ☐ As only some of the required additional search fees were timely paid by the applicant, this international search report covers only those claims for which fees were paid, specifically claims Nos.:

4. ☐ No required additional search fees were timely paid by the applicant. Consequently, this international search report is restricted to the invention first mentioned in the claims; it is covered by claims Nos.:

Remark on Protest ☐ The additional search fees were accompanied by the applicant's protest and, where applicable, the payment of a protest fee.

☐ The additional search fees were accompanied by the applicant's protest but the applicable protest fee was not paid within the time limit specified in the invitation.

☐ No protest accompanied the payment of additional search fees.

Form PCT/ISA/210 (continuation of first sheet (2)) (January 2015)